



UNIVERSITY
OF TRENTO

DOCTORAL SCHOOL IN PHYSICS, XXVI CYCLE

ENGINEERING & CHARACTERIZATION OF
A GFP-BASED BIOSENSOR FOR PH AND
CHLORIDE INTRACELLULAR
MEASUREMENTS

Ph.D. thesis of:

FRANCESCO ROCCA

University of Trento,

CNR-Institute of Biophysics

Tutor:

Daniele Arosio

CNR-Institute of Biophysics

TRENTO, 24th APRIL 2014

And those who were seen dancing were
thought to be insane by those who
could not hear the music.

Declaration

I confirm that this is my own work. The use of all material from other sources has been properly and fully acknowledged.

Abstract

ClopHensor, a new fluorescent ratiometric GFP-based biosensor, is a powerful tool for non-invasive pH and chloride quantification in cells.

ClopHensor is a chimeric construct, with the pH- and chloride-sensing E²GFP linked to the reference red protein DsRed-monomer, whose fluorescence is used as reference signal. E²GFP dissociation constant of about 50 mM (at pH = 7.3) makes it ideal for quantifying physiological chloride concentration. However, chloride affinity of E²GFP strongly depends on pH value in solution: precise chloride measurement requires also a pH measurement. By ratio-imaging technique, three different excitation wavelengths are necessary for a pH and chloride concentration estimation.

With the goal to reduce the number of excitation wavelengths required for ratio-imaging technique, in this thesis I present a detailed study of H148G-V224L-E²GFP, selected among several E²GFP-variants for its improved photophysical and spectroscopic characteristics.

H148G-V224L-E²GFP exhibits a chloride affinity and a pH sensitivity similar to *ClopHensor*. Its emission spectra interestingly display two distinct emission peaks at 480 nm and 520 nm after excitation at 415 nm. Importantly, fluorescence emission spectra collected at various pH values also display a clear isosbestic point at 495 nm. This property allows the innovative possibility of pH and chloride concentration determination using only two excitation wavelengths.

Moreover, while being chloride independent, the 520-to-495 (nm) ratio displays a pK_a value of about 7.3, centered in the physiological pH range. These characteristics make it ideal for quantifying intracellular pH changes and chloride fluxes in physiological conditions.

Applications in living cells of this new biosensor demonstrated its usefulness for ratio-imaging analysis.

H148G-V224L-E²GFP+DsRed was successfully expressed in neuron-like cells, as proof-of-concept that ratio-imaging analysis can be performed also in neuron-like cells.

These results are very promising for *H148G-V224L-E²GFP+DsRed* future expression in brain neurons, where chloride plays a crucial role in neuronal activity.

Purified *H148G-V224L-E²GFP* was successfully uploaded in polymeric varterite nanospheres to characterize their endocytosis pathways in cells.

Contents

1	Introduction	1
1.1	Green fluorescent protein	3
1.2	Chloride in living organisms	5
1.3	Chloride-sensitive probes	6
1.3.1	Microelectrodes	6
1.3.2	Fluorescent Cl-sensitive probes	8
2	Goal of this project	35
3	Materials & Methods	37
3.1	Materials	37
3.2	Equipment	42
3.2.1	Protein purification	42
3.2.2	Spectroscopic analysis (in-vitro)	43
3.2.3	Microscopic analysis (in-cell)	46
3.3	Lab Protocols	49
3.3.1	In-vitro pH and chloride titration	49
3.3.2	In-cell experiment	55
4	Results	61
4.1	Site-specific mutants	62
4.1.1	Mutant V224L-E ² GFP	62
4.1.2	Mutant V224Q-E ² GFP	69
4.1.3	Mutant V224N-E ² GFP	75
4.1.4	Mutant L42H-V224L-E ² GFP	81
4.1.5	Mutant H148G-E ² GFP	86
4.1.6	The mutant: H148G-V224L-E ² GFP	94
4.1.7	Mutant H148D-V224L-E ² GFP	119
4.1.8	Site-specific mutants results	123
4.2	Random mutagenesis	124

4.2.1	P192A-E ² GFP	124
4.2.2	K101E-E ² GFP	125
4.2.3	S202N-E ² GFP	125
4.3	In-cell applications	128
4.3.1	Uptake in cells of already-purified biosensor	128
4.3.2	Intracellular functional characterization	131
4.3.3	pH and chloride distribution in neuron-like cells	133
5	Conclusions	139

List of Figures

1.1	resolution comparison for biological imaging techniques	2
1.2	<i>Aequorea victoria</i> jellyfish	3
1.3	GFP ribbon diagram	3
1.4	GFP molecule in cartoon style	4
1.5	Schematic representation of Cl-sensitive microelectrode	7
1.6	Schematic experiment with microelectrodes	7
1.7	Structural formula of SPQ and MQAE	9
1.8	Bleaching effect on <i>Quinolinium</i> compounds	10
1.9	3D structure of GFP and YFP	11
1.10	Spectral characteristics of the most important FPs	12
1.11	<i>Clomeleon</i> , schematic representation	14
1.12	<i>Clomeleon</i> , chloride affect and FRET efficiency	14
1.13	Time-course titration of SuperClomeleon in hippocampal neurons	18
1.14	<i>SuperClomeleon</i> outperforms <i>Clomeleon</i>	19
1.15	Effect of pH on chloride affinity	20
1.16	Representation of Cl-Sensor construct	20
1.17	Design and spectroscopic fluorescent properties of <i>Cl-Sensor</i>	21
1.18	Clophensor: E ² GFP and DsRed	22
1.19	Ribbon representation of E ² GFP with chloride ion	23
1.20	E ² GFP chloride quenching on fluorescence excitation spectra	24
1.21	Typical fluorescence isotherm for chloride binding	25
1.22	Fluorescence decay time	25
1.23	pH effect on chloride dissociation constant	26
1.24	Thermodynamic model for E ² GFP binding	26
1.25	Net number of proton exchanged during chloride binding	27
1.26	pH effect on intensity and shape of E ² GFP excitation spectrum	28
1.27	Stereo view of E ² GFP and YFP chromophore region	29
1.28	Ribbon representation of E ² GFP with chloride ion	30

1.29	<i>ClopHensor</i> spectroscopic features fat different pH and chloride concentrations	31
1.30	Excitation spectra of <i>ClopHensor</i> at different pH values	31
1.31	Ratio between emission fluorescence at different excitation	32
1.32	Ratio between E ² GFP and DsRed emission as chloride indicator	33
1.33	E ² GFP chloride dissociation constant dependence on pH	34
3.1	AKTA-FPLC	42
3.2	FPLC purification steps	43
3.3	EnSpire Plate Reader	44
3.4	Epifluorescence configuration	45
3.5	90° angle fluorescence configuration	46
3.6	Spectrophotometer Jasco V550	46
3.7	iMic equipment	48
3.8	Spectroscopic characterization spectra	50
3.9	Chloride effect on fluorescence	53
3.10	pH effect on fluorescence	54
3.11	Kd changes with pH	55
4.1	Representation of the chloride binding pocket	62
4.2	E ² GFP 3D-structure	63
4.3	V224L-mutant emission spectra	64
4.4	Comparison of chloride affinity for V224L-E ² GFP and E ² GFP	65
4.5	Chloride affinity at different pHs	65
4.6	pH effects on V224L-E ² GFP excitation fluorescence intensities	67
4.7	E ² GFP 3D-structure	69
4.8	Chloride quenching effect on emission spectra for V224Q-E ² GFP	70
4.9	Chloride affinity of V224Q-mutant at different pHs	71
4.10	pH effect on V224Q-E ² GFP fluorescence spectra	72
4.11	pH effect on V224Q-E ² GFP absorption spectra	73
4.12	E ² GFP 3D-structure	75
4.13	Chloride quenching effect on V224N-E ² GFP	76
4.14	Chloride dissociation constant is affected by pHs	77
4.15	pH effect on V224N-E ² GFP fluorescence spectra	78
4.16	Analysis of pH effect on V224N-E ² GFP fluorescence spectra	79
4.17	Representation of the chloride binding pocket	81
4.18	E ² GFP 3D-structure	81
4.19	Chloride quenching effect on L42H-V224L-E ² GFP fluorescence intensity	82
4.20	pH effects on L42H-V224L-E ² GFP excitation fluorescence	84

4.21	L42H-V224L-mutant K_d is affected by pH	85
4.22	E ² GFP 3D-structure	86
4.23	pH effect on H148G-E ² GFP fluorescence intensities	87
4.24	Emission isosbestic point in H148G-E ² GFP	88
4.25	Chloride effect on H148G-E ² GFP fluorescence intensity, at physiological pH	89
4.26	Fluorescence intensity of H148G-E ² GFP at increasing chloride concentration	90
4.27	H148G-E ² GFP chloride dissociation constant (K_d) depends on pH	90
4.28	Excites State Proton Transfer	92
4.29	Emission spectra in case of ESPT failure	93
4.30	E ² GFP 3D-structure	94
4.31	H148G-V224L-mutant fluorescence spectra at different chloride concentration	96
4.32	H148G-V224L-E ² GFP fluorescence intensity at increasing chloride concentration	97
4.33	K_d depends on pH	97
4.34	pH effect on fluorescence intensity	99
4.35	pH effect in isosbestic point	100
4.36	Graphics representation of filters used for pH analysis of H148G-V224L-E ² GFP	100
4.37	Ratio between H148G-V224L-E ² GFP main emission peak and isosbestic band	101
4.38	<i>Ratio-pH</i> 520/495 is independent from chloride concentration	102
4.39	Absorbance spectra for native and denaturated GFP mutant	103
4.40	Relative brightness	104
4.41	Van't Hoff isothermal analysis	105
4.42	Van't Hoff isothermal analysis comparison	106
4.43	pH effect on green, cyan and red channel	107
4.44	In-cell pH calibration	108
4.45	Examples of pH analysis in cells	109
4.46	<i>Ratio-pH</i> is chloride independent	110
4.47	pH analysis is independent from microscope setup parameters	110
4.48	Autofluorescence contribution	112
4.49	Chloride effect on green, cyan and red channel	113
4.50	Chloride quenching effect on Cl-ratio	114
4.51	K_d at different pH	115
4.52	Example of chloride analysis in cells	116

4.53	R^0 and R^{inf} are pH independent	117
4.54	E ² GFP 3D-structure	119
4.55	Fluorescence emission intensity quenching effect	120
4.56	pH effect on H148D-V224L-E ² GFP fluorescence spectra shapes and intensities	121
4.57	Chloride dissociation constant at different pH values	124
4.58	Chloride dissociation constant at different pH values	125
4.59	S202N-E ² GFP chloride dissociation constant and pH sensibility	126
4.60	S202N-E ² GFP pH effect on fluorescence spectra	127
4.61	Vaterite nanosphere loaded with H148G-V224L-E ² GFP uptaken in HEK293 cells	129
4.62	Expression of H148G-V224L-E ² GFP+DsRed biosensor in CHO- K1 cell	131
4.63	Monitoring of chloride concentration in response to GlyR activation	132
4.64	Schematic representation of a typical neuron cell	133
4.65	Transmission-light images of NSC-34 neuron-like cells	134
4.66	DsRed fluorescent signal from not-differentiated NSC-34	135
4.67	pH map inside an NSC-34 neuron-like cell	136
4.68	H148G-V224L-E ² GFP with DsRed expressed in neuron-like NSC- 34	137
4.69	DsRed intensity in different cell lines	138

List of Tables

3.1	Composition of buffers without chloride at different pH range .	38
3.2	Composition of buffers with chloride at different pH range . . .	39
3.3	Chloride titration table for FluoroMax -1	51
3.4	Chloride titration table for FluoroMax -2	51
3.5	Chloride titration table for Enspire	52
4.1	Recap of site-specific E ² GFP main spectroscopic characteristics.	123

Chapter 1

Introduction

Fluorescence microscopy has become an essential tool to study biological events in living cells, tissues and animals.

The main advantage of fluorescence imaging over all other imaging techniques (e.g. electron microscopy) lies in its compatibility with live specimens, allowing minimally invasive and dynamic experiments.

Many imaging techniques are widely used for medical and physiological studies. Positron emission tomography (PET) and magnetic resonance imaging (INMR) allow a real-time analysis of animal and human body, but their spatial resolution is limited to $\sim 1\text{ mm}$, drastically limiting their application in cells. At the opposite end of resolution spectrum there is electron microscopy (EM) with its molecular-level spatial resolution, but its applications are very invasive, biological samples must be fixed, denying the possibility of any dynamic experiments on living cells.

Between these two extremes, fluorescence microscopy is the only imaging technique able to provide a wide range of temporal and spatial resolution, working both on fixed and living samples. It is characterized by spatial resolution at organelles-level in cells (it is possible to resolve the nucleus, the endoplasmatic reticulum and the Golgi apparatus) and it can be exploited for dynamic measurements (e.g. tracking proteins and biomolecules and studying changes in concentration variations of proton and other biological relevant molecules and ions)[22].

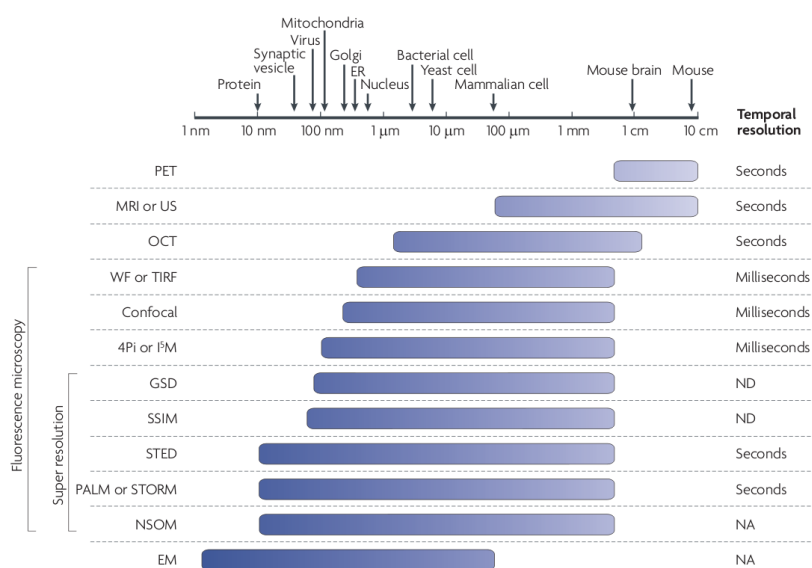


Figure 1.1: Comparison of temporal and spatial resolution of biological sample imaging techniques. PET, positron emission tomography; MRI, magnetic resonance imaging; US, ultrasounds; OCT, optical coherence tomography; WF, widefield microscopy; TIRF, total internal reflection fluorescence; GSD, ground-state depletion; SSIM, structured-illumination microscopy; STED, stimulated emission depletion; PALM, photoactivated localization microscopy; STORM, stochastic optical reconstruction microscopy; NSOM, near-field scanning optical microscopy; EM, electron microscopy. The temporal resolution is not applicable (NA) for EM and NSOM because they work with static sample, and it is not determined (ND) for GSD and SSIM. Notes: the given average size of biological samples may widely vary among different cell lines and species; the spatial resolution is given at the focal plane.

During the last few decades important efforts have been spent on fluorescent protein mutagenesis in order to engineer and develop new biosensors for in-living-cells microscope experiments[68].

Fluorescent probes, engineered for quantitative analysis of intracellular distribution of various proteins and ions, have been widely exploited to obtain crucial information of both physiological and pathological conditions in biological organisms at a cell-component precision level[14].

1.1 Green fluorescent protein

Green fluorescent protein (GFP) is a fluorescent molecule, from the *Aequorea victoria* jellyfish, deeply exploited on biological imaging studies¹.

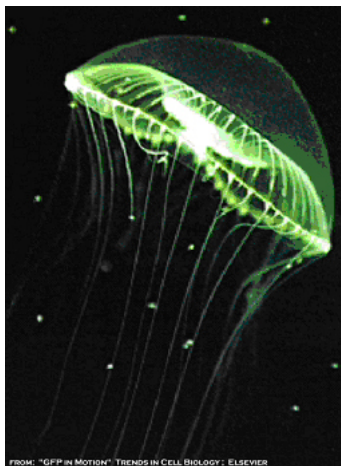


Figure 1.2: *Aequorea victoria* jellyfish

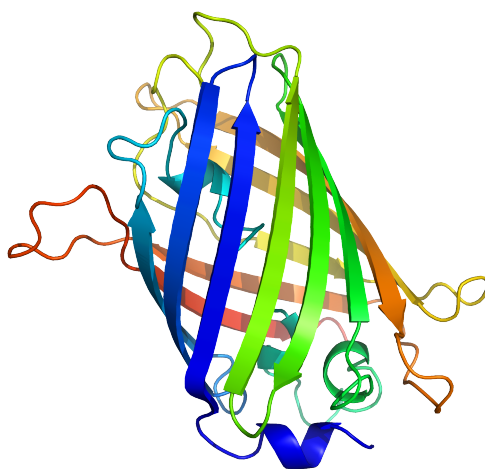


Figure 1.3: GFP ribbon diagram, with highlighted the eleven β -sheets forming the chromophore protective scaffold

GFP, as extracted from the jellyfish, is characterized by bright green fluorescence, with a quantum yield (QY) of 0.79. Its major excitation peak is in

¹Martin Chalfie, Osamu Shimomura, and Roger Y. Tsien were awarded the 2008 Nobel Prize in Chemistry for their discovery and development of the green fluorescent protein.

the UV region at 395 nm, with a second one at 475 nm in the blue region. Its main emission is centered in the green portion of the visible spectrum, at 510 nm[76].

GFP fluorescent signal is generated by its chromophore, located in a cylinder-shaped β -barrel structure (Figure 1.4). Chromophore is formed by cyclization reactions of the tri-peptide Ser65–Tyr66–Gly67, during a post-translational modification process named *maturation*[61]. Chromophore interactions with sidechain residues and with surrounding hydrogen-bonding network define the color, intensity and photostability of GFP fluorescence.

The tightly-packed nature of the β -barrel structure² prevents solvent molecules to reach the chromophore, protecting its fluorescence from quenching by water and other solvents. The high stability of GFP structure in several environmental conditions, its spontaneous autocatalytic formation of the chromophore (no specific cofactors are requested[63]), the possibility to alter its spectral properties by mutagenesis and its genetically-encoded fluorescence makes GFP family extremely attractive for a wide variety of biological applications.

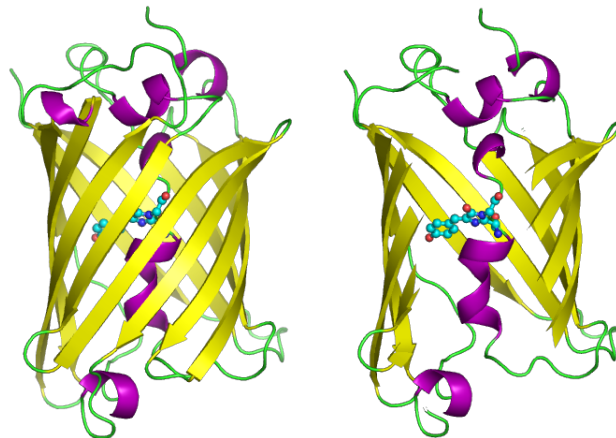


Figure 1.4: GFP molecule in cartoon style (the second with the side of the beta barrel cut away to reveal the chromophore)

The GFP gene is often used as a reporter of expression in cell and molecular biology[59] and many animals have been engineered to express GFP as a proof that a particular gene is expressed in a specific organism. GFP gene can be introduced into organisms (bacteria, yeast, fungi, plant, fly and mammalian cells

²GFP high-resolution structure has been characterized by x-ray crystallography [57], online available on PDB database.

including human) and maintained in their genome through cell transformation, breeding or injection with a viral vector.

GFP has also been widely used in biosensing, to built fluorescent genetically-encoded probes optimized for intracellular microscope in living specimens[38].

Minimally invasive optical techniques (e.g two-photon microscopy[73, 84]) and super-resolution techniques (STED, STORM and PALM [22]) have been applied to GFP-based probes imaging in order to direct study intracellular processes minimizing sample damaging and alterations.

1.2 Chloride in living organisms

Chloride is the most abundant anion in cells of every biological organism. It is involved in many different physiological processes, from neurotransmission to regulation of pH, cell volume, water-salt balance, fluid secretion and resting membrane potential stabilization[71].

Chloride homeostasis, intracellular concentration and permeability are key parameters finely tuned in cells by a wide variety of Cl-selective channels and Cl-transporters[15].

Misregulation of $[Cl^-]$ homeostasis in cells often leads to severe phenotypes[5] and diseases, such as cystic fibrosis, myotonia congenita, congenital chloride diarrhea, inherited hypercalciuric nephrolithiasis, Bartter's and Gitelman's syndromes, hyperekplexia and epilepsy (for instance in epilepsy, variations of intracellular chloride concentration is known to be involved during a seizure)[35, 36, 40, 42, 44, 69, 70].

Chloride is also crucial in the physiology of the nervous system: the main inhibitory synapses both in peripheral and in central neuronal circuits are the GABAergic and glycernergic synapses, both of them operating by means of Cl-selective channels[28].

Despite the crucial role of chloride ions in several cellular processes, a detailed knowledge on the chloride regulating mechanisms has yet to be achieved, for physiological and pathological conditions.

This lack of knowledge is mostly due to technical difficulties in quantitative monitoring and estimating chloride fluxes in living cells. Intracellular chloride concentration measurements in neuron cells, but also in may other cell lines, is very challenging.

High sensitivity and wide dynamic range are fundamental features of chloride-sensitive probes in order to provide a reliable estimation of chloride concentration and fluctuations.

1.3 Chloride-sensitive probes

The most common chloride-sensitive probes can be gathered in two distinct categories: microelectrodes and fluorescent dyes.

1.3.1 Microelectrodes

Widely used from 1960s to 80s, microelectrodes allowed chloride distribution analysis and dynamic measurements.

The first chloride-sensing electrode was simply based on a small tip ($\sim 2\mu m$ of diameter) with a fine *AgCl* wire covered by a protective glass capillar[37] (Figure 1.5).

This type of electrodes were able to respond to chloride changes very slowly, in the order of some minutes, and they were difficult to manage during intracellular measurements. Moreover, further experiments demonstrated that this type of electrode always reported a chloride concentration higher than real concentration in intracellular environment[56].

Electrodes were then modified and improved, measuring chloride via a liquid chloride exchanger[82] and quantifying its concentration from analysis of membrane resting potential (acquired with a separated electrode) and electrical voltage variations directly due to chloride ion fluxes[2]. A schematic representation of this version of microelectrodes applied to a cell (the central circle) is reported in the top of Figure 1.6: chloride concentration and membrane potential were recorded with the use of three microtips. In the bottom of Figure 1.6 is shown a typical recorded signal for chloride and membrane potential.

It is important to notice the time-scale, in the order of several minutes, to understand the difficulties in using this kind of equipment to measure in-cell fast chloride transients.

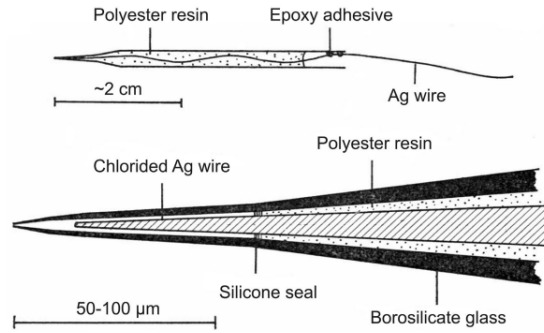


Figure 1.5: Schematic representation of first-design microelectrode for chloride measurements. The complete electrode (top image) and its enlarged tip view (bottom image) are represented[56].

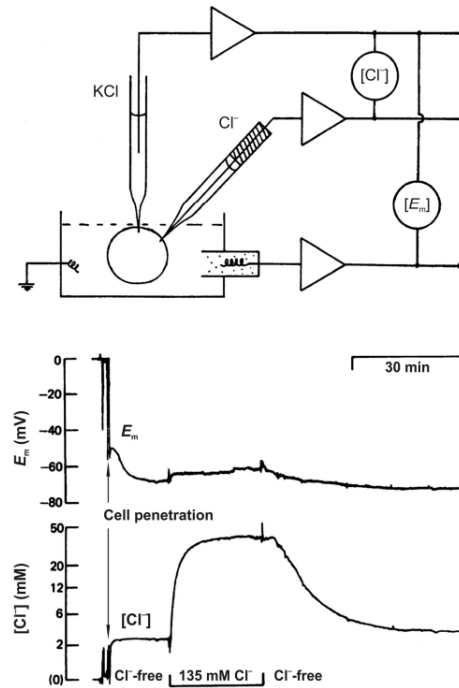


Figure 1.6: Top: diagram showing the basic experimental setup for $[Cl^-]$ measurements using microelectrodes[74]. Bottom: example of simultaneous recording of membrane potential E_m and chloride concentration $[Cl^-]$. Notes the very slow chloride variations recorded, in the order of minutes[2]

Results from experiments with Cl-sensitive micro-electrodes, in spite of all their complications and drawbacks, had a great importance on chloride understanding, demonstrating that $[Cl^-]$ in cells is significantly different than the

theoretical predicted passive distribution: chloride ions must be transported in an some active way through the cell membrane[65].

Although micro-electrodes have shown their potential in chloride measurements in cells, several technical complications limited their spread application: they are not able to follow fast kinetics (their typical response is in the minute time-scale) and they can't assure reliable results without significantly damaging cells (with a dimension of some micrometer, tips damage cells integrity during insertion and measurement). Moreover, mechanical insertion of micro-electrodes inside cells may alter their natural chloride distribution, leading to biased results[14].

1.3.2 Fluorescent Cl-sensitive probes

Exogenous fluorescent probes

Fluorescent-based chloride-sensitive probes have been the next step, with their non-invasive possibility to monitor chloride distribution and dynamical changes in different cell types.

Presence of heavy-atom ions, as iodine or bromide, decrease fluorescence of many fluorophores, while chloride ion is less affecting and only few fluorophores are subjected to chloride quenching[25].

In 1869 the first chloride quenching effect was observed on fluorophore *Quinine*, and this knowledge opened the way towards more efficient Quinine-based chloride-sensitive probes.

Quiolinium (Quinine-based chloride indicators) are based on the halides ability to quench fluorescence arising from heterocyclic organic compound with a quaternary nitrogen ring, present in *Quinine* and preserved in its most two famous and important mutants: SPQ[33] and MQAE[47]. Their chemical structure is reported in Figure 1.7, where the nitrogen rings for chloride quenching are visible.

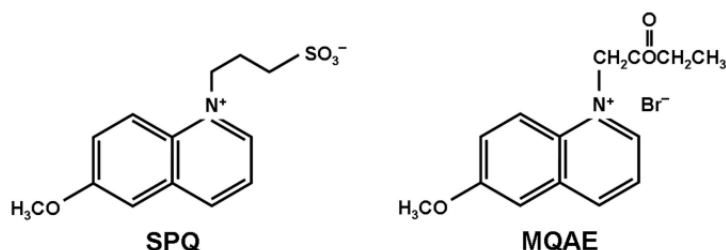


Figure 1.7: Structural formula of Quinine-based chloride indicators SPQ and MQAE

A relation between fluorescence intensity and chloride concentration is provided by Stern-Volmer equation:

$$\frac{F_0}{F} = 1 + K_{SV} \cdot [Cl^-] \quad (1.1)$$

where F_0 is the fluorescence intensity in absence of halide and F in presence of $[Cl^-]$ in solution; K_{SV} is the Stern-Volmer characteristic quenching constant, related to the dissociation constant by $Kd = 1/K_{SV}$.

SPQ [6-methoxy-N-(3-sulfopropyl)quinolinium] is excited with ultraviolet light (at 320 nm) and emits in a single broad blue emission peak at 450 nm. Its fluorescence emission intensity is not altered by cations, phosphates, nitrates, and sulfates, but it is strongly quenched by chloride ions, with a $Kd^{Cl} \sim 8.5 \text{ mM}$ [32].

MQAE [6-methoxy-N-(6-methoxyquinolyl)-acetoethyl ester] exhibits same spectroscopic characteristics as SPQ, but an higher chloride sensitivity. Unlike SPQ, can easily permeate through the plasma membrane[47], resulting in a very short incubation time (10-minutes incubation of brain slices is enough for bright stained neurons[48]). Longer incubation times however lead to severe neuron deterioration, as it happens with SPQ.

In general, *Quinolium* compounds have an appropriate chloride sensitivity for in-cells measurements, selectivity and rapid response to $[Cl^-]$ changes, with readout unaffected by pH. As drawback, they require ultraviolet excitation, with consequent strong bleaching effect³[55] (as visible in Figure 1.8), limiting experiments duration and allowing only a low acquisition rate (0.2-2 frames per minute); *Quinolium* compounds also suffer of significant leakage rate[77, 48] and exhibit intense neuron toxic effect after incubation longer than an hours[67].

³Bleaching effect may however be reduced by the use of two-photon-excitation technique[48].

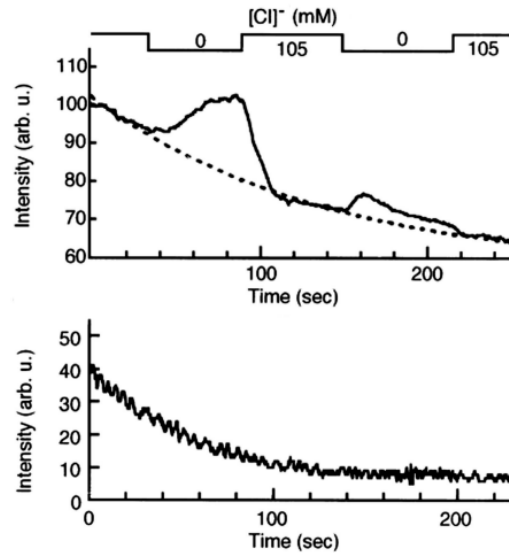


Figure 1.8: Example of continuous fluorescence measurements on cells loaded with MQAE. Note the rapid baseline degradation (top and bottom traces) and the drastic decrease (in the top trace) in fluorescence response to the second chloride adding from 0mM to 150mM[55]

These exogenous fluorescent dyes must be uploaded in cells from the external medium by endocytic pathways[39], and can't be directed to specific sub-cellular location[39]. Another consequence of their exogenous-nature is their cell penetration, which changes significantly from cell to cell[7].

Genetically-encoded fluorescent probes

The most recent approaches is based on endogenously expressed chromophores (instead than exogenously added probes).

The discover that fluorescent proteins (FP family) derived from GFP exhibit chloride and pH sensitivity marked the beginning of the genetically-encoded probes era.

Conventional dyes (i.e. not genetically-encoded as GFP) must be uploaded in cells from the external medium, while GFP-based biosensors are instead directly expressed inside the cells: GFP-vector may be integrated in cells genome in a stable way or just encoded in a transient and temporary way. They can be directed to preselected subcellular compartment by genetic engineering procedures, fusing the probe with a specific-designed sequence tag[11, 43, 76]. Their spectroscopic characteristics are well appropriate for noninvasive and

high-resolution imaging in living specimens[30] allowing chloride estimation exactly in specific cell compartment[8].

GFP-based genetically-encoded probes are characterized by a natural intracellular expression concentration normally in the order of some $1 - 100 \mu M$, several order of magnitude less than chloride concentration ($6 - 60 mM$ in neurons), with consequent minimum buffering effect on $[Cl^-]$ estimation[14].

Recent studies have exploited these very attractive spectroscopic characteristics of GFP-variants to monitor intracellular pH[39], calcium Ca^{2+} concentration [52], halide ions concentration[3], interaction protein-protein [85], tyrosine kinase activity [75], redox status in living cells[18] and molecule tracking at subcellular level[23]. GFPs have also found important applications in neurobiology fields, measuring neuronal activity and neuron-circuit activity at cellular level[46].

Before the introduction of fluorescent probes, neurobiological studies were performed exploiting electrophysiological procedures and protocols, whose readouts were not always reliable[49].

GFPs fluorescent nature allows neurobiological studies using fluorescence and optical techniques; however, monitoring small and fast changes of target molecule concentrations for neuronal signaling is still challenging[4, 41].

YFP: yellow fluorescent protein

In the last decade, genetically-encoded optical probes have been widely used to noninvasive monitor chloride concentration in cells, mostly triggered by the discover of the halide-binding property of the yellow fluorescent protein.

Yellow fluorescent protein (YFP) is a GFP-derived genetically-encoded fluorescent protein, obtained by GFP with mutations T203Y/S65G/V68L/S72A. It is brighter than GFP, with red-shifted excitation/emission spectra[20].

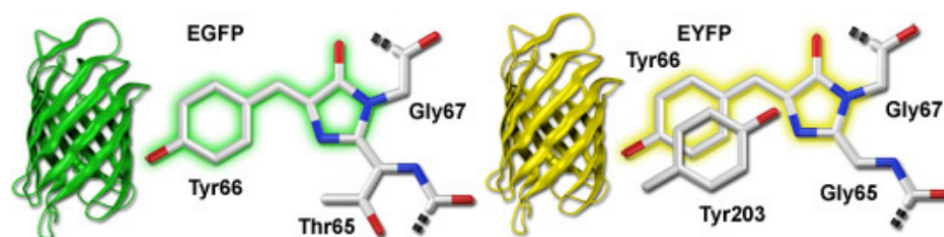


Figure 1.9: 3D structure of GFP and YFP, with zoom on the different chromophore structure

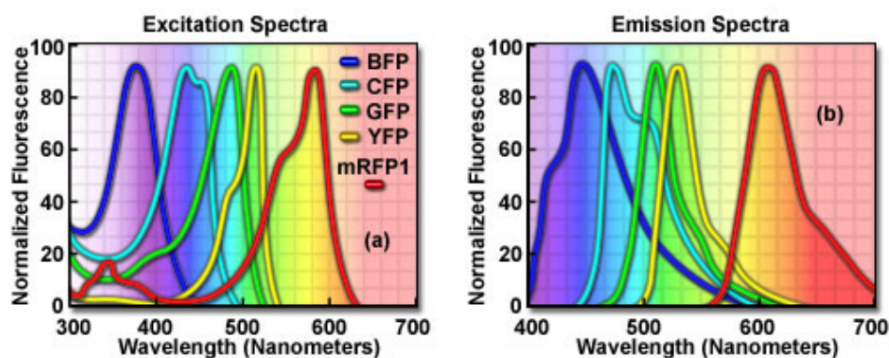


Figure 1.10: Spectral characteristics of the most important FPs, with excitation spectra (left panel) and emission spectra (right panel)

YFP fluorescence is quenched by small anions[80], so it has been immediately engineered as chloride-indicator[80]. This sensitivity is due to halide binding near the chromophore, which appears to alter the ionization constant of the chromophore and then its fluorescence emission[34]. YFP chloride affinity is in the order of some hundreds milliMolar at physiological pH (but it is very pH sensitive)[81].

YFP fluorescence is also pH-dependent, as for all the others FPs.

In the physiological pH range, YFP sensitivity to chloride is very low, with consequent limitations in using this FP-variant as efficient in-cell chloride indicator. To improve YFP spectroscopic characteristics, libraries of YFP-mutants were generated, in which residues close to the halide binding site were randomly mutated[24]. Among many chloride sensitive variants obtained, the mutations H148Q and V163S were able to reduce YFP chloride affinity below the 100 *mM* [24].

Ratiometric genetically-encoded fluorescent probes

The major drawback affecting in-vivo usage of YFP, and in general all FPs-based biosensors, is that the probe analyte concentration has a direct effect on final fluorescence intensity measured. Therefore, determine whether fluorescence intensity changes are due to chloride quenching or to variations in probe concentration is not possible, considering also the complications caused by photobleaching effect.

An independent protein concentration measurements is then required during every experiment.

This problem has been solved by constructing chimaera, fusion-proteins containing a chloride-sensitive part and a reference part (chloride independent).

The ratiometric approach can eliminate data distortion caused by photobleaching, variable cell thickness, stability of illumination lines, excitation path length and of course probe concentration variations, compensating also a possible non-uniform probe distribution inside each cell[27].

The most important milestone was achieved in 2000, constructing a ratiometric YFP-based chloride indicator: *Clomeleon*[41].

Clomeleon

*Clomeleon*⁴ is a fusion-protein composed of two distinct fluorescent protein, Cyan Fluorescent Protein (CFP) and a YFP-variant named Topaz (GFP-S65G-S72A-K79R-T203Y-H231L) connected by a short flexible linker of 24 aminoacids (in Figure 1.11 a representation of the construct and a cartoon of the full biosensor)

Clomeleon's principle of work is based on fluorescence-resonance-energy-transfer (FRET, see Box on page 16) between CFP (insensitive) and YFP-Topaz (sensitive to chloride).

The presence of a chloride isosbestic point in emission spectra (i.e. an emission wavelength whose intensity is chloride independent) as visible in Figure 1.12 allows the use of this construct as a ratiometric probe for chloride concentration estimation.

⁴The construct was named *Clomeleon* as an allusion to the FRET-based genetically-encoded calcium indicator *Cameleon*

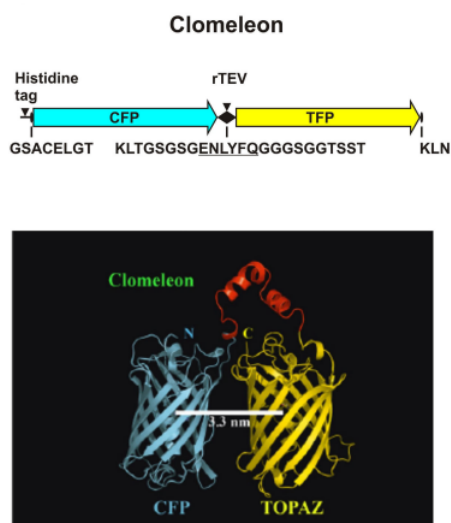


Figure 1.11: Schematic representation of the Clomeleon vector and its 3D final construct structure

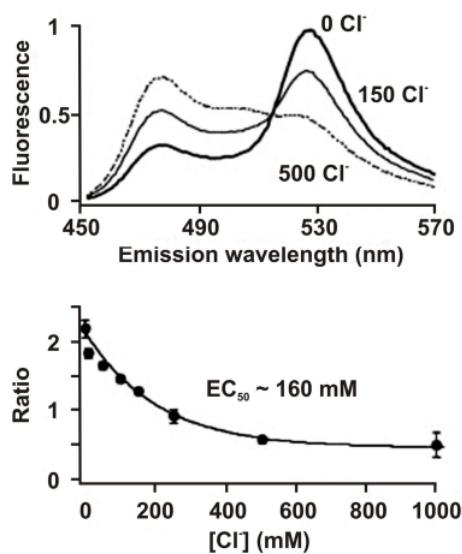


Figure 1.12: Top: presence of chloride isosbestic point in emission spectra, allowing this probe to be a ratiometric chloride estimator. Bottom: Emission intensity ratio between Donor and Acceptor decreases at increasing chloride concentration, even with a sensibility very low ($EC_{50} \sim 160 \text{ mM}$)[41]

Chloride binding to Topaz reduces its emission intensity, leading to a decrease in FRET efficiency. As consequence, emission intensity ratio between

Topaz (FRET-acceptor) and CFP (FRET-donor) is reduced as chloride concentration increases (Figure 1.12).

Clomeleon, unlike other organic probes, exhibits excitation upon visible light, limiting bleaching effect otherwise significant with UV excitation. Other interesting *Clomeleon* spectroscopic features are good s/n, safer cell loading procedure, absence of leakage from cells and the possibility to target different type of cells when using specific promoters. Moreover, it is characterized by high fluorescent stability[60].

Clomeleon has the great advantage to be a ratiometric probe. The possibility to perform ratiometric chloride concentration measurements allows optical experiments which are just minimally affected by variations in specimen thickness, excitation light intensity and *Clomeleon* concentration. These advantages makes *Clomeleon* a perfect tool to monitor chloride in cells even with complicated geometry, such as neurons and retina cells [41, 60].

A severe limitation for this ratiometric chloride-sensitive probe, as for all the others YFP-based indicators, is its intrinsic pH dependence and its slow reaction-time to chloride. Moreover, CFP and Topaz may bleach with different time-rate, distorting the signal readout.

The most significant disadvantage is however its chloride sensitivity, too low to be used for highly accurate chloride estimation inside cells: a chloride dissociation constant $Kd^{Cl} > 160mM$ is relatively far from physiological chloride concentration range (in the order of some milliMolar [4, 14]).

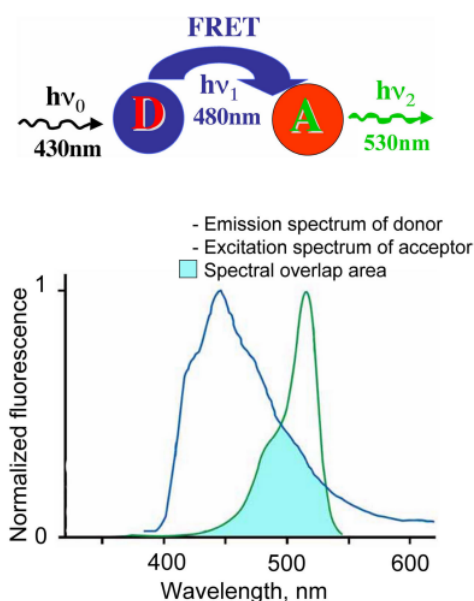
Development of chloride probes with sensitivity closer to physiological chloride values would mean obtaining powerful tools for a precise and accurate $[Cl^-]$ measurements in living samples.

FRET

Fluorescence resonance energy transfer (FRET) is a nonradiative dipole–dipole interaction between two chromophores, with energy direct transferred from a donor molecule (D) to the acceptor one (A).

For this phenomenon to take place, some conditions must be fulfilled:

- Donor emission spectrum and acceptor absorption spectrum must overlap
- Donor and acceptor must be at short distances, less than 10nm
- Donor emission dipole and acceptor absorption dipole must have favourable orientation
- Both fluorophores must have a high quantum yield



The FRET efficiency has a strict relation with the distance r between the two fluorophores:

$$E = \frac{1}{1 + \left(\frac{r}{R_0}\right)^6}$$

where R_0 is a distance, characteristic for each fluorophores pair, at which the energy transfer efficiency is the 50% of the maximum.

FRET is a very powerful tool for protein-protein interaction studies, being extremely sensitive to short-range distance variations.

SuperClomeleon

A *Clomeleon*-based new probe has been developed by a multi-stage genetic manipulation strategy of *Clomeleon*[26].

The main steps of this procedure, detailed described by *Grimely et al. 2013* [26], consisted in YFP single-point mutations directed to improve its chloride affinity and signal-to-noise ratio while enhancing its FRET response to chloride changes.

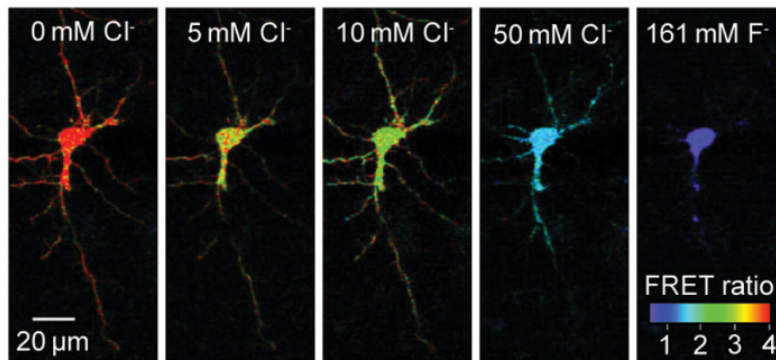
The most promising chloride-sensitive probe from this screening procedure, *SuperClomeleon*, exhibits two chloride binding sites near the chromophore, which leads to an increased chloride affinity up to $Kd^{Cl} \sim 30 \text{ mM}$ (at $pH = 7.1$).

This enhanced sensitivity carries as counterpart a rise in chromophore pK_a and a consequent brightness decrease: the YFP chromophore can exist in four possible conformation (anionic, cationic, zwitterionic and neutral, according to pH), of which only the anionic form is fluorescent[20]. With an increased chromophore pK_a , the concentration of the anionic chromophore (i.e. the fluorescent form) is decreased, therefore diminishing sensor brightness.

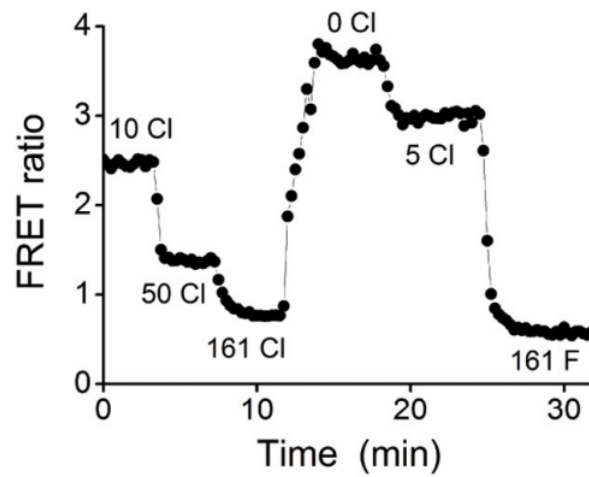
In *SuperClomeleon* this proton interference is sufficiently balanced to arrive to a compromise: sacrifice part of brightness to drastically improve chloride sensitivity.

SuperClomeleon has shown its ability to measure chloride concentration in neurons (Figure 1.13a) and to report fast chloride changes in-cell (Figure 1.13b) with improved signal-to-noise ratio if compared to *Clomeleon* (Figure 1.14a) and with higher FRET-ratio signal (Figure 1.14b).

Unfortunately, pH has still an effect both on chloride affinity and on fluorescence intensity (Figure 1.15). Moreover, being based on FRET, this pH dependence is intrinsically present in *SuperClomeleon*.

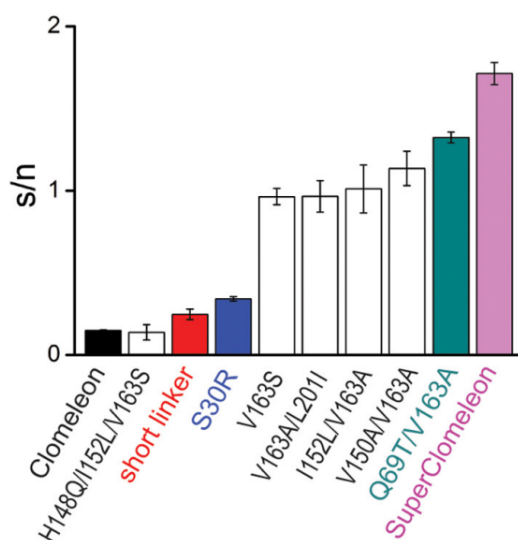


(a) Titration of SuperClomeleon in hippocampal neurons, with in false-color Cl^- -dependent changes in FRET-ratio[26]

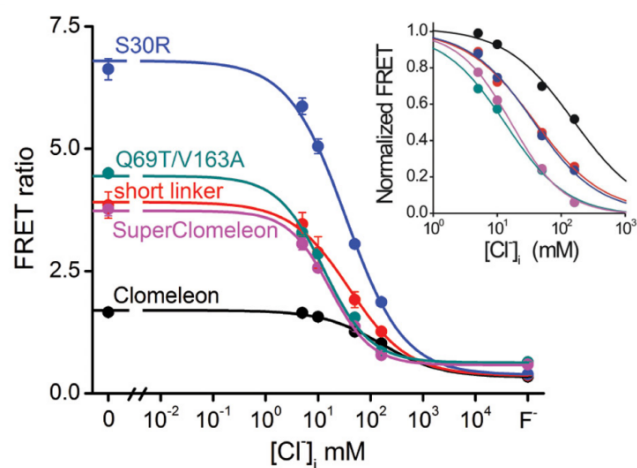


(b) Time course in FRET-ratio changes in response to $[\text{Cl}^-]$ changes: SuperClomeleon is able to follow fast chloride changes in cells shown in Figure 1.13a[26]

Figure 1.13: Time-course titration of SuperClomeleon in hippocampal neurons



(a) Signal-to-noise estimation for several *Clomeleon* variants: *SuperClomeleon* shows a s/n orders of magnitude better than *Clomeleon* and other YFP-variants



(b) Chloride titration curves, for several *Clomeleon* variants, to visualize the superior FRET-ratio of *SuperClomeleon* if compared to *Clomeleon*. In the inset the same data are normalized for their minimum and maximum ratio value, in order to compare the different chloride sensibility: *SuperClomeleon* is far more sensitive than *Clomeleon*

Figure 1.14: *SuperClomeleon* outperforms *Clomeleon* both in signal-to-noise ratio and in FRET-ratio signal intensity[26]

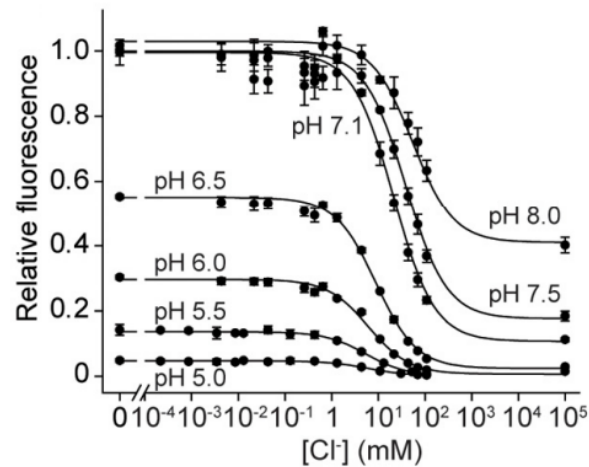


Figure 1.15: Effect of pH on chloride affinity: the higher the pH and the more the construct is fluorescence, but losing dynamic range of chloride sensibility[26]

SuperClomeleon offers an improved sensitivity to chloride fluxes in comparison with *Clomeleon*, even if it is characterized by a great pH interference, both on FRET efficiency and on chloride sensitivity.

SuperClomeleon is not able to estimate pH, so a previous and independent pH estimation is necessary to assure a precise *SuperClomeleon* FRET-ratio-based chloride measurements.

Cl-sensor

Cl-sensor[49] is substantially based on *Clomeleon* construct, but with specific mutations on YFP (YFP/H148Q/I152L/V163S).

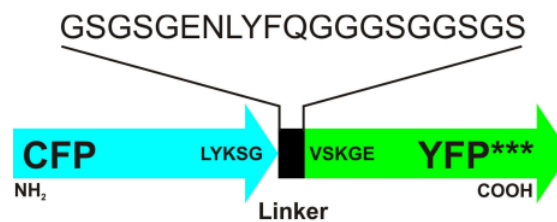
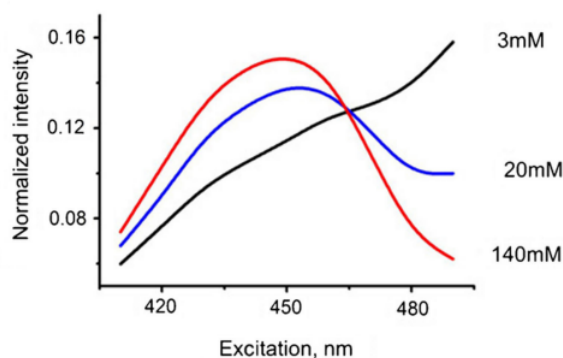


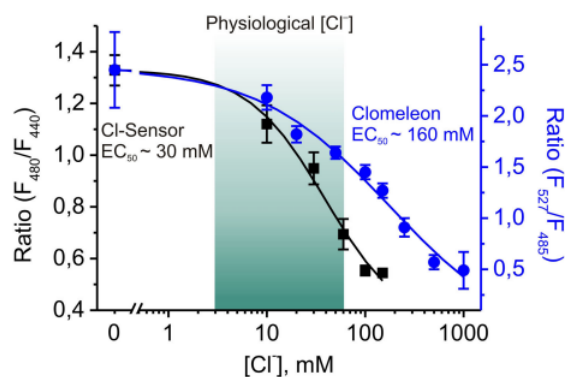
Figure 1.16: Representation of Cl-Sensor construct (***) indicates the YFP with the three mutations -H148Q -I152L -V163S) [49]

Cl-sensor spectral properties exhibit two important features:

- the normalized excitation spectra, acquired at different chloride concentration, shows a chloride isobestic point at 465 nm (Figure 1.17a). This feature allows *Cl-sensor* to be used as a ratiometric sensor in excitation
- this probes exhibits a high chloride sensitivity ($EC_{50} = 25 \pm 5 \text{ mM}$ at physiological pH), about 5-folds higher than *Clomeleon* (Figure 1.17b)



(a) Normalized excitation spectra for different chloride concentration (from 3mM to 140mM). Note the chloride isobestic point at 465nm, where chloride doesn't influence fluorescence intensity.



(b) Comparison of chloride sensitivity for *Cl-Sensor* (in black) and *Clomeleon* (in blue) with highlighted the physiological chloride concentration range. *Cl-sensor* is characterized by a chloride sensitivity more than 5-folds higher than *Clomeleon*.

Figure 1.17: Design and spectroscopic fluorescent properties of *Cl-Sensor*[49]

Cl-sensor keeps all the advantageous features of *Clomeleon*, such as visible light excitation, no leakage from cells and possibility to be directed to specific cell types with specific promoters. As counterpart, as *Clomeleon* it exhibits a high pH sensitivity affecting chloride concentrations measurements, making an absolute chloride estimation not-trivial.

Several works have however demonstrated the powerful characteristics of *Cl-Sensor* in monitoring chloride concentration, in different experimental conditions, during neurons development[54, 83].

ClopHensor

YFP and its variants used in *Clomeleon*, *SuperClomeleon*, *Cl-sensor* and in all other genetically-encoded chloride indicators (as *YFpH* and *pHlameleons*[41, 21, 49]), are characterized by a dual sensitivity: the chloride ions sensitivity makes them suitable chloride-sensitive genetically-encoded probes, but their fluorescence intensity emission is also sensible to pH.

This double dependence complicates measurements analysis: if the concentration of proton and chloride changes simultaneously (cellular processes often co-regulates Cl^- and H^+ concentration[66]) it is not possible to distinguish the two effect in order to obtain an absolute and independent chloride concentration measurement.

This issue has been solved with the introduction of *ClopHensor*[4], a genetically-encoded fusion-protein able of simultaneous Cl^- and H^+ concentration measurements in several cell lines[4, 53].

ClopHensor is formed by the fusion of E²GFP (EGFP+T203Y) and Discosoma red fluorescent protein (DsRed⁵), as schematically shown in Figure 1.18.

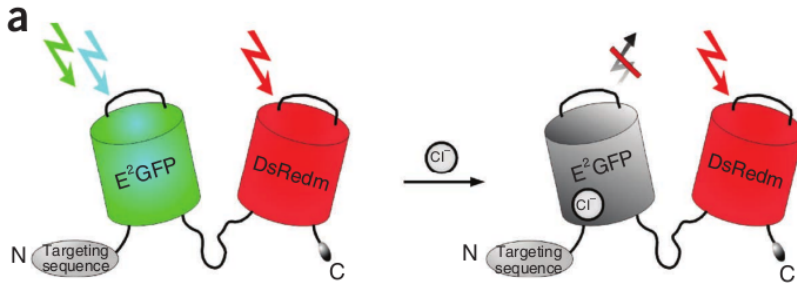


Figure 1.18: E²GFP and DsRed are fused with a flexible linker of 20 aminoacids. Chloride binding on E²GFP induces its static quenching, while not affecting DsRed fluorescence.[4]

ClopHensor is based on non-FRET measurements and it is able to performs at the same time both *pH* and $[Cl^-]$ measurements[4, 83], overcoming difficulties associated with $[Cl^-]$ monitoring in presence of *pH* fluctuations around physiological values.

⁵DsRed has been reported to suffer of intracellular aggregation problems when expressed in neurons. In *Clophensor* it is then planned to be substitute with *tdTomato*[62]

Red moiety DsRed has been chosen as reference because its fluorescence is insensitive both to chloride and to proton, and fairly separated from the green emission of E²GFP. Spectroscopic studies[4] have also revealed that DsRed does not interfere with E²GFP advantageous spectroscopic features[3].

E²GFP: ClopHensor sensitive component *ClopHensor* is still one of the most sensitive and reliable biosensor for chloride and pH measurements in living cells. Its powerful characteristics are hidden in its sensitive component: a GFP-based fluorescent protein, obtained from the Enhanced-GFP (EGFP - GenBank Accession n.U76561) adding the single mutation T203Y, named E²GFP.

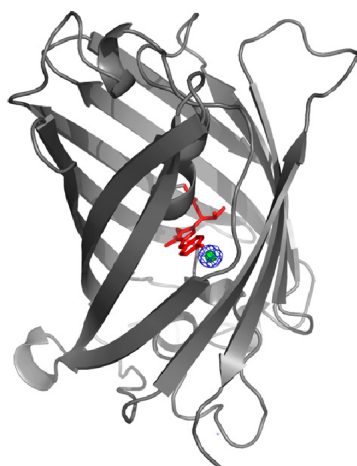


Figure 1.19: Ribbon representation of E²GFP with chloride ion (green sphere) inserted in the binding pocket near the chromophore (in red). In blue is represented the chloride electron density map.[3]

E²GFP fluorescence intensity is very chloride sensible, as resulting from spectra in Figure 1.20: with emission set at 523 nm, E²GFP excitation spectra were acquired at increasing chloride concentration (up to 1M) for three different pH conditions (acid $pH = 4.95$, physiological $pH = 7.05$ and basic $pH = 9.3$)[3].

When chloride concentration is increased, fluorescence intensity drops off uniformly in the whole spectral range.

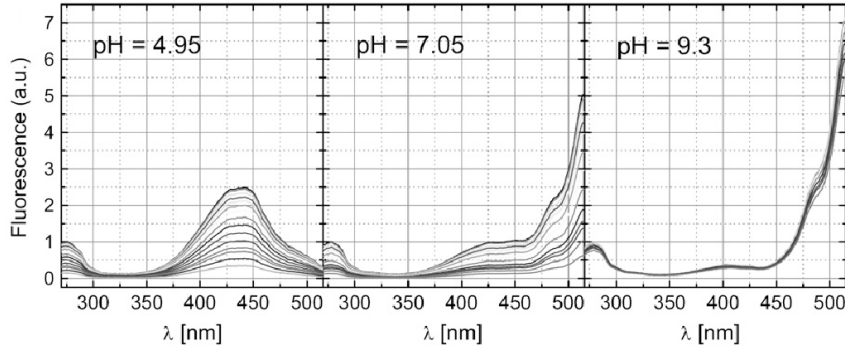


Figure 1.20: E²GFP fluorescence excitation spectra (normalized at 278nm for protein concentration) collected at emission fixed at 523nm. Increasing chloride concentration, from $[Cl^-] = 0\text{ mM}$ to $[Cl^-] = 1\text{ M}$, correspond to a decrease in fluorescence intensity (at three different pH values: 4.95 - 7.05 - 9.30, from left to right)[3]

Chloride titration on fluorescence intensity data were normalized and fitted with a 1:1 binding equation:

$$F = \frac{F_0 + F_1 \cdot \frac{[Cl^-]}{Kd}}{1 + \frac{[Cl^-]}{Kd}} \quad (1.2)$$

where F_0 is the fluorescence intensity without halogen in solution, F_1 the intensity at infinite halogen concentration, F is the fluorescence at that particular chloride concentration $[Cl^-]$ and Kd the halogen-GFP dissociation constant, directly representing the halogen sensitivity.

Equation 1.2 allows a precise determination of the Kd without the necessity to perform titration at halogen saturation concentration (often experimentally inaccessible).

In Figure 1.21 is reported a typical isothermal from chloride titration (at pH=5.2), where fluorescent intensity have been normalized and fitted with Equation 1.2.

Remarkably, fluorescence intensity goes asymptotically to zero at infinite halogen concentration (within its statistical errors).

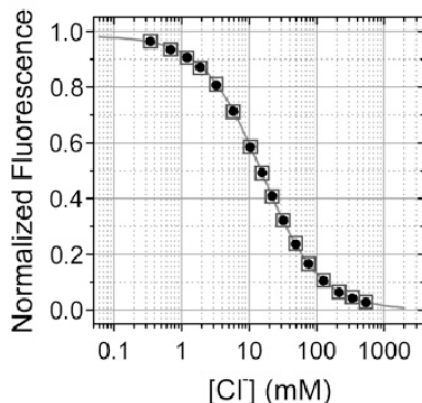


Figure 1.21: Typical fluorescence isotherm obtained at $pH = 5.2 \pm 0.05$ analyzing fluorescence intensity variations (integrating excitation and emission data) at different chloride concentration. Solid line is the fit with Equation 1.2, returning a $Kd^{Cl} = 15.4 \pm 0.2 \text{ mM}$ [3]

To unambiguously verify that E²GFP fluorescence intensity is quenched by chloride via *static* quenching, E²GFP excited state fluorescence decay time has been analyzed.

Fluorescence decay data at pH 7.4 and 9.4 are shown in Figure 1.22, acquired both in absence of chloride and with $[Cl^-] = 1 \text{ M}$: they exhibit a single lifetime, unaffected neither by the chloride presence nor by the pH, as expected in case of static quenching.

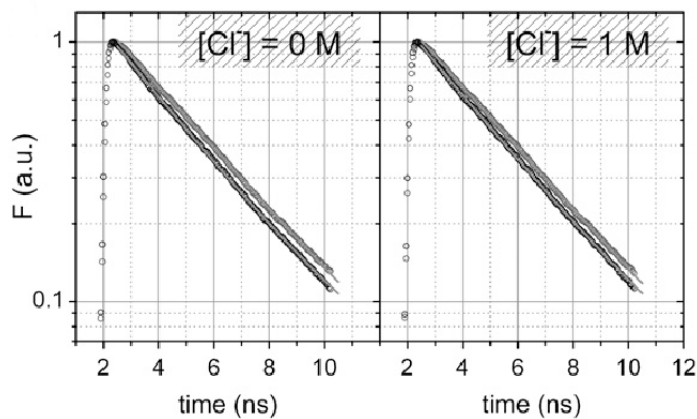


Figure 1.22: Fluorescence decay time at pH 7.4 (left) and 9.4 (right), with and without chloride. Static quenching effect is confirmed by the fact that chloride doesn't influence decay time, at any pH.[3]

The E²GFP chloride dissociation constant Kd^{Cl} is affected by pH, as reported in Figure 1.23: the strong interplay between H^+ and Cl^- binding causes a falling of E²GFP chloride affinity by more than three orders of magnitude in the pH range from 4.5 to 10.

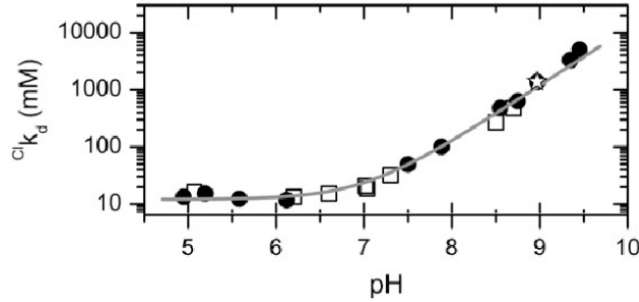


Figure 1.23: The change of the logarithm of chloride dissociation constant as function of pH is represented by the strong interplay between proton and chloride binding on E²GFP. Data reported are derived from fluorescence experiments (solid circles) and from absorption (open square).[3]

This strong interaction between pH and halogen-binding affinity has been described with a statistical thermodynamic model, accounting for just two interacting binding sites, one for the halogen and one for the proton[17]

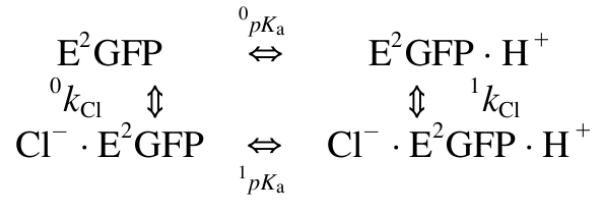


Figure 1.24: Thermodynamic model for E²GFP binding to proton H^+ or to chloride Cl^- , in a model where two distinct and specific binding sites are present on the protein[3]

In Figure 1.24 $^0K_{aCl}$ and $^1K_{aCl}$ are the association chloride constant to the unligated and proton-ligated E²GFP forms, while 0pK_a and 1pK_a are likewise the logarithm of the proton association constant to the unligated and chloride-ligated forms of E²GFP.

To estimate all the thermodynamic parameters of Model 1.24, chloride affinity dependence on pH was analyzed[3] over the entire pH-range of E²GFP stability (in Figure 1.23). This dependence is clearly characterized by only one plateau (at pH values lower than 6). It is therefore possible a precise estimation of only two of the independent thermodynamic constants in Scheme 1.24:

${}^0pK_a = 7.01 \pm 0.13$ for the proton binding in absence of chloride

$\frac{1}{{}^1K_{aCl}} = {}^1K_{dCl} = 12.1 \pm 0.1 \text{ mM}$ for the chloride binding at saturated proton conditions, i.e. acid pH)

The chloride dissociation constant in absence of proton (i.e. in basic conditions) results higher than 10^{44} mM and it is not well determined. Its extremely high value suggests a large coupling free-energy between chloride and proton.

Furthermore, the net number of proton exchanged upon chloride binding (as shown in Figure 1.25) suggests that at acid pH value (lower than 6.0) chloride binding is not associated with any proton exchange, while at basic pH (higher than 8.0) chloride binding is related to one proton binding.

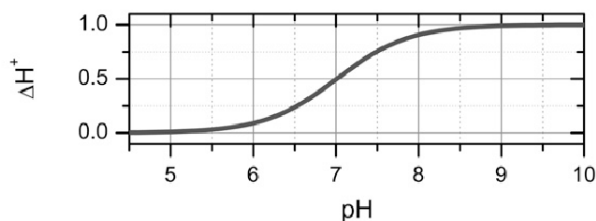


Figure 1.25: Net number of proton exchanged during chloride binding, according to data of Figure 1.23 on the facing page[3]

To summarize, chloride binding requires the presence of a proton. In acid pH conditions the protein is protonated, and chloride can be easily bounded, while at basic pH (i.e. absence of proton) the E²GFP chloride affinity is far lower.

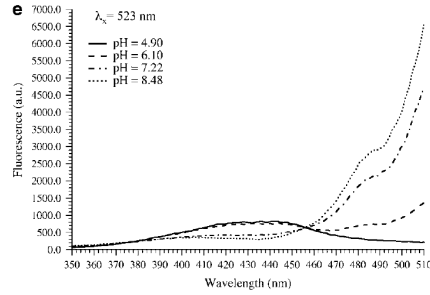
Moreover, E²GFP x-ray crystal structure analysis has revealed that the $E^2GFP + Cl^-$ complex structure is compatible only with the protonated protein form[3].

Fluorescence excitation spectra collected at various pH values clearly show intensity changes due to pH effects (Figure 1.26a). These changes can be described with a two-state protonation equilibrium, characterized by a $pK_a = 6.78 \pm 0.05$ [9] as reported in Figure 1.26b.

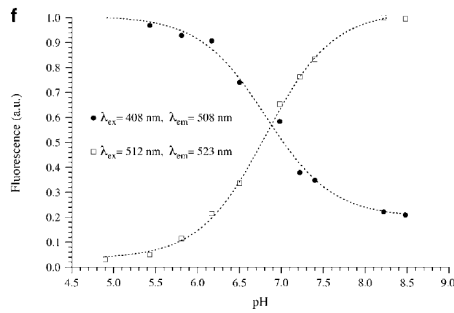
E²GFP fluorescence intensity is then very affected by pH, having a $pK_a \simeq 6.8$ well-within the physiological pH range. E²GFP pH-induced fluorescence

intensity variations can be exploited to precisely measure pH values in the physiological pH range.

The presence of an excitation wavelength whose associated green fluorescence emission is not affected by pH is extremely useful in ratio-imaging technique for pH and chloride concentration measurements. E²GFP has this pH-independent excitation at $\lambda_{\text{isobestic}} = 458 \text{ nm}$ [4, 9] and it is then able to independently measure pH and chloride concentration by ratio-imaging technique[4].



(a) Excitation spectra at different pH values (from 4.9 to 8.48) for emission fixed at 523 nm[9]



(b) Fluorescence intensity dependence upon pH for the protonated (solid circle) and deprotonated (open squares) form of E²GFP[9]

Figure 1.26: pH effect on intensity and shape of E²GFP excitation spectrum

Characterized by a $pK_a \simeq 7$ and the presence of the excitation isobestic point, E²GFP has the great advantage to be able to measure pH without necessity to add any other external probe (as instead was necessary with previous chloride biosensors[41, 49]). With the knowledge of the pH, it is then possible to calculate the correct chloride dissociation constant to be used to correctly estimate chloride concentration.

E²GFP x-ray crystal structure is similar to the YFP structure[79]. The phenol ring of residue Y203 is in face-to-face configuration $\pi-\pi$ stacking interaction with the chromophore plane. E²GFP specific mutations alter the chromophore

region, as shown in Figure 1.27 with the comparison of chromophore cavity structure for E²GFP and YFP:

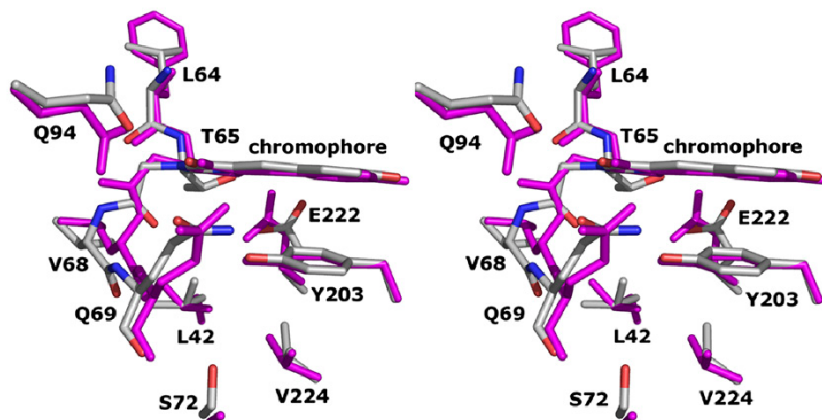


Figure 1.27: Stereo view of chromophore region of E²GFP and, in magenta, superimposition of YFP chromophore region.[3]

E²GFP is characterized by a high chloride affinity ($Kd_{Cl} \approx 12 - 15 \text{ mM}$ for pH range < 7.0), with also a relative high $pK_a \sim 7.0$. Its halogen affinity is linked to pK_a , with a progressive loss of chloride affinity when $pH \gtrsim pK_a$.

At physiological pH value ($pH \simeq 7.2$) E²GFP exhibits a chloride dissociation constant of $Kd \sim 35 \text{ mM}$, appropriate for precise chloride concentration intracellular measurements and similar to the improved variants of Clomeleon[49, 26] and YFP[24].

In contrast of all YFP-variants used in previous ratiometric chloride-sensitive biosensors[24, 26, 49], E²GFP is characterized by the ratiometric ability of sensing the environmental pH in a way independent from chloride concentration[9].

This pH-measurement ability is the great advantage of *ClopHensor*: the quantification of chloride concentration, whose binding is affected by pH, can now be performed over the actual pH value directly acquired by *ClopHensor* itself.

ClopHensor: principles of work Chloride ions sensitivity of YFP-variants *Clomeleon*, *SuperClomeleon*, *Cl-sensor*, *etc.* is strongly affected by pH. This double dependence complicates measurements analysis, being not possible to distinguish the two effect in order to obtain an absolute and independent chloride concentration measurement. A previous pH measurements is necessary, but all YFP-based biosensor are not able to perform this task, requiring then the use of a second pH-sensitive external probe.

This issue was solved with the introduction of *ClopHensor*[4], a new genetically-encoded fusion-protein able of simultaneous Cl^- and H^+ concentration measurements thanks to the particular spectroscopic characteristics of its sensitive component: a GFP-based fluorescent protein named E²GFP (previously described on page 23).

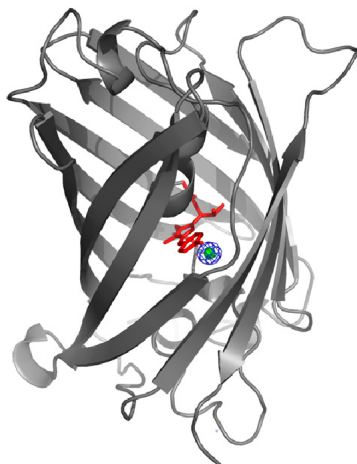
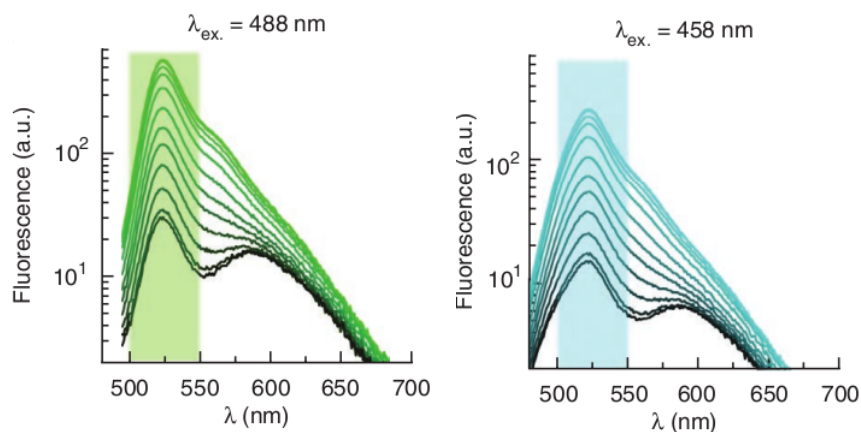


Figure 1.28: Ribbon representation of E²GFP with chloride ion (green sphere) inserted in the binding pocket near the chromophore (in red).[3]

When E²GFP is excited at its main excitation peak $\lambda_{exc,gfp} = 488\text{ nm}$ its emission fluorescence intensity is chloride sensible [4, 9] as reported in Figure 1.29a, but like all proteins of GFP family is at the same time also affected by pH[51].

To be able to measure chloride effect on fluorescence is necessary to avoid somehow this pH influence. With E²GFP it is possible to solve this issue exploiting its isosbestic point in excitation spectrum: when E²GFP is excited at this particular wavelength ($\lambda_{isosbestic} = 458\text{ nm}$, Figure 1.30) its emission intensity is constant and independent from pH variations[4, 9], being however chloride sensible (as shown in Figure 1.29b: fluorescence intensity is quenched by increasing chloride concentration as happens for Figure 1.29a).

Emission intensity of E²GFP is then affected by chloride and pH when it is excited at its main excitation peak $\lambda_{exc,gfp}$, while it is affected only by chloride when it is excited at its isosbestic wavelength $\lambda_{isosbestic}$.



(a) Emission spectra of *ClopHensor* upon excitation at 488 nm[4] (b) Emission spectra of *ClopHensor* upon excitation at 458 nm[4]

Figure 1.29: Emission spectra of *ClopHensor* upon excitation at 488 nm and 458 nm (Graph *a* and *b*): for both graphs chloride concentration varies from 0 mM (lightest-color line) to 1 M (darkest-color line) with consequent fluorescence intensity quenching. The shaded area stand for a graphic representation of the collected emission range used in microscopy acquisition with living cells. These spectra have been acquired at constant $pH = 6.9$: for graph *a* this is necessary (pH influences fluorescence intensity emission upon excitation at 488 nm) while in graph *b* pH wouldn't affect its spectra (they have been acquired for excitation at the isosbestic point).

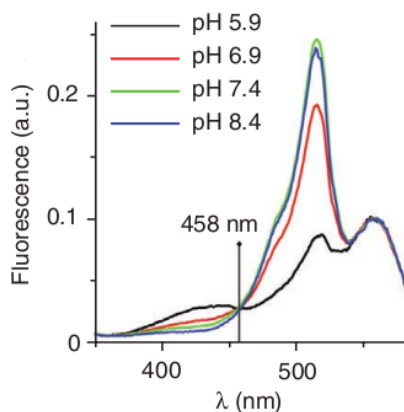
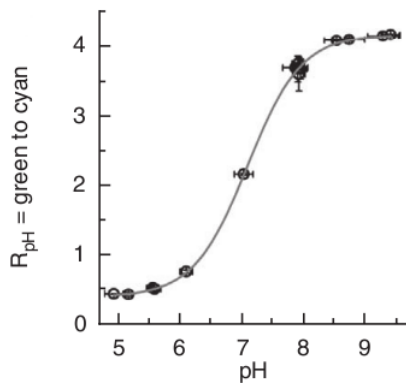


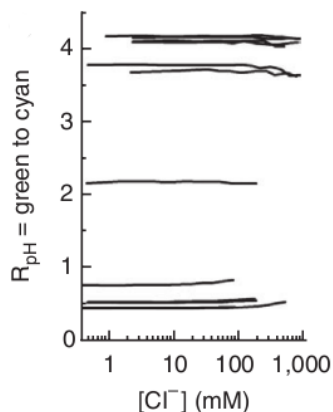
Figure 1.30: Excitation spectra of *ClopHensor* acquired at different pH values as indicated (for emission set at 590 nm). Note the presence of the capital isosbestic point at 458 nm.[4]

E^2GFP shows always the same chloride affinity regardless the excitation wavelength used[4], so the ratio between the emission intensity under excitation at main excitation peak and under excitation at isosbestic point wavelength is not affected by chloride (Figure 1.31b) but still sensible to pH (in Figure 1.31a).

This ratio is named “*ratio-pH*”.



(a) Ratio between the fluorescence intensity emission for excitation at 488 nm and at 458 nm, at various pH. A clear pH dependence is present, allowing the use of this ratio as a pH-indicator[4]



(b) Ratio between the fluorescence intensity emission for excitation at 488 nm and at 458 nm, at various $[Cl^-]$ for different pH. At any pH value this ratio is always not sensible to chloride concentration variations, it is always constant in spite of $[Cl^-]$ increase.[4]

Figure 1.31: Ratio between emission fluorescence for excitation at 488 nm and 458 nm: pH sensible while $[Cl^-]$ insensible

In-vivo pH sensitivity of E²GFP is characterized by a $pK_a = 6.8 \pm 0.05$ [4], falling in the physiological pH range (approximately from pH 6.7 to 7.5[12]). This characteristic donates to *ratio-pH* a very high pH sensitivity in this useful pH range.

The presence of an isosbestic excitation point is also necessary for chloride measurement: the ratio between green fluorescent emission upon excitation at the isosbestic point (signal sensible to chloride but not to pH) and DsRed emission for excitation at its main excitation wavelength $\lambda_{exc,red} = 543\text{nm}$ (signal independent both from chloride and pH[4]) is directly related to chloride concentration (in figure1.32).

This ratio is named “*ratio-Cl*”.

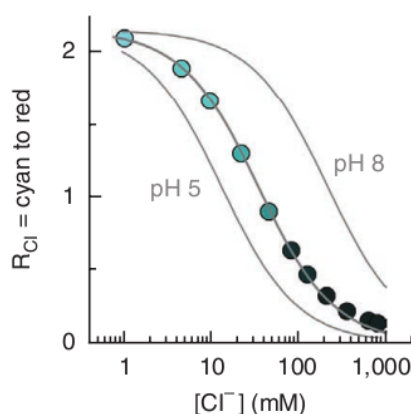


Figure 1.32: The ratio between E²GFP emission upon excitation at the isosbestic point and DsRed fluorescence is directly related to chloride concentration, but is also affected by pH[4]

E²GFP has a chloride sensitivity characterized by a $Kd^{Cl} \sim 35\text{mM}$ [3] (at $pH \simeq 7.2$, the physiological value), suitable to measure chloride concentration in physiological range (in cells in non-pathological conditions the chloride concentration is in the order of some milliMolar [4, 14]).

The accuracy and precision which characterize E²GFP pH and chloride readouts are obtained thanks to its particular pK_a and Kd^{Cl} values, both falling inside the physiological range of pH values and chloride concentration in cells.

The main drawback of *ClopHensor* is the dependence of its chloride sensitivity (expressed by Kd^{Cl}) to environmental pH value[3]: as consequence of cooperative proton and halide binding[3, 10], *ClopHensor* chloride dissociation

constant Kd drastically increases for $pH > pK_a$ of the chromophore, as clearly reported in Figure 1.33.

Unfortunately, E²GFP has a $pK_a = 7.01 \pm 0.01$ [3] falling well-within the the physiological pH range (from pH 6.7 to 7.5[12]), severely limiting the measurement robustness in case of even little pH shifts.

Before performing a chloride measurements, a previous pH estimation is then necessary in order to compute the correct Kd^{Cl} value at that particular pH.

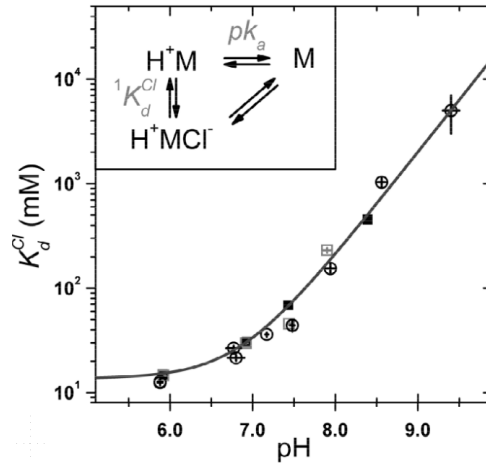


Figure 1.33: E²GFP chloride dissociation constant (Kd^{Cl}) dependence on pH, with spectrophotometer in vitro (solid square) and with confocal microscope in cells (open square and circle). In the inset is shown the chloride (Cl) and proton (H) binding scheme to E²GFP (M) in hypothesis of infinite cooperativeness.[4]

E²GFP is sensible to chloride but also to pH, so *ClopHensor* itself is able to measure both these parameters without needing any other external probes, but these operations require three excitation wavelengths: the excitation of E²GFP at its main excitation peak $\lambda_{exc,gfp}$, the second excitation at the isosbestic point wavelength $\lambda_{isosbestic}$, and the DsRed excitation $\lambda_{exc,red}$.

The necessity to use three excitation wavelengths requires a complicated microscope setup, expensive system with not-trivial alignment, optimization and maintenance. These issues are enhanced in the view of future applications with two-photon-excitation microscopy in deep live tissue imaging.

In this research E²GFP mutants are engineered, to remove pH dependence and allowing a direct chloride concentration measurements without the previous needing of a pH estimation. In this way the chloride measurements will require only two excitation wavelengths, meaning a cheaper and easier to maintain and optimize microscope setup.

Chapter 2

Goal of this project

This project aims to build a *ClopHensor*-based biosensor able to precisely measure chloride concentration in cells requiring ONLY TWO EXCITATION WAVELENGTHS (instead of three as *ClopHensor*).

The necessity to use three excitation wavelengths requires a complicated microscope setup, expensive system with not-trivial alignment, optimization and maintenance. These issues are enhanced in the view of future applications with two-photon-excitation microscopy in deep live tissue imaging.

Our efforts have been focused on improving the *ClopHensor* sensitive component by engineering and characterizing several E²GFP-mutants.

The perfect E²GFP-mutant must keep the E²GFP extraordinary ability to measure chloride concentration in cells (i.e. mutants with a $Kd^{Cl} \sim 3 \div 60 \text{ mM}$) with a readout no more sensitive to pH effects, at least in the physiological pH range (characteristic of GFP-mutants with $pK_a \gtrsim 8$).

Increasing pK_a of E²GFP-variants to values outside physiological pH range (i.e. to $pH \gtrsim 8$) is the way we've chosen to improve *ClopHensor*'s readout, stabilizing the Kd to its optimal value for a wide pH range (until $pH \sim pK_a$). In this context, even relatively large pH fluctuations around physiological $pH = 7.2$ would cause almost no deviations when recording chloride concentration.

Because of the low chloride transmembrane ratio and driving force (chloride reversal potential E_{Cl} is usually very close to the resting potential of the cells), reliable monitoring of intracellular chloride requires extremely sensitive biosensors[14].

Various E²GFP-mutants are here engineered and characterized, as possible candidates for an optimized version of *ClopHensor*, as described in the *Result* chapter.

Chloride affinity was obtained by analyzing changes in emission and excitation fluorescence intensity of GFPs in solutions at increased chloride concentrations for different pHs. The pK_a parameter was obtained analyzing fluorescence emission and absorbance spectra in buffers at different pHs without the presence of chloride.

Other relevant biophysical properties (folding fraction and brightness) of GFP mutants were measured, owing to their strong impact on in-vivo measurements.

For a fine thermodynamic description of the molecules a Van't Hoff analysis is also carried out.

These characterization experiments are all performed using multiplate reader and spectrofluorometer for a faster and accurate analysis.

Chapter 3

Materials & Methods

3.1 Materials

Bacterial culture growth

Prokaryotic cells for recombinant GFP-mutants expression were grown in LB medium

- **Luria Broth medium (LB medium)**

Bacto-Tryptone	10	g
Bacto-yeast extract	5	g
NaCl	10	g
ddH ₂ O	1	l

Add NaOH 5M to arrive pH7.

Autoclave at 15psi (1.05 Kg/cm²) at 120°C for 20 minutes to sterilize.

Add Ampicillin before use.

Protein purification

Protein purification from bacterial lysate was performed by FPLC (further described in Section 3.2.1 on page 42). Three different buffer are required for the purification process

- **Washing buffer (W buffer)**

Diethanolamine (DEA)	20	mM
Potassium sulfate (K ₂ SO ₄)	50	mM
ddH ₂ O	500	ml

Add protease inhibitor and adjust to pH 8.5 using sulfuric acid 30%
Filter with 0.22 μ m membrane filters.

- **Elution Buffer (E buffer)**

Washing buffer (W)	100	ml
d-Desthiobiotin	2.5	mM

Filter with 0.22 μ m membrane filters

- **Regeneration buffer (R buffer)**

Dilution of Strep-tag[®] regeneration buffer with HABA 10x (IBA, #2-1002-100) in ddH₂O water. Filter with 0.22 μ m membrane filters.

GFP fluorescence in-vitro titration

pH and chloride effects on GFP-mutants were in-vitro analyzed, diluting GFP-mutants in buffer at specific pH and chloride concentration.

The buffer ionic strength was always kept constant at $I = 1 M$. In buffer without chloride that halogen was replaced with the same molarity of sodium sulfate.

To adjust the pH value we used NaOH or sulfuric acid (H₂SO₄) 30%.

- **Buffer without chloride (Base buffer)**

pH < 5.5		
Acetic acid (H ₂ SO ₄)	50	mM
Sodium sulfate (Na ₂ SO ₄)	333	mM
ddH ₂ O	to 500	ml
5.5 < pH < 8		
Phosphate buffer	100	mM
Sodium sulfate (Na ₂ SO ₄)	333	mM
ddH ₂ O	to 500	ml
pH > 8		
Diethanolamine (DEA)	50	mM
Sodium sulfate (Na ₂ SO ₄)	333	mM
ddH ₂ O	to 500	ml

Table 3.1: Composition of buffers without chloride at different pH range

- **Buffer with chloride (Adding solution)**

pH < 5.5		
Acetic acid (H2SO4)	50	mM
Sodium chloride (NaCl)	1	M
ddH2O	to 500	ml
5.5 < pH < 8		
Phosphate buffer	100	mM
Sodium chloride (NaCl)	1	M
ddH2O	to 500	ml
pH > 8		
Diethanolamine (DEA)	50	mM
Sodium chloride (NaCl)	1	M
ddH2O	to 500	ml

Table 3.2: Composition of buffers with chloride at different pH range

GFP fluorescence in-cell titration

Cells were grown at 37°C and 5% CO₂ in medium DMEM complete (DMEM + 10% FBS + 4mM glutamine + 100unit penicillin and 0.1mg streptomycin).

Eukaryotic cells were transfected with Effectene (*Effectene transfection reagent, Qiagen, #301425*) following Effectene protocol. Standard protocols were optimized with the use of a double amount of DNA (i.e. 800 ng of DNA for cell cultured in 35mm Petri dishes).

To in-cell calibrate GFP-mutants, cells internal pH and chloride conditions were set with the use of ionophores (see further for details), equilibrating the cell conditions with those of the external buffer. External cell growth buffer was Hepes-based, with pH and [Cl] as desired.

Like in in-vitro experiment buffers (Table 3.1 on the preceding page), the ionic strength constant was kept constant. In buffer without chloride we replaced that halogen with the same molarity of sodium and potassium gluconate. pH was adjust by using NaOH or sulfuric acid 30%.

- **Buffer without chloride (Base buffer)**

Hepes	20	mM
Magnesium sulfate (MgSO ₄)	0.6	mM
Sodium gluconate	38	mM
Potassium gluconate	100	mM
ddH ₂ O	to 250	ml

- **Buffer without chloride (Base buffer)**

Hepes	20	mM
Magnesium sulfate (MgSO ₄)	0.6	mM
Sodium Chloride (NaCl)	138	mM
ddH ₂ O	to 250	ml

pH value have been adjusted with NaOH or sulfuric acid (H₂SO₄) 30%.

Ionophores

Ionophores are lipid-soluble molecule able to transport specific ions across the lipid bilayer of the cell membrane.

A mix of different ionophores was used:

- *Nigericin sodium salt* (N7143 Sigma-Aldrich): ionophore which disrupts membrane potential and stimulates ATPase activity in mitochondria. It's a efficient K⁺ carrier (K⁺ > Rb⁺ ≥ Cs⁺ >> Na⁺). Dissolved 10mg in 1ml CHCl₃.
- *Valinomycin* (V0627 Sigma-Aldrich): very efficient potassium ionophore. Insoluble in water, dissolve in MeOH (10mg in 1ml MeOH).
- *Carbonyl cyanide 3-chlorophenylhydrazone CCCP* (C2759 Sigma-Aldrich): H⁺ ionophore, inhibits the pH gradient and activated Cl⁻ uptake. Dissolve 100mg in 10ml MeOH.
- *Tributyltin chloride* (T50202 Sigma-Aldrich): used to replace halogens in organic compounds for hydrogen.

A ionophore stock 100x were prepared mixing all the ionophores as follows:

Nigericin	560	μl
Valinomycin	830	μl
CCCP	153	μl
Tributyltin Cl	4.3	μl
ddH ₂ O	to 15	ml

Prokaryotic and eukaryotic cells

- BL21(DE3) Competent Cells (*Agilent Technologies #200131*) are an all-purpose strain for high-level protein expression and easy induction. They were used for GFP-mutant production for in-vitro experiments.
- HEK293 (Human Embryonic Kidney 293 cells) are an immortalized cell line originally derived from human embryonic kidney cells grown in tissue culture. HEK 293 cells are very easy to grow and transfect and have been widely used in cell biology research. This cell line was used for in-cell calibration of GFP-mutant response to pH and chloride.
- NSC-34 (Mouse Motor Neuron-Like Hybrid cell) is a hybrid cell line, produced by fusion of motor neuron and embryonic mouse spinal cord cells with mouse neuroblastoma. These cells express many properties of motor neurons, including choline acetyltransferase, acetylcholine synthesis, storage and release and neurofilament triplet proteins. Therefore, these immortalized motor neuron-like cells are often used as a model for the investigation of neuronal function and differentiation.

3.2 Equipment

Several different equipment and instruments were required to perform a full and complete characterization of GFP mutants, specially focusing on spectroscopic and microscopic analysis.

3.2.1 Protein purification

After protein production by E.Coli, the GFP mutants were purified from bacterial clear lysate using a fast protein liquid chromatography ÄKTA-FPLC system (Pharmacia, GE Healthcare) .

Fast Protein Liquid Chromatography (FPLC)

Ion exchange is the most common FPLC strategy. A resin is chosen so that the protein of interest will bind to the resin by a charge interaction while in buffer W (the washing buffer) but become dissociated and return to solution in buffer E (the elution buffer).

A protein mixture (containing the one of interest) is dissolved in 100% buffer W and pumped into the resin column by ÄKTA pumps system. The protein of interest binds to the resin while all the other components are carried out in the buffer. The proportion of elution buffer E is gradually increased from 0% to 100% according to a programmed change in concentration (the "gradient"). At some point during this process the bounded proteins dissociates and appears in the effluent. The effluent passes through a detector which measure protein concentration (by absorption of ultraviolet light at a wavelength of 280nm). As the protein is eluted it appears in the effluent as a "peak" in protein concentration and can be collected for further use.



Figure 3.1: AKTA-FPLC system, with in evidence the several fraction collecting tubes

IBA Strep-Tactin column (*Strep-Tactin® Superflow® high capacity cart. H-PR, IBA #2-1234-001*)[1] was used. Its resin contains an engineered strep-

tavidin named Strep-Tactin. GFP-mutants were produced by bacteria directly with a special flag, the Strep-tag II, a short peptide (it contains just 8 amino acids WSHPQFEK, so it has a minimal effect on protein structure and function), which binds with high selectivity to Strep-Tactin present in the column. The Strep-tag II allows affinity chromatography under physiological conditions, enabling native, active Strep-tagged proteins to be purified in a single step.

The binding affinity of the Strep-tag II to Strep-Tactin ($Kd = 1\mu M$) is nearly 100 times higher than normal streptavidin.

After a short washing step, gentle elution of purified recombinant protein is performed by addition of low concentrations of d-desthiobiotin. D-desthiobiotin is a stable, reversibly binding analog of biotin, the natural ligand of streptavidin, so here is used as a competitor of Strep-tag II in binding the resin. After the complete elution, the column can be regenerated washing with R buffer (regeneration buffer) which contains HABA (4-hydroxyazobenzene-2-carboxylic acid), able to dissociate d-desthiobiotin from the resin.

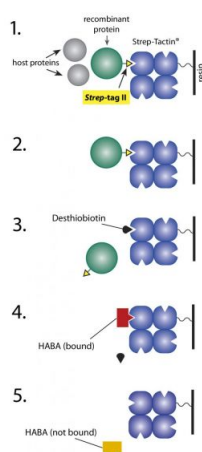


Figure 3.2: Purification steps in a Strep-tactin column: 1) host proteins and our recombinant protein pass through the column resins; 2) only the recombinant protein is retained by the resin thanks to the interaction of strep-tag with strep-tactin; 3) the elution buffer contains d-desthiobiotin, which detach the protein and can be collected; 4) desthiobiotin is removed using HABA in regeneration buffer 5) washing the resin with ddH₂O it's ready for a new purification

3.2.2 Spectroscopic analysis (in-vitro)

Fluorescence spectral characteristics of purified GFP mutants were analyzed with two different type of spectrofluorometer: an Enspire Multimodal Plate Reader (PerkinElmer) and a FluoroMax-4 (Horiba Scientific). Absorbance

spectra were acquired using spectrophotometer V-550 (Jasco inc.)

EnSpire Multimodal Plate Reader

The EnSpire Multimode Plate Reader is a high performance, compact and configurable instrument designed with quadmonochromators, top and bottom reading configuration and well scanning mode.

It's important to highlight the presence of four monochromators, two in excitation and two in emission, providing an optimal signal to noise ratio and improving confidence in results. Moreover it is extremely flexible due to its ability to select any wavelength necessary for excitation and emission, providing to the cleanest possible fluorescence signal.

EnSpire scanning capabilities saves time in acquiring fluorescence spectra in 96-well plates, making this instruments very suitable for spectroscopic characterization of a large number of GFP-mutant and for fast and precise pH-chloride titration experiments. Thanks to its easy-to-create protocol system, fluorescence acquisition protocol can be run automatically but the software, making unnecessary the continuous presence of the user.

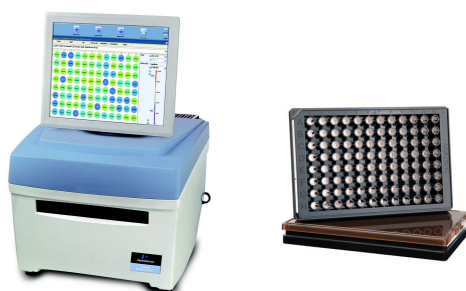


Figure 3.3: EnSpire Multimodal Plate Reader, with in evidence the touch screen during well-labeling procedure. For our experiment the standard 96-well plate black were used.

Epifluorescence configuration: EnSpire Multimode Plate Reader works in *epifluorescence* configuration, widely common in fluorescence spectroscopy-microscopy for biological sample. In this setup excitation light is focalized by an objective on the sample from above (or from under, if the system is *inverted*). Fluorescence emission light is collected from the same objective used for excitation, and is direct to the detector. Special filters (called Dichroic mirrors) are able to remove excitation light, allowing only emission signal to be detected.

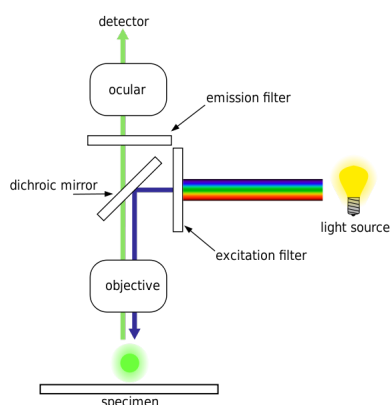


Figure 3.4: Epifluorescence configuration

FluoroMax-4

When the goal is obtaining high quality spectra, and the speed is not so critical, the best way is using a FluoroMax.

The source is a very stable and long-life Xenon lamp, enabling UV-VIS excitation. The two excitation and two emission monochromators assure a precise control in wavelength, and by its fast moving (up to 80nm/s) it's possible a fast spectra recording. The slits themselves are bilaterally, continuously adjustable from the computer in units of bandpass. This preserves maximum resolution and instant reproducibility of any spectrum. Emission detector electronics employ photon-counting for the ultimate in low-light-level detection.

90-degrees configuration: Fluorescence emission is most often measured at a right angle (90°) relative to the excitation light direction. This geometry is used in order to avoid interference of the transmitted excitation light, as happens when placing the detector in front of the excitation line (180°)[19].

This geometry is also very useful for a better signal-to-noise ratio: monochromators are not perfect, they transmit some stray light (light with other wavelengths than the targeted) and have a wavelength-independent transmission. When measuring at a 90° angle, only the light scattered by the sample causes this stray light resulting in a better signal-to-noise ratio and lowering the detection limit by approximately a factor 10000 [64] when compared to the 180° geometry.

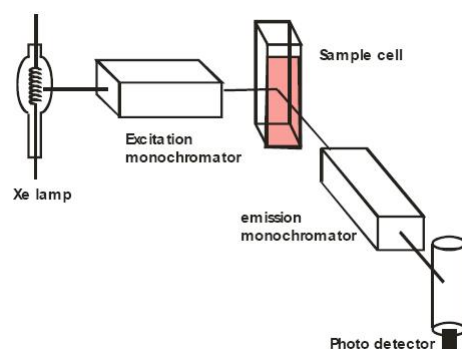


Figure 3.5: 90° angle fluorescence configuration

Spectrophotometer V550

The Jasco V550 UV/VIS spectrophotometer has a wavelength range of 190nm to 900nm provided by a deuterium lamp and a tungsten iodine lamp. The instrument is capable of absorbance measurements with wavelength scanning speed from 10nm/min, for high precision absorbance values, up to 4000nm/min for fast acquisition.



Figure 3.6: Spectrophotometer Jasco V550

3.2.3 Microscopic analysis (in-cell)

To analyze characteristics of GFP-mutants in cells, I used the iMic microscope (Till Photonics).

iMic microscope

iMic is a widefield microscope from Till Photonics, characterized by fast acquisition rate, filter-selected excitation and emission and fast z-stack acquisition. It is suitable for in-cell ratio-imaging pH and chloride analysis.

State-of-the-art fluorescence imaging requires a variety of peripheral equipment, highly sensitive cameras, fast stabilized light sources and special optical

features. The flexibility of the iMIC allows upgrading with additional modules and items to tailor the system according to specific applications.

- **Setup:** multi level systems designed with modular concept (Figure 3.7a on page 48)
- **Detector:** QImaging Retiga 2000DC CCD digital camera. for low-light fluorescence, high-dynamic-range and high-speed acquisitions. Characterized by 1600 x 1200 resolution, with pixel-size of 7.4 μm and QE 55% at 500nm (Figure 3.7b on page 48)
- **Objectives:**
 - Olympus UPlan FLN 10x / 0.30 Air
 - Olympus Plan-N 40x / 0.65 Air
 - Olympus Plan 100x / 1.25 Oil
- **Focus drive:** a lead screw for coarse focus (25 mm dive range with resolution less than 1 μm , with 2 mm/s speed) and a piezo crystal for fine focus (250 μm z-range with 50 nm resolution)
- **Illumination:**
 - *transmission:* a solid state monochromatic green LED, with a Long distance Phase contrast condenser NA 0.55;
 - *epifluorescence:* light source is a Oligochrome (Figure 3.7c on page 48), an ultra fast filter switching device with a fully digital high precision galvanometer driven mirror. Thanks to its 150W Xenon lamp can cover UV-VIS excitation wavelength range (from 320 nm to 700 nm) with continuously variable intensity control 0–100%. It can hosts up to 5 equally illuminated filter positions, switched in less the 3ms, and a light condenser ACT to avoid unnecessary waist of light.

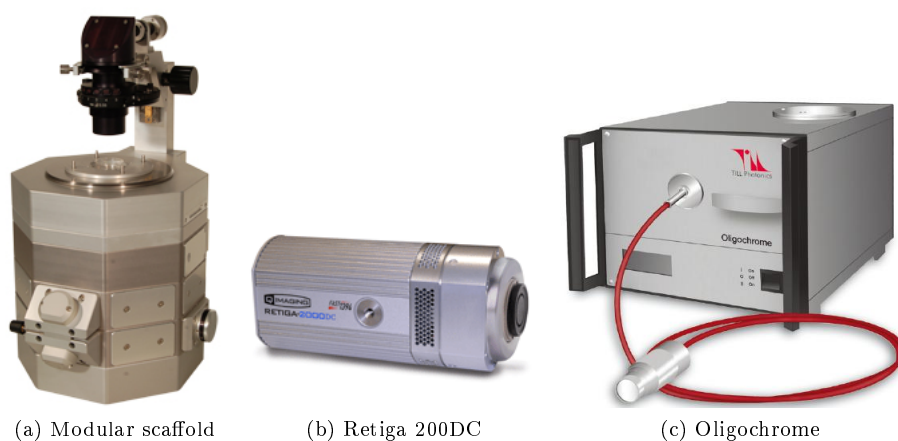


Figure 3.7: iMic equipment

- **x-y stage:** fully integrated stage, with mechanical travel x-y range of 25x25 mm, high resolution positioning (less than 1 μm) and fast moving (up to 7.5 mm/s)
- **Excitation filter-set:** the with light emitted by the Xenon lamp in the Oligochrome is filter with:
 - *ET 402/15x* (Chroma Technology Corporation) for generic blue fluorescent proteins excitation
 - *ET 415/20x* (Chroma Technology Corporation) for green fluorescent protein GFP-mutants
 - *ET 490/20x* (Chroma Technology Corporation) for green fluorescent protein GFP-mutants
 - *ET 543/35x* (Chroma Technology Corporation) for generic red fluorescent protein excitation
- **Dichroic mirrors:**
 - *69002bs* (Chroma Technology Corporation) for Dapi-Fitc-TxRed
 - *ZT442rdc* (Chroma Technology Corporation) with wavelength cut at 450nm, for GFP
 - *Di01 R488/561 25x36* (Semrock inc.) dual edge dichroic beamsplitter for simultaneous detection of GFP and red protein signal

- **Emission filter-set:** a fully automatic filterwheel is placed before the detector, hosting filters:
 - *FF01 520/15-25* (Semrock inc.) for GFP main emission peak
 - *FF01 498/20-25* (Semrock inc.) for emission isosbestic point in particular GFP mutants
 - *ET 460/36m* (Chroma Technology Corporation) for generic blue fluorescent proteins emission
 - *FF01 512/630-25* (Semrock inc.) dual band bandpass filter for simultaneous detection of GFP and red protein signal

3.3 Lab Protocols

3.3.1 In-vitro pH and chloride titration

To measure chloride and pH effect on protein, titration assays were carried out starting from two different solutions, prepared with buffer described in section 3.1 on page 38:

- *Adding solution:* at the pH and protein concentration I want to perform my experiment, with a chloride concentration of 1M
- *Base solution:* at exactly the same pH and protein concentration of previous Adding solution, but without chloride

In this way, when mixing the two solutions, there was not variation in pH and in protein concentration, only differences in chloride concentration affect fluorescence signal. It was possible to perform chloride titration at different pH values, to estimate the dependence of chloride affinity constant K_d with proton concentration in solution.

To measure the pH effect on fluorescence at a certain chloride concentration (usually it is performed in absence of chloride) this is simply done by preparing different samples of Base buffer, at different pH values, in which is present always the same protein concentration, so that the only free parameter is the proton concentration.

Fluorescence excitation and emission

To completely characterize a completely unknown fluorescent protein, even before analyzing its chloride affinity or pH dependence, it's necessary to know its excitation and emission properties.

As general rule, we performed the first emission spectrum fixing the excitation at 278nm (ultraviolet light), the excitation wavelength for the aromatic aminoacids present in the major part of fluorescent proteins. If some of these excited aromatic aminoacids are close to protein chromophore (as happens in GFP) they transfer part of their energy to cromophore, which gets excited and can then riemits light as fluorescence.

Even if this is not a direct excitation of the chromophore, this first spectrum is extremely important because we can detected the emission spectrum of our protein, and in particular we can know the exact emission wavelength.

With this knowledge we perform an excitation spectrum, fixing the correct emission wavelength, now related only to the chromophore properties.

Now the protein excitation peak is exactly known, so the last spectrum can be performed: an emission spectrum with excitation wavelength fixed no more at 278nm, but at the excitation peak as just discovered. In this way we are sure to excite directly the chromophore, without the mediating effect of aromatic aminoacids. The collected emission spectrum is thus directly related to protein fluorescence characteristics.

To sum up, three steps are crucial to characterize an unknown fluorescent protein:

Spectrum-A Exciting the protein at 278nm and recording the emission spectrum, to know the emission peak (Figure 3.8a on page 50)

Spectrum-C Performing an excitation spectrum with emission fixed at the main emission peak discovered in spectrum-A. Now we know the protein chromophore excitation peak (Figure 3.8c on page 50)

Spectrum-B Emission spectrum obtained fixing the excitation wavelength as just detected in spectrum-C. In case in spectrum-C are present more than one excitation peak, spectrum-B must be performed at each excitation wavelength (Figure 3.8b on page 50)

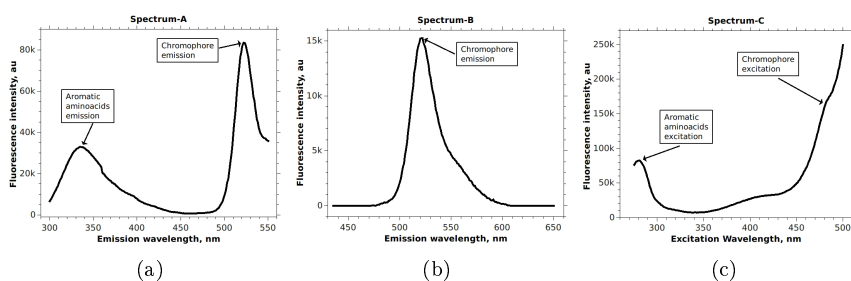


Figure 3.8: Spectroscopic characterization spectra

These spectral characteristics may vary with pH values.

Titration using FluoroMax-4

In the spectrofluorometer FluoroMax-4, the sample is only one quartz cuvette, so the titration is performed by subsequent adding of different volumes of Adding solution (V_{Add}) in the cuvette, containing at the beginning only Base solution (line #1).

As reported in Table 3.3 on page 51 and Table 3.4 on page 51, after each adding the spectroscopic analysis is performed at a different chloride concentration (C_{Final}):

#	V_{Initial} [μl]	C_{Initial} [mM]	V_{Add} [μl]	C_{Add} [mM]	V_{Final} [μl]	C_{Final} [mM]
1	1960	0.0	0	1000	1960	0.0
2	1960	0.0	2	-	1962	1.0
3	1962	1.0	2	-	1964	2.0
4	1964	2.0	5	-	1969	4.6
5	1969	4.6	10	-	1976	9.6
6	1976	9.6	15	-	1994	17.1
7	1994	17.1	20	-	2014	26.8
8	2014	26.8	30	-	2044	41.1
9	2044	41.1	50	-	2094	64.0
10	2094	64.0	100	-	2194	106.7
11	2194	106.7	200	-	2394	181
12	2394	181	400	-	2794	298
13	1500	298	400	-	1900	446
14	1900	446	500	-	2400	561
15	2400	561	500	-	2900	637
16	1500	637	500	-	2000	728
17	1000	728	1200	-	2200	876

Table 3.3: Chloride titration table, for subsequent adding in FluoroMax-4.

#	V_{Initial} [μl]	C_{Initial} [mM]	V_{Add} [μl]	C_{Add} [mM]	V_{Final} [μl]	C_{Final} [mM]
1	1900	0.0	0	1000	1900	0.0
2	1900	0.0	10	-	1910	5.2
3	1910	5.2	30	-	1940	20.6
4	1940	20.6	80	-	2020	60
5	2020	60	150	-	2170	125
6	2170	125	300	-	2470	130
7	2470	130	1000	-	3470	455
8	1470	455	1000	-	2470	675
9	0	675	2000	-	2000	1000

Table 3.4: Chloride titration table for faster properties screening.

Titration using Enspire Multimodal Plate Reader

Enspire can perform automatic analysis up to 96 different samples using the 96-well plates (OptiPlate-96, PerkinElmer). Each well contains E²GFP-mutant at different pH and chloride concentration, so its complete pH and chloride characterization can be carried out in a shorter time than with FluoroMax-4, with the same amount of materials.

In Table 3.5 is reported the typical chloride titration on each plate line

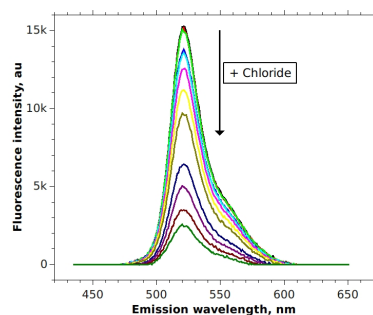
#	$V_{Initial}$ [μ l]	$C_{Initial}$ [mM]	V_{Add} [μ l]	C_{Add} [mM]	V_{Final} [μ l]	C_{Final} [mM]
1	150	0	0	1000	150	0.0
2	149	0	1	1000	150	6.7
3	148	0	2	1000	150	13.3
4	146	0	4	1000	150	27
5	144	0	6	1000	150	40
6	141	0	9	1000	150	60
7	137	0	13	1000	150	87
8	132	0	18	1000	150	120
9	110	0	40	1000	150	267
10	90	0	60	1000	150	400
11	50	0	100	1000	150	667
12	0	0	150	1000	150	1000

Table 3.5: Chloride titration table for Enspire.

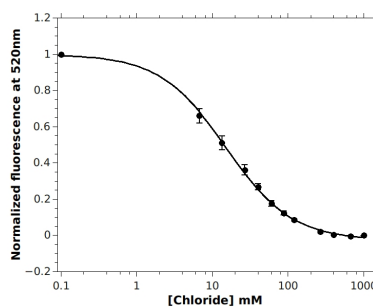
Fluorescence intensity analysis for chloride quantification

In presence of chloride ions GFP-mutants undergo static quenching: their fluorescence emission intensity is reduced, and this reduction is directly related to chloride concentration present in solution (Figure 3.9a).

In Figure 3.9b is reported this quenching effect on the emission intensity at 520nm for increasing chloride concentration.



(a)



(b)

Figure 3.9: Fluorescence intensity is reduced by increased chloride concentration

Data shown in Figure 3.9b can be fitted with equation [3]:

$$F = \frac{F_0 + F_1 \cdot \frac{[Cl]}{K_d}}{1 + \frac{[Cl]}{K_d}} \quad (3.1)$$

This equation, valid for a binding of protein:ions 1:1 as it is in our cases, relates the fluorescence intensity F with the chloride concentration present in the solution $[Cl]$ through the *chloride dissociation constant* K_d .

This constant represents the affinity of the protein for the chloride (the lower this K_d value is, the more sensitive to chloride the protein is). When in solution is present a chloride concentration exactly as the K_d the emission fluorescence intensity is half of the zero-chloride fluorescence intensity.

Values F_0 and F_1 are the fluorescence intensity at zero chloride concentration (the maximum intensity possible for that fluorophore) and at infinite chloride concentration (the lower intensity due to chloride quenching) respectively.

All fitting results are here indicated as *Average \pm Std.Error*.

Fluorescence intensity analysis for pH quantification

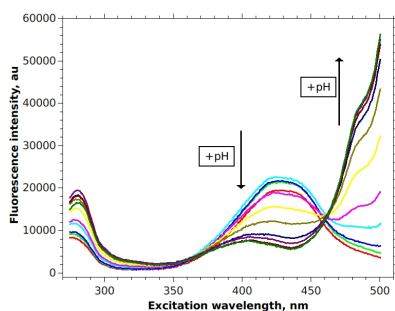
It is widely reported [3, 9] that GFP fluorescence intensity is strongly affected by pH value.

This effect is clearly visible in the example in Figure 3.10a, with the different excitation spectra at several pH values (from pH 5 to 9).

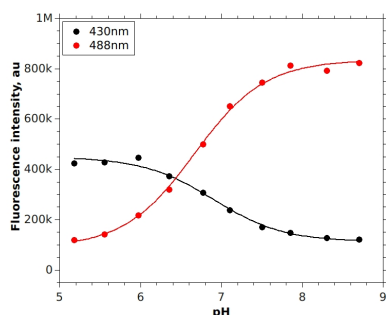
The intensity variations can be collected at any wavelength (as shown on Figure 3.10b) and they can be fitted with Equation 3.2

$$F = \frac{A_1 + A_2 \cdot 10^{(pK-pH)}}{1 + 10^{(pK-pH)}} \quad (3.2)$$

Constants A_1 and A_2 indicate the minimum and maximum values that fluorescence can reach (i.e. the two plateau visible in Figure 3.10b), F stands for the fluorescence intensity measured at certain pH , while pK is a constant value described as the pH values at which fluorescence intensity reaches the middle point between the two plateau. All fitting results are here indicated as *Average \pm Std.Error*.



(a)



(b)

Figure 3.10: Fluorescence intensity is affected by changes in pH values

Analysis of chloride affinity dependence to pH

The chloride dissociation constant K_d , describe in Section 3.3.1, is affected by pH values. GFP-mutant chloride affinity depends on the proton concentration in solution.

A typical behavior is shown in Figure 3.11: at acid pH values the chloride affinity is always constant at the value called K_d^1 , while at basic pH it increases significantly.

This data are analyzed with the Formula 3.3, relating the variations in chloride affinity with the environmental proton concentration; K_d^1 is the affinity constant at infinite high proton concentration (pH extremely acid), and indicates the affinity constant of the fully protonated GFP specie; the pH value at which the K_d is double than K_d^1 is named pK_a . All fitting results are here indicated as *Average \pm Std.Error*.

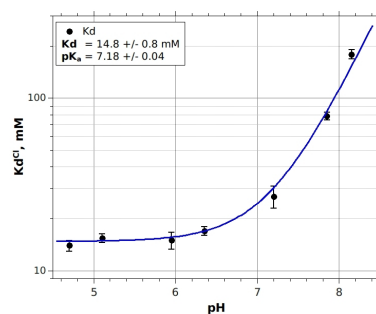


Figure 3.11: A typical variation of chloride affinity with pH

$$Kd = Kd^1 \frac{1 + 10^{(pK_a - pH)}}{10^{(pK_a - pH)}} \quad (3.3)$$

It is important to notice that, for pH higher than this pK value, the affinity constant increases continuously in an exponential trend.

3.3.2 In-cell experiment

To calibrate GFP-mutant response in cells at different pH and chloride concentration, cells internal pH and $[Cl^-]$ have been equilibrated to the external buffer conditions.

This equilibration have been obtained with the use of specific ionophores, organic molecules which increase the cell membrane permeability to some ions (Section 3.1 on page 40).

Equilibration medium have been prepared at desire pH and chloride concentration mixing properly the buffers described in Section 3.1 on page 39.

Set the desired pH and [Cl] conditions inside cells

Cell growth medium (DMEM complete) was removed, then cells were washed several times with sterile PBS before adding the equilibration medium (at desired pH and $[Cl^-]$).

After an incubation of 3 minutes, the medium was removed and new equilibration medium was added.

This procedure was repeated for 5 times, to assure pH and chloride conditions equilibration inside the cells.

During ratio-imaging acquisition, cells are always kept in this equilibration medium.

Neuron-like cells differentiation

NSC-34 is a hybrid cell line produced by fusion of neuroblastoma with mouse motoneuron-enriched primary spinal cord cells

Undifferentiated NSC-34 can be grown in standard complete DMEM medium (*DMEM +10% FBS +4mM glutamine +100unit penicillin and 0.1mg streptomycin*).

For their differentiation in neuron-like cells it is necessary to reduce the amount of FBS to 1% [45]. To complete differentiation process, the medium must never be changed for 5-7 days, just with addings of $1\mu M$ retinoic acid every 2 days. Retinoic acid is not strictly necessary for differentiation, but it induces¹ cells projection of longer processes (associated with axons) in spite of short ones (associated to dendrites).

Ratio-imaging acquisition protocol

Three channels are required in ratio-imaging acquisition:

1. pH and $[Cl^-]$ sensitive channel, obtained by green moiety emission
2. $[Cl^-]$ sensitive channel, but pH independent, obtain thanks to the isosbestic point of the green moiety
3. Reference channel, independent from pH and $[Cl^-]$, obtained by the red moiety

¹Personal experimental observation.

In the analysis further shown in *Result* chapter, each channel have been acquired at these conditions:

1. Excitation at 415/10 nm, emission at 520/20 nm, camera exposure time at 6000 milliseconds
2. Excitation at 415/10 nm, emission at 495/20 nm, camera exposure time at 6000 milliseconds
3. Excitation at 543/20 nm, emission with long pass filter LP 620 nm, camera exposure time 200 milliseconds

Ratio-imaging analysis protocol

Once the three channels have been acquired, the background must be subtracted for each image (may be different from image to image)

The brightest image, usually the red one, is then duplicated and it is converted in a mask.

Mask is a particular image elaboration with pixel intensity set at 1 or NaN (Not a Number): 1 for those pixels which, in the original image, had an intensity higher than a threshold, or NaN for those pixels whose intensity was below that threshold. The mask image is a schematic representation of what the software will consider “cell” (associated with 1) and what “background” (associated with NaN).

Mask image is multiplied, pixel by pixel, to all the three images. In this way the pixel intensities whose represented the cell signal are not modified (they are multiplied by 1) while the background is set to NaN, which will not be considered by software in doing any further operation.

From the ratio (pixel by pixel) between image 1) and 2) it is possible to obtain a cell map whose pixel intensity can be directly converted in pH values; from the ratio between image 2) and 3) it is possible to obtain a chloride concentration distribution map.

A previous calibration is required to perform this conversion.

Ratio-imaging: a theoretical view pH and [Cl] maps

A complex analyte:biosensor 1:1 has an equilibrium stoichiometry governed by the Grynkiewicz equation[4, 27]. For a generic ratiometric chloride probe Grynkiewicz equation can be written as:

$$[Cl^-] = Kd^{Cl} \cdot \left(\frac{R - R_{free}}{R_{bound} - R} \right) \cdot \left(\frac{S_{D,free}}{S_{D,bound}} \right) \quad (3.4)$$

In ratio imaging, the ratiometric value R stands for $R = \frac{S_N}{S_D}$, where S_N and S_D indicates the generic signal at the numerator and denominator of the ratio analysis, respectively.

In the specific case of *ClopHensor*, S_N is the fluorescence green emission signal at the isosbestic point (i.e. the signal which intensity is pH-independent, but always chloride sensible) while S_D is the red moiety emission signal (independent from pH and chloride).

Free and *Bound* indicates signal acquired in absence of chloride or in full chloride-bound conditions.

ClopHensor red moiety is DsRed, independent from chloride, so $S_{D,free} = S_{D,bound}$. Moreover, $S_{N,bound} = 0 \rightarrow R_{bound} = 0$ because E²GFP bound to chloride undergoes static quenching and it is not fluorescent.

R_{free} is the R plateau value in absence of chloride, R_{bound} the plateau for the full chloride-bound, while Kd^{Cl} indicates the chloride dissociation constant characteristic of that specific biosensor-variant.

Likewise, for a generic ratiometric pH probe, the Grynkiewicz equation is:

$$pH = pK_a + \log\left(\frac{R - R_A}{R_B - R}\right) + \log\left(\frac{S_{D,A}}{S_{D,B}}\right) \quad (3.5)$$

R_A and R_B are the R values in acid and basic conditions, respectively.

In the specific case of *ClopHensor* analysis, R is calculated using for S_N the fluorescence emission signal at the green main emission peak (signal pH and chloride dependent) and for S_D the fluorescence green emission signal at the isosbestic point (signal sensible only to chloride).

$S_{D,A}$ and $S_{D,B}$ stands for the isosbestic green fluorescence signal in acid or basic conditions, signal which is independent from pH, so $S_{D,A} = S_{D,B}$.

With the considerations above mentioned, equations 3.4 and 3.5 can be simplified as follow:

$$[Cl^-] = Kd^{Cl} \cdot \left(\frac{R_{free} - R}{R}\right) \quad (3.6)$$

$$pH = pK_a + \log\left(\frac{R - R_A}{R_B - R}\right) \quad (3.7)$$

For *ClopHensor*, chloride dissociation constant Kd^{Cl} is influenced by pH. This dependence is expressed by the equation[3, 32]:

$$Kd_{(pH)}^{Cl} = Kd_1^{Cl} \cdot \frac{1 + 10^{(pK_a - pH)}}{10^{(pK_a - pH)}} \quad (3.8)$$

Once known pK_a , and estimated pH in the region of interest, the corresponding $Kd_{(pH)}^{Cl}$ can be calculated with Equation 3.8. Kd_1^{Cl} is the chloride dissociation constant of the fully-protonated GFP-mutant form, experimentally determinate.

Chloride concentration values are calculated according to Equation

$$[Cl^-] = Kd_{(pH)}^{Cl} \cdot \left(\frac{R_{Cl}^0 - \alpha R_{Cl}}{\alpha R_{Cl}} \right) \quad (3.9)$$

where R_{Cl}^0 is a setup-dependent parameter which must be experimentally determined performing single measurements in absence of chloride (pH is indifferent).

α is the ratio between the excitation intensities at which the two images of each ratio-analysis have been acquired.

In conclusion, rewriting and simplifying Equations 3.7 and 3.9, it is possible to obtain the equations which calibration data have been fitted with:

$$\alpha R_{pH} = \frac{R_B + R_A \cdot 10^{(pK_a - pH)}}{1 + 10^{(pK_a - pH)}} \quad (3.10)$$

$$\alpha R_{Cl} = \frac{R_{Cl}^0}{1 + \frac{[Cl^-]}{Kd_{(pH)}^{Cl}}} \quad (3.11)$$

Chapter 4

Results

In this chapter the engineered E²GFP mutants are presented and their properties discussed with respect to their use in a new optimized version of ClopHensor, in place of the sensitive moiety E²GFP.

Each GFP-mutant here described was obtained by mutagenesis of E²GFP. Mutagenesis is a molecular biology techniques able to modify DNA sequence of proteins. It is possible to substitute a particular aminoacid of a precise position in the protein structure with another one of choice (*site-specific* mutagenesis) or performing the same substitution process in a random way, exploiting natural replication errors of specific polymerasis¹ (*random* mutagenesis). These new DNA plasmids are inserted in competent bacteria of the E.Coli family (BL21-de3) with “bacterial transformation” process. These bacteria easily accept and incorporate exogenous DNA (they are specifically engineered for this purpose). Bacteria naturally express proteins as contained in their genomic background, and then they also express exogenous DNA plasmid codifying for E²GFP mutants. Bacteria are then lysate by sonication, and E²GFP-mutants are purified and separated from all other bacterial proteins using affinity purification columns in FPLC (see Section 3.2.1 on page 42). Proteins so purified are ready to be used in all spectroscopic characterizations and analysis described in this chapter.

During spectroscopical characterization, particular attention was paid to chloride affinity and pH sensitivity: ideal chloride affinity would be $Kd^{Cl} \sim 3 \div 60 \text{ mM}$ to precise measure chloride concentration in cells, and pH independence should be assured by a $pK_a \gtrsim 8$.

¹Class of enzymes associated to polymerization of nucleic acids.

4.1 Site-specific mutants

High-resolution crystal structure of E²GFP (pdb code: 2o2b) was a valuable tool to study the protein structure and identify possible residues for rational site-specific mutagenesis.

Mutations were directed to preserve the chloride sensitivity typical of E²GFP, or if possible even to improve it in order to be more sensitive to smaller chloride concentration changes.

New mutants must also be less pH sensitive (at least in the physiological pH range), with a chloride affinity pH independent in that pH range. In this way a direct chloride measurement would be possible with the use of just two excitation wavelengths (instead of three as required by ClopHensor).

Each mutation had always a double effect, playing a role in modifying both proton affinity and chloride sensitivity at the same time. For each new mutant designed and purified, both pH effect (expressed by pK_a) and chloride affinity (by Kd^{Cl}) were analyzed and quantified.

4.1.1 Mutant V224L-E²GFP

E²GFP high-resolution crystal structure (pdb code: 2o2b) suggests further optimization of the chloride-sensing domain, in particular on the way to theoretically increase chloride sensitivity.

Figure 4.1 shows schematic representation of E²GFP chloride-binding cavity (volume $\approx 10 \text{ \AA}^3$; colored in orange) hosting the chloride atom. The same binding site also contains a single water molecule (colored in red) linked with an H-bond to the chloride (at distance 3.2 \AA).

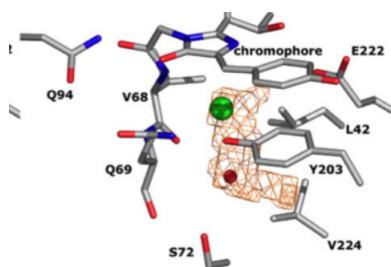


Figure 4.1: Representation of the chloride binding pocket derived from high-resolution crystal structure. Chloride ion and water molecule are represented as a green and red sphere, respectively, and V224 residue is well visible near the water molecule.

To understand the influence of this water molecule on chloride affinity, mutation V224L was designed. Solvent accessibility to the chloride binding cavity

will be reduced, without modifying the electrical charge distribution surrounding the chromophore.

Mutation V224L replaces VALINE² with LEUCINE³ in position 224. This substitution theoretically brings interesting effects on protein properties:

- LEUCINE-224 faces towards the water molecule, and with its longer side-chain (it has in its side-chain a $-\text{CH}_2$ group more than VALINE) leaves no more space for the water molecule to be hosted in the binding pocket. In this conditions only the chloride atom will be present near the chromophore. This characteristic is expected to increase chloride sensitivity, decreasing Kd .
- Both VALINE and LEUCINE present the same $-\text{CH}_3$ terminal group, in order to not alter the original E²GFP electrostatic distribution surrounding the chromophore. pK_a is expected to be the same as for E²GFP

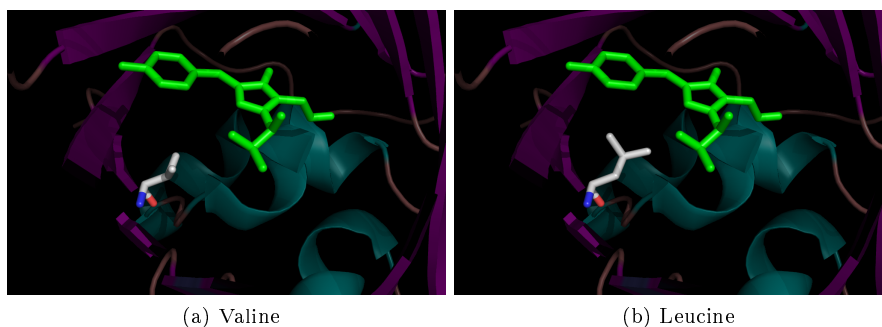


Figure 4.2: E²GFP structure, with highlighted the chromophore (in green) and the 224-residue (gray for carbon, red for oxygen, blue for nitrogen)

In-vitro characterization

Chloride dependence The longer side chain of the new aminoacid LEUCINE in position 224 should fill the chloride binding pocket, leaving enough space for the chloride insertion (for consequent quenching effect on chromophore) but preventing the presence of the water molecule.

To analyze chloride quenching effect on fluorescence intensity, emission spectra (under excitation at 430 nm) have been acquired at increasing chloride concentration, from 0 *mM* (upper black line) to 1000 *mM* (the lower line, in dark-green), to cover all the possible chloride concentration conditions in cells

²nonpolar, hydrophobic aminoacid

³an hydrophobic amino acid due to its aliphatic side chain. Longer than valine, it maintain the same electrical charge

(Figure 4.3). Each of these spectra were acquired at constant pH (=5.2, at this conditions chloride affinity is less influenced by pH) to avoid pH variation influence on chloride binding.

In figure 4.3 a significant fluorescence intensity decrease is visible already with low chloride concentration in solution, meaning this mutation has a strong positive effect on chloride binding affinity.

Chloride quenching effect for E²GFP (red dots) and V224L-mutant (black dots) at pH = 5.2 were compared (Figure 4.4). Each dot represents the normalized fluorescence emission intensity, measured at the main emission peak wavelength, at different chloride concentration present in solution.

This analysis revealed a significant improvement in chloride affinity: the V224L-mutant has $Kd^{Cl} = 1.2 \pm 0.2 \text{ mM}$, more then 10-fold lower than E²GFP ($Kd^{Cl} = 20 \pm 1 \text{ mM}$) at that pH value.

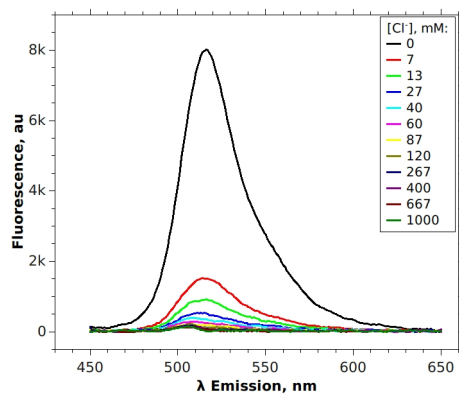


Figure 4.3: V224L-mutant emission spectra (excitation at 430 nm) at chloride concentration increasing from 0 *mM* (upper black line) to 1 *M* (lower dark green line) at pH=5.2

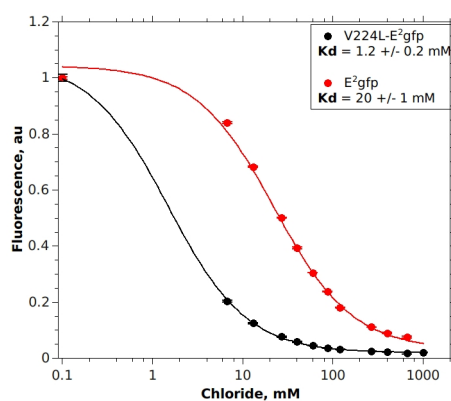


Figure 4.4: Comparison of fluorescence intensity quenching effect, at different chloride concentration, for V224L-E²GFP (black dots) and E²GFP (red dots) at pH=5.2

This very low chloride dissociation value is valid only at acid pH because this extreme chloride affinity is very pH dependent.

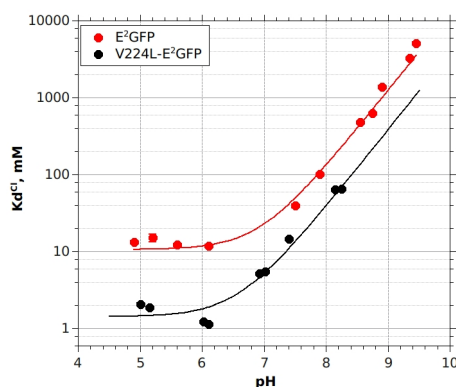


Figure 4.5: Chloride affinity at different pH values for V224L-E²GFP (black dots, $Kd = 1.2 \pm 0.2$ mM, $pK_a = 6.6 \pm 0.1$), compared with E²GFP (red dots, $Kd = 11.7 \pm 0.8$ mM, $pK_a = 7.1 \pm 0.2$)

This pH effect has been analyzed performing chloride titration experiments, as performed at $pH = 5.2$, also for different pHs.

Variation of Kd with pH is here reported in Figure 4.5: black points represent Kd^{V224L} , characterized by a constant $Kd = 1.2 \pm 0.2$ mM at acid pH values, and a sudden loss of chloride binding ability at higher pH values (this variation is fitted with Equation 3.1, resulting in a $pK_a = 6.6 \pm 0.1$).

V224L-E²GFP is then more sensitive to chloride, it is able to detect chloride concentration in solution far below the limit of E²GFP. V224L chloride affinity

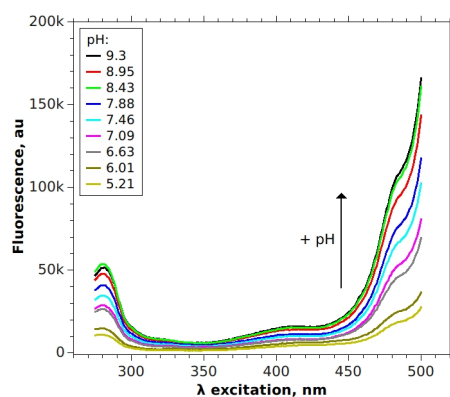
is anyway more dependent on the environmental pH: in the physiological pH range its Kd value is very dependent to pH fluctuations.

pH dependence In the previous section, the very high pH dependence of this new mutant was shown monitoring chloride affinity at different pH values. To have a complete view on pH effects on V224L-variant, its pH dependence has also been studied measuring the way pH affects excitation spectra.

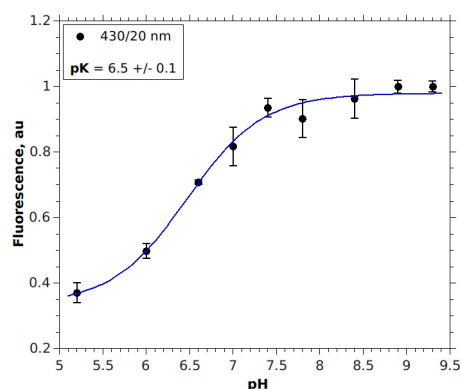
Excitation spectra (with emission wavelength fixed at 520 nm) have been acquired at different pH values, from acid pH (the first spectrum has been acquired at $pH = 5.2$) to very basic solution (until $pH = 9.3$) in order to cover the whole physiological pH range in cells[12].

A summary of these pH-titration spectra is shown in Figure 4.6a on the facing page: with the dark-yellow line representing the acid conditions, excitation spectra intensity always increases as pH increases in solution, arriving at very basic conditions with the black-line spectrum.

Fluorescence intensity is very pH dependent. The intensity in the band 420–440 nm at several pH values, and the strong influence of pH on fluorescence is clearly visible in Figure 4.6b. This influence is characterized by a $pK_a = 6.5 \pm 0.1$, result is in perfect agreement with pK_a previously obtained from chloride affinity pH dependence (see Section 4.1.1 on page 63).



(a) V224L-mutant excitation spectra (emission at 500 nm) in the pH range from 5.2 (dark-yellow line) to 9.3 (black line)



(b) Fluorescence intensity variations (analyzed in the fluorescent band 430/20 nm), at different pH values

Figure 4.6: pH effects on V224L-E²GFP excitation fluorescence intensities

The most important characteristic of these excitation spectra pH titration is the absence of an isobestic point: varying pH values, fluorescence intensity is never constant at any wavelength. To efficiently separate the effects of pH and chloride quenching during post-acquisition data analysis it is extremely useful the presence of an isobestic point.

Conclusions New aminoacid LEUCINE is longer than VALINE, and it fills deeper in the chloride binding pocket taking the space previously occupied by a water molecule. With this mutation, only the chloride ion is now present in the binding pocket near the chromophore.

The absence of this water molecule promotes the chloride insertion in the binding pocket, giving the protein a very high chloride sensitivity. Chlo-

ride affinity of V224L- variant ($Kd^{Cl} = 1.2 \pm 0.2 mM$) was improved by approximately one order of magnitude with respect to the E²GFP ($Kd^{Cl} = 15 \pm 0.2 mM$). This feature make V224L extremely sensitive to chloride concentration in very low chloride conditions.

As counterpart, VALINE substitution with LEUCINE affects proton affinity, lowering pK_a below 7. Indeed, chloride affinity is strongly affected by pH in the physiological pH range, small changes in pHs causes great variations in chloride affinity. A pH measurement is then always necessary before any chloride quantification analysis, as with E²GFP.

This mutant is also lacking in the isosbestic point in excitation, required to efficiently separate pH and chloride contribution on fluorescence signal variation. Missing the isosbestic point, V224L-mutant can not be used in ratio-imaging.

However, studying V224L-mutant, the importance of position 224 has arisen. Facing directly the chloride binding pocket in the proximity of the chromophore, aminoacid in position 224 plays an important role both for chloride affinity and for proton sensitivity.

Other 224-mutants will be engineered exploiting the two major variables position -224 offers: side-chain length for chloride affinity and aminoacid residual electrical charge for pH sensitivity.

4.1.2 Mutant V224Q-E²GFP

The residue at position 224 plays an important role in defining spectroscopic characteristics of GFPs. Position 224 faces directly the chloride binding pocket, very close to the chromophore.

As highlighted for mutant V224L (Section 4.1.1), the residue side chain length influences chloride affinity, removing the water molecule from the binding pocket and leaving space only for chloride ion. Considering the proximity of residue 224 to the chromophore, it is rational to infer the importance of electrical charge carried by aminoacid 224 in defining the chromophore dependence on proton concentration (i.e. the pH effects).

A new mutation was introduced in position 224. Side chain length and electrical charge of the new aminoacid was expected to increase chloride affinity (decreasing Kd value to milliMolar range) and decrease pH sensitivity (increasing pK_a to values higher than 8).

GLUTAMINE presents a side chain longer than VALINE and even longer than LEUCINE (mutant V224L described in Section 4.1.1) having two -CH₂ groups in its chain. GLUTAMINE presents also a positive electric charge. This effect should increase chromophore pK_a , making this protein pH insensitive in the physiological pH range.

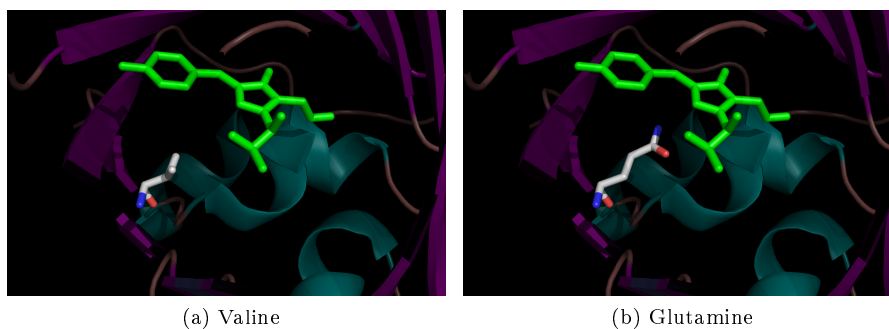


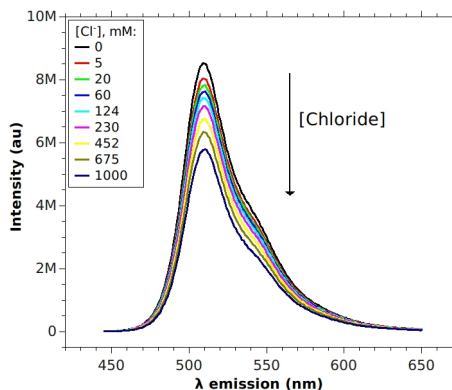
Figure 4.7: E²GFP structure, with highlighted the chromophore (in green) and the 224-residue (gray for carbon, red for oxygen, blue for nitrogen)

In-vitro characterization

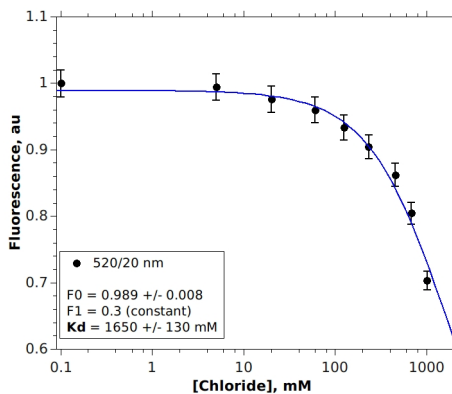
Chloride dependence Emission spectra, under excitation fixed at 425 nm, have been acquired at increasing chloride concentrations, from absence of chloride to 1000 mM, as already performed for V224L-mutant (Figure 4.8a).

A quantification of chloride affinity is reported in Figure 4.8b, analyzing fluorescence intensity at the main emission peak (520/20 nm) for each chlo-

ride concentration of Figure 4.8a. This mutant is characterized by a very low chloride sensitivity: with a $Kd^{Cl} = 1650 \pm 130 \text{ mM}$ at $\text{pH} = 7.2$ it is not appropriate to measure chloride concentration in living organisms⁴.



(a) Emission spectra (excitation at 425 nm) at increased chloride concentration from 0 mM (upper black line) to 1 M (lower blue line) at $\text{pH}=7.2$



(b) Fluorescence intensity decreases only at very high chloride concentration ($\text{pH}=7.2$)

Figure 4.8: Chloride quenching effect on emission spectra for V224Q-E²GFP

V224Q-mutant is sensitive to chloride only at very high ion concentration, but remarkably it is also insensitive to proton concentration (at least in the physiological pH range): its chloride dissociation constant remains pH independent until very basic pHs. This pH dependence is characterized by the very high $pK_a = 8.68 \pm 0.08$ (as reported in Figure 4.9, almost 2 pH-unit higher the E²GFP).

⁴There are no biological samples, physiological or pathological, with a chloride concentration in the working range of V224Q mutant

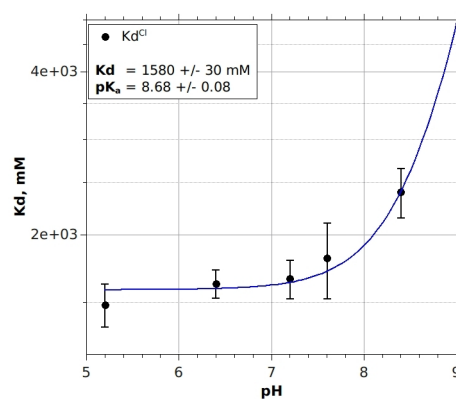


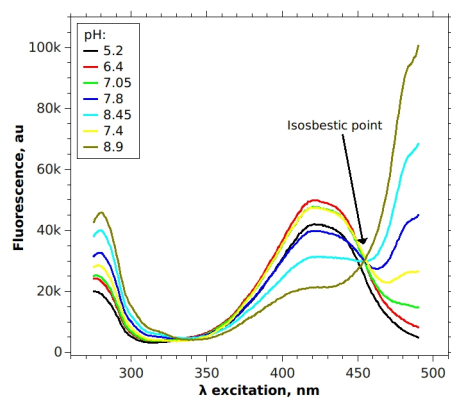
Figure 4.9: Chloride affinity of V224Q-mutant remains constant until very basic pH values

pH dependence V224Q-mutant excitation spectra (with emission fixed at 510 nm) have been performed at pH values from 5.2 to 8.9 (Figure 4.10a).

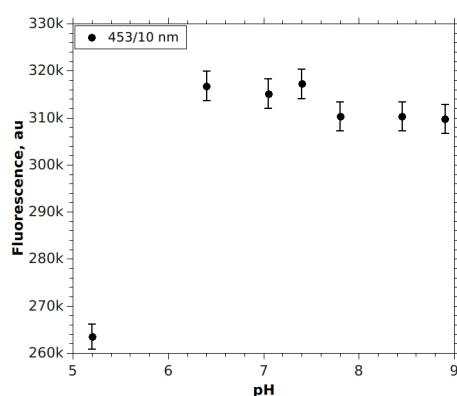
The first characteristic to be noticed is the presence of an isosbestic point at 453 nm (Figure 4.10b).

pH effects on excitation fluorescence intensity are reported in Figure 4.10c: analyzing pH dependence at wavelength shorter or longer the isosbestic point wavelength (453 nm) a $pK_a > 8$ is always obtained (8.1 ± 0.1 and 8.2 ± 0.3 , respectively), confirming its pH independence.

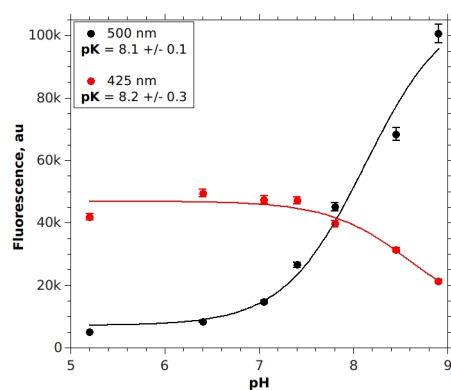
This results remark the importance of this position not only for its influence on chloride affinity, but also for proton affinity.



(a) Excitation spectra (for emission at 510 nm) performed at different pH values, from 5.2 (black line) to 8.9 (dark green line). To notice the presence of the isosbestic point, at 453 nm



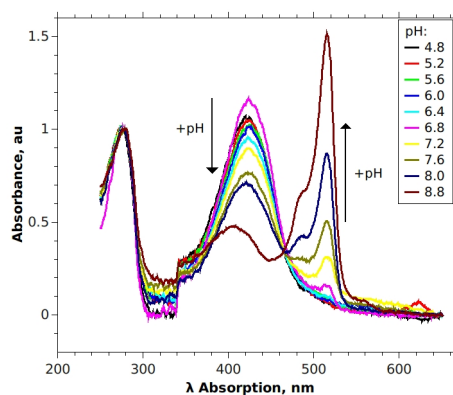
(b) Isosbestic band presence is confirmed at 453/10 nm



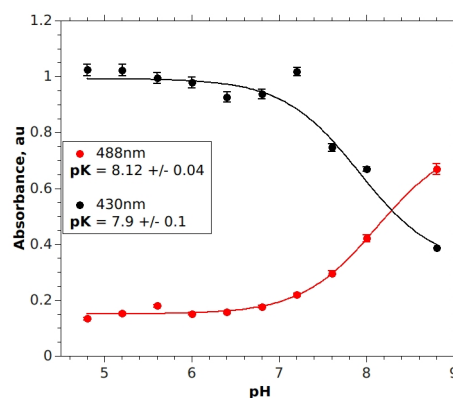
(c) Fluorescence intensity variations, from spectra in Figure 4.10a, analyzed at 425 nm and 500 nm. Both these positions are affected by pH at the same way, characterized by the same high pK_a

Figure 4.10: pH effect on V224Q-E²GFP fluorescence spectra

This basic pK_a values obtained from fluorescence analysis has also been confirmed by absorbance experiment.



(a) Absorption spectra at different pH values



(b) Absorption variations at two wavelengths for different pHs

Figure 4.11: pH effect on V224Q-E²GFP absorption spectra

In Figure 4.11a are reported the absorbance spectra for V224Q-mutant, acquired from $pH = 4.8$ (violet spectrum) to 8.8 (dark red spectrum): the isosbestic point presence is confirmed, and also the pK_a value higher than 8 (Figure 4.11b), consistent with what previously obtained.

Conclusion Mutant V224Q-E²GFP presents a very low sensitivity to chloride concentration: the long GLUTAMINE's chain obstructs the chloride entrance in the binding pocket, reducing drastically V224Q-mutant chloride affinity to the order of Molar. This mutant is then not useful as chloride biosensor in physiological conditions.

However, this mutation interestingly reduces proton affinity: the positive-

charge chain causes an increase of pK_a to values higher than 8 (starting from 7 for E²GFP) making this protein very pH-insensitive in physiological pH range. Moreover, the presence of isosbestic point in excitation is preserved.

Due to its very low chloride sensitivity, this mutant is not appropriate for my project, so no further analysis in-cells are performed.

4.1.3 Mutant V224N-E²GFP

Aminoacids in position 224 have shown their important role in modifying chloride affinity and pH sensitivity.

Facing directly inwards the chloride binding pocket entrance, aminoacid-224's side chain length influences chloride accessibility to binding pocket, strongly modulating the chloride dissociation constant K_d . Electrical charge of the residue position modifies electrical conditions surrounding the chromophore, leading to different pH sensitivity than original pK^{E2GFP} .

As described in section 4.1.2 on page 69, the long side chain of GLUTAMINE mutation in position 224 obstructs the chloride entrance in the binding pocket, reducing drastically V224Q-mutant chloride affinity.

ASPARAGINE has instead a side-chain shorter than GLUTAMINE and as long as VALIN, having just one -CH₂ group in its chain, so it should keep the same extremely high chloride sensitivity as the valine mutation V224L (Section 4.1.1) avoiding the obstruction problems of GLUTAMINE (V224Q, section 4.1.2).

The ASPARAGINE residual group is instead kept the same as GLUTAMINE: thanks to its -NH₂ group a positive end near the chromophore is presents, whose electrostatic effect should increase chromophore pK, as happened with V224Q (section 4.1.2), making this protein insensitive to pH in physiological range.

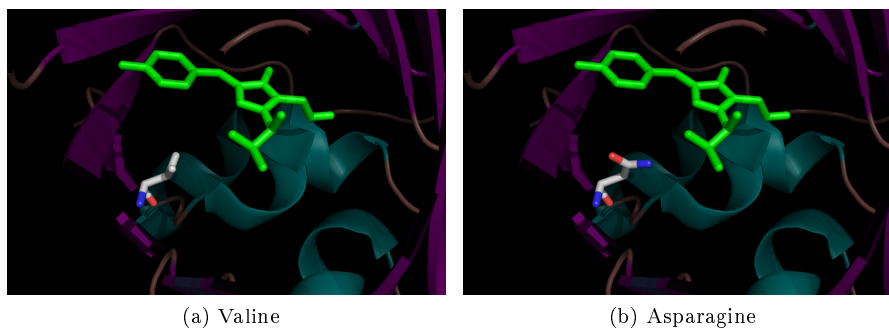


Figure 4.12: E²GFP structure, with highlighted the chromophore (in green) and the 224-residue (gray for carbon, red for oxygen, blue for nitrogen)

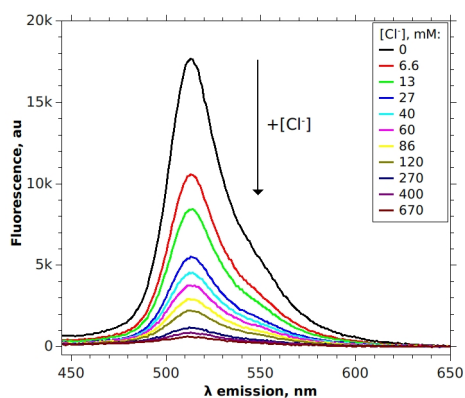
In-vitro characterization

Chloride Dependence Emission spectra have been acquired, upon excitation at 435 nm, at several chloride concentration.

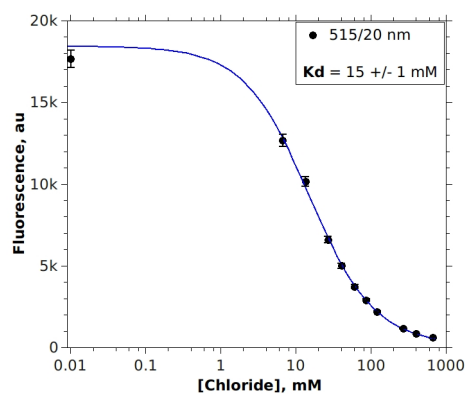
In Figure 4.13a is reported the chloride quenching effect on emission spectrum at $pH = 5.3$: emission intensity decreases as chloride concentration in

solution increases.

Intensity decreasing has been analyzed selecting the emission intensity at the main emission peak 515 nm (with bandwidth of 20 nm) for each chloride concentration. Resulting plot is reported in Figure 4.13b: chloride affinity of V224N-mutant is characterized by a $Kd^{Cl} = 15 \pm 1 \text{ mM}$. This value falls well-within the physiological chloride concentration in cells, giving this mutant an excellent chloride sensitivity in the physiological range.



(a) Emission spectra fluorescence intensity is reduced (excitation at 435 nm) due to increased chloride concentration: the highest intensity is emitted at absence of chloride in solution (black spectrum) while for higher $[Cl^-]$ (e.g. $c = 1 \text{ M}$ for dark-red spectrum) fluorescence intensity is strongly quenched and reduced ($pH=5.3$)



(b) Fluorescence intensity quenching (analyzed at 515/20 nm) for increasing chloride concentration in solution, at $pH = 5.3$

Figure 4.13: Chloride quenching effect on V224N-E²GFP emission fluorescence spectra

ASPARAGINE residual group has the same electrical charge of GLUTAMINE,

so it is rational to expect this V224N-mutant to have the same high pK than V224Q-mutant. V224N-mutant electric charge is however located not so close to the chromophore as it was with glutamine in V224Q-mutant (now the side-chain is shorter) and this may have effects on the way pH influences chloride sensitivity.

To study pH effect on chloride affinity, V224N-mutant chloride dissociation constant was analyzed at different pH values.

Results are reported in Figure 4.14: this mutant has a chloride affinity extremely dependent on pH, with a very acid $pK_a = 6.1 \pm 0.2$.

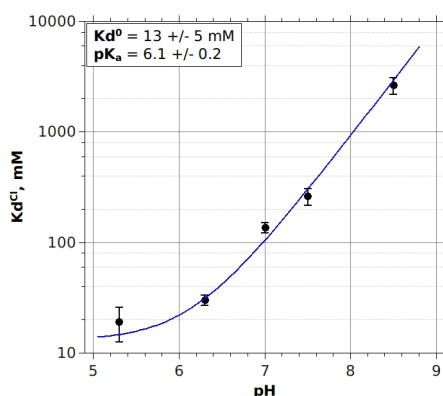
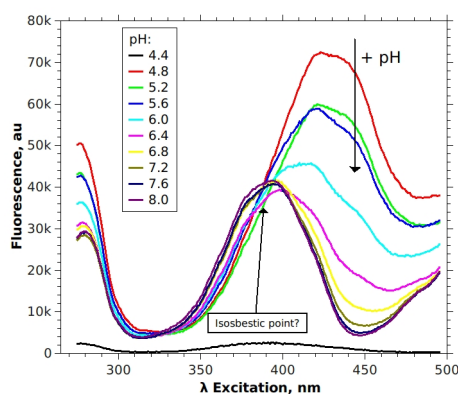


Figure 4.14: V224N-E²GFP chloride dissociation constant Kd is affected by pHs: in the physiological pH range even little pH changes causes drastic variations in Kd value

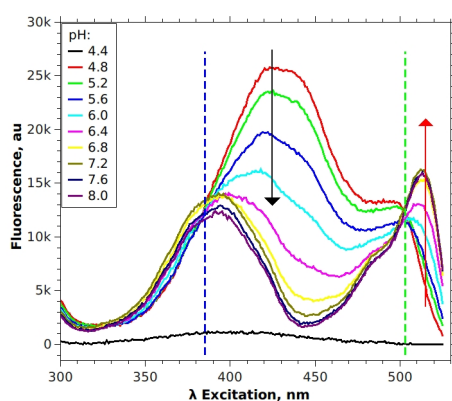
pH dependence As for previous mutants, pH dependence was characterized analyzing excitation spectra at different pH values (Figure 4.15a, emission fixed at 515 nm).

pH still affects fluorescence intensity, but the most abnormal characteristic is the presence of a not well defined isosbestic point at 385 nm (instead that at 460-470 nm as for all the other mutants).

To shed light on this unusual pH effect on excitation spectra, additional spectra were performed (Figure 4.15b) with emission wavelength at 545 nm. In this way it was possible to analyze excitation properties in spectral regions before prohibited due to overlap of zero-order Rayleigh scattering.



(a) Excitation spectra (for emission at 515 nm) at increasing pH values

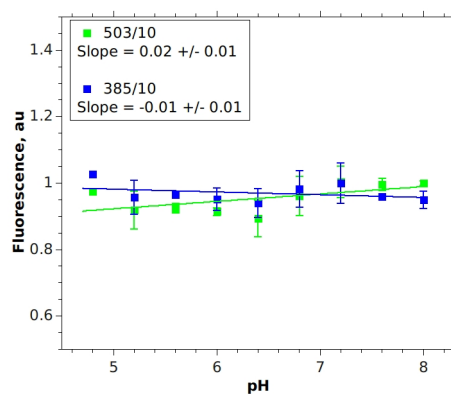


(b) Excitation spectra (for emission at 545 nm) at increasing pH values

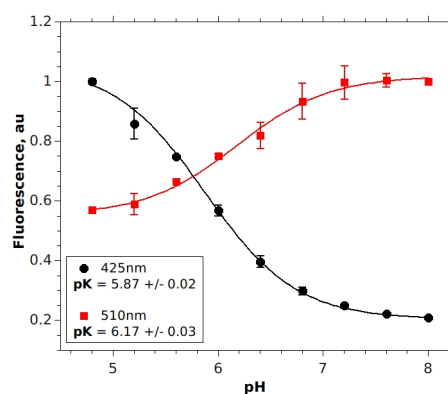
Figure 4.15: pH effect on V224N-E²GFP fluorescence spectra, increased from 4.8 (red spectrum) to 8.1 (wine spectrum).

In this extra spectral region a new isosbestic point appears at 503 nm, very red-shifted than “normal” wavelengths (around 460 nm), while confirming the presence the unusual blue isosbestic point at 385 nm. Analysis of these isosbestic wavelength intensities, with 10 nm bandwidth, confirms their pH-independence: in Figure 4.16a linear fits of fluorescence intensity versus pHs give slope values comparable to zero.

To characterize pH effect on excitation spectra, fluorescence intensity of Figure 4.16a has been analyzed at 425 nm and 510 nm (with 20 nm bandwidth).



(a) Fluorescence intensity at 385 nm and 503 nm is pH independent: V224N has two isosbestic points in excitation.



(b) Fluorescence intensities, here reported at different pH values, are highly affected by pHs

Figure 4.16: Analysis of pH effect on V224N-E²GFP fluorescence spectra

V224N-mutant fluorescence intensity is very pH sensible, characterized by a $pK \sim 6$ (Figure 4.16b), confirming the low pK obtained with previous chloride affinity experiments (Figure 4.14 on page 77).

Conclusions Aminoacid in position 224 is located near the chromophore and it faces right inwards the chloride binding pocket entrance. Its electrostatic charge and the steric effect of its side-chain have a direct influence on chloride affinity, proton affinity, and excitation spectra.

Aminoacids with a side-chain longer than VALINE (the original aminoacid -224 in E²GFP) like LEUCINE and ASPARAGINE (V224L and V224N mutants) increase chloride affinity: their longer side chains fill the binding pocket, leaving space only for the chloride ion, preventing water molecule entrance (in E²GFP a water molecule is present in the binding pocket together with the chloride

ion[3]). Aminoacid with a too long side chain, like GLUTAMINE (V224Q) instead obstruct the chloride entrance to the binding pocket, making the GFP-mutant chloride insensitive (K_d around Molar).

The electrical charge of aminoacids affects pH dependence of fluorescence. Replacing nonpolar aminoacid, like VALINE and LEUCINE, with positive-charged one like GLUTAMINE (V224Q) pK_a increases higher than 8, meaning the mutant is pH insensitive (in physiological pH range).

This electric effect is however mediated by the distance between the aminoacid residue and the chromophore. V224N-mutant has the positive-charged ASPARAGINE in position 224 (positive like GLUTAMINE), but more distant to the chromophore than GLUTAMINE would be: the results is a very pH-dependent GFP, with an acid pK_a around 6. Moreover, this positive-charged residue, placed at that particular intermediate distance from the chromophore, leads to very particular excitation spectra shapes, characterized by the presence of two isosbestic points at not-usual wavelengths.

4.1.4 Mutant L42H-V224L-E²GFP

Studying crystal protein structure and focusing on chloride binding pocket, also position 42 appeared interesting because it is located very close to the chromophore, and it is oriented towards the chloride binding pocket (see Figure 4.17).

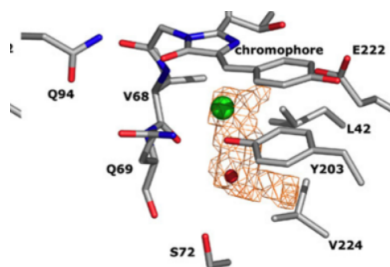


Figure 4.17: Representation of the chloride binding pocket from high resolution crystal structure. Chloride ion is represented as a green sphere

The rationale behind mutagenizing this position was to create an “electrostatic clamp” to attract chloride into the binding pocket, improving chloride affinity.

To achieve this task, the original nonpolar LEUCINE has been replaced with a basic HISTIDINE: the new positive electrostatic charge should attract the negative chloride ion near the chromophore.

The template used for this mutation was not the original E²GFP, but the variant V224L-E²GFP.

V224L-E²GFP (described in Section 4.1.1) is extremely chloride sensitive, and with this mutation it was predicted to reach even higher level of sensitivity.

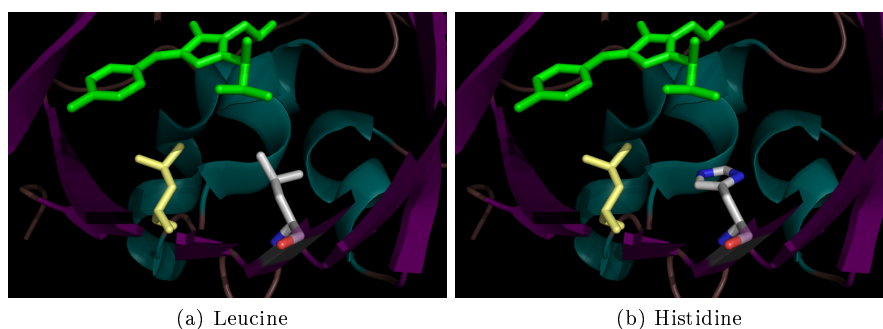
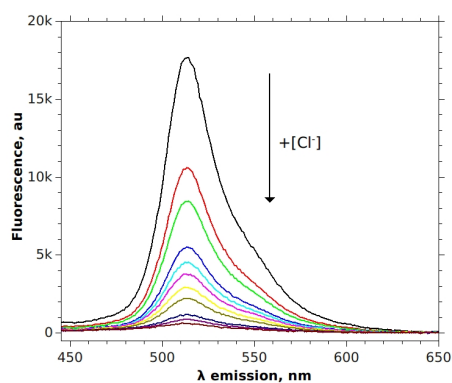


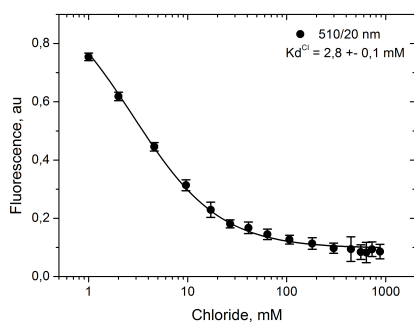
Figure 4.18: E²GFP structure, with highlighted the chromophore (in green), the leucine-224 (in yellow) and the 42-residue (gray for carbon, red for oxygen, blue for nitrogen)

In-vitro characterization

Chloride dependence L42H-V224L-mutant chloride dependence was studied following the standard procedure described for previous mutants, acquiring fluorescence spectra at increasing chloride concentration.



(a) L42H-V224L-E²GFP emission spectra (for excitation at 420 nm) at increased chloride concentration, from 0 mM (upper black line) to 1 M (lower dark-red line) at constant pH=5.2. Fluorescence spectra intensity decreases as chloride concentration is increased.



(b) Normalized fluorescence intensity measured at main emission peak (510/20 nm): the chloride quenching effect on fluorescence intensity is clearly visible as the chloride concentration increases.

Figure 4.19: Chloride quenching effect on L42H-V224L-E²GFP fluorescence intensity

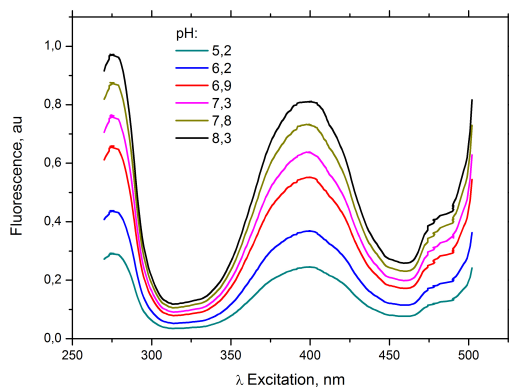
As reported in Figure 4.19, emission fluorescence spectra upon excitation at 420 nm are strongly quenched by chloride in solution. A very low Kd^{Cl} of 2.8 ± 0.1 mM (at pH=5.2) confirms this strong chloride affinity, almost one order of magnitude lower the E²GFP, but very similar to V224L-variant.

Electrostatic clamp doesn't seem to play a role, L42H-V224L-mutant is

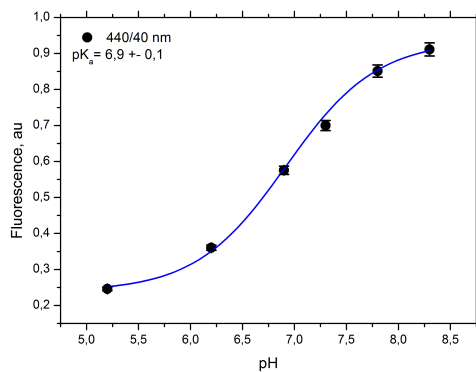
characterized by a very high chloride sensitivity, but still very similar to its template V224L-variant.

pH dependence Excitation spectra acquired at different pH values were analyzed to characterize L42H-V224L-mutant pH dependence, following protocol already applied to the other E²GFP-mutants

Resulting pH effect on fluorescence spectra are reported in Figure 4.20a. Fluorescence intensity variations analysis at the main excitation wavelength ($\lambda = 400/40\text{ nm}$), reported in Figure 4.20, results in an extremely low $pK_a = 6.9 \pm 0.1$. Moreover, like for its template V224L-E²GFP, also L42H-V224L-variant resulted without an isobestic point (Figure 4.20a).



(a) Excitation spectra (with emission fixed at 510 nm) from pH=5.2 (cyan line) to pH=8.2 (black line): fluorescence intensity is strongly pH dependent



(b) Main excitation peak ($\lambda = 400/40 \text{ nm}$) shows a marked fluorescence intensity variations at different pH values

Figure 4.20: pH effects on L42H-V224L-E²GFP excitation fluorescence

Also chloride affinity is then expected to be very dependent on pH. In order to check this dependence, chloride titration previously carried out at pH=5.2 has been performed in the range from pH=5.2 to pH=8.5.

L42H-V224L-mutant is characterized by a chloride affinity strongly dependent on pH. Analysis of this dependence returned a $pK_a^{Kd} = 6.91 \pm 0.08$, in perfect agreement with what obtained with pH titration on fluorescence intensity (Figure 4.20).

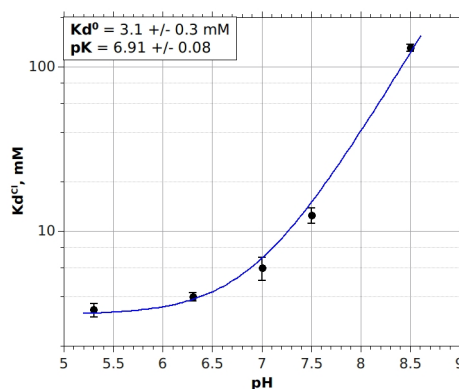


Figure 4.21: Chloride dissociation constant is affected by pH: L42H-V224L-mutant chloride affinity is strongly pH dependent in the physiological pH range ($6.8 < pH < 7.5$)

Conclusions Site-specific mutation L42H aims to create a positive electrostatic clamp to attract chloride ion (negative charged) near the chromophore, in order to improve E²GFP-mutant chloride affinity.

This task was not achieved. In fact chloride affinity resulted in the same range of the template V224L-E²GFP (less than 3 mM) so this mutation doesn't improve chloride sensitivity.

While not affecting chloride affinity, this new positive charge alters the normal electrostatic environment in the chromophore surroundings, modifying the way fluorescence is affected by pH: this GFP-variant fluorescence is very sensitive to proton concentration. Also its chloride dissociation constant is very sensitive to pH, making a pH estimation still necessary before any chloride measurement.

Another important drawback is the missing of excitation isosbestic point.

It is always more evident the strong interplay that aminoacid mutations have both on chloride affinity and on proton sensitivity (K_d and pK).

4.1.5 Mutant H148G-E²GFP

Beside protein crystal structure, an accurate literature screening has been performed, in order to obtain information and suggestion on specific mutations which can reduce pH sensitivity (i.e. GFP variants with $pK > 8$).

As reported in literature [13, 29] mutation H148G leads to an increase in protein pK_a to values 7.8.



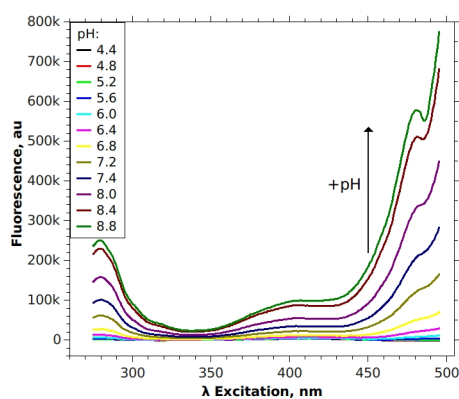
Figure 4.22: E²GFP structure, with highlighted the chromophore (in green) and the 148-residue (gray for carbon, red for oxygen, blue for nitrogen)

Its chloride sensitivity has never been tested, so in this section pH and chloride affinity are analyzed.

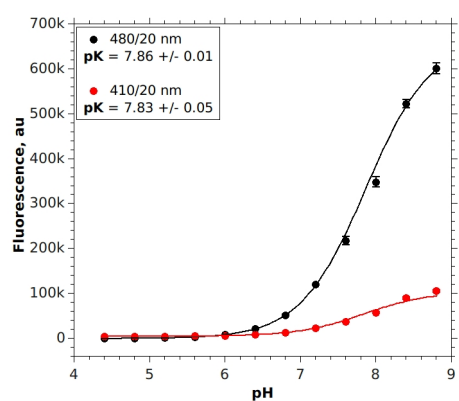
In-vitro characterization

pH titration To confirm predicted pK from literature, excitation spectra have been acquired as for all the other mutants, varying pH from 4.4 to 8.8 (emission wavelength fixed at $\lambda = 518 \text{ nm}$).

In Figure 4.23a is reported the clear pH effect on fluorescent spectra. Analyzing intensity variation at 410 nm and at 480 nm (Figure 4.23b) H148G-E²GFP is characterized by a $pK \simeq 7.85$, perfectly confirming literature results.



(a) Excitation spectra exhibit changes in intensities at different pH values, from acid (lower blue line, at $pH = 4.4$) to basic pH ($pH = 8.8$, green spectrum)

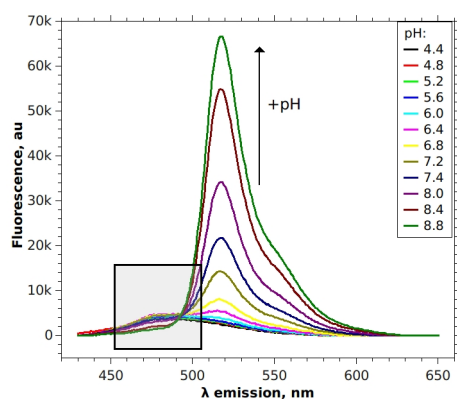


(b) pH effect quantification on fluorescence intensity at 410 nm and 480 nm

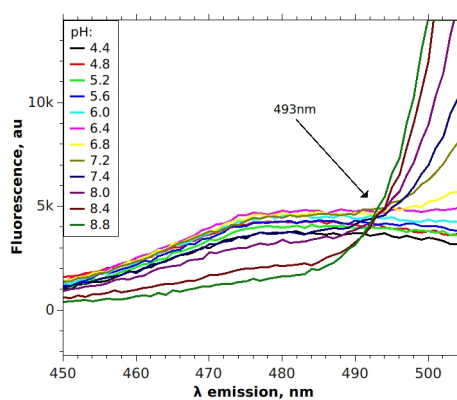
Figure 4.23: pH effect on H148G-E²GFP fluorescence intensities

Beside this improvement in proton sensitivity, mutation H148G carries a great drawback: excitation isosbestic point is lost.

H148G-mutant has however a reason to be highlighted, presenting an unexpected and intriguing characteristic. pH titration on emission spectra usually doesn't present notable characteristics, pH dependence obtained from those spectra is exactly what is observed in excitation spectra, providing no new information. Unexpectedly, for H148G-E²GFP an isosbestic point is present in emission at 493 nm (Figure 4.24, for excitation at 410 nm).



(a) H148G-E²GFP emission spectra show unusual isosbestic point

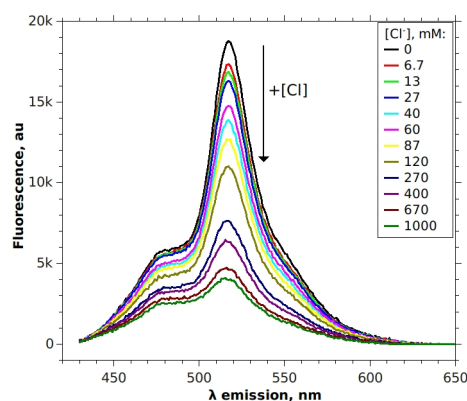


(b) Zoom on isosbestic point in Figure (a)

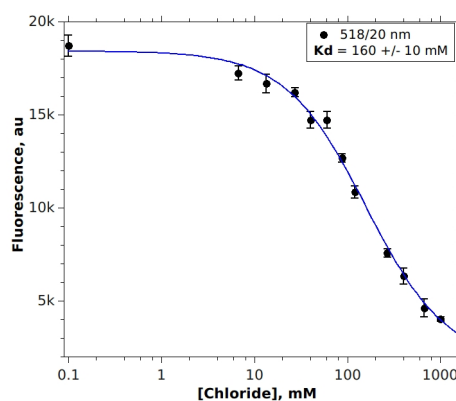
Figure 4.24: Emission isosbestic point in H148G-E²GFP

This isosbestic point is not clear, not well defined and with a very low intensity. However, this emission isosbestic point will be the key features of the most promising E²GFP-mutant so far engineered and characterized (further described in Section 4.1.6 on page 94).

Chloride titration Standard analysis already described was performed on emission spectra in order to characterize H148G-mutant chloride dissociation constant. Resulting emission spectra are reported in Figure 4.25a with evident the fluorescence intensity reduction due to chloride quenching effect. Dissociation constant governing this quenching was quantified in $Kd^{Cl} = 160 \pm 10 \text{ mM}$ (analyzing fluorescence quenching at 518/20 nm upon 410 nm excitation) in Figure 4.25b. With this high Kd value, this mutant is not appropriate to measure chloride concentration in physiological conditions.



(a) Fluorescence emission spectra at different chloride concentration, from 0 mM (black line) to 1 M (dark green line)



(b) Fluorescence intensity variations, at different chloride concentration, at main emission peak wavelength (518/20 nm)

Figure 4.25: Chloride effect on H148G-E²GFP fluorescence intensity, at physiological pH

An interesting information arises during comparison of K_d obtained analyzing emission isosbestic wavelength ($\lambda_{Isosb.} = 493/20\text{ nm}$) and main emission peak wavelength ($\lambda_{Peak} = 518/20\text{ nm}$).

As shown in Figure 4.26, also the emission isosbestic point is affected by chloride quenching in the same way as the main emission peak ($Kd_{518nm}^{Cl} = 160 \pm 10\text{ mM}$ and $Kd_{493nm}^{Cl} = 170 \pm 20\text{ mM}$).

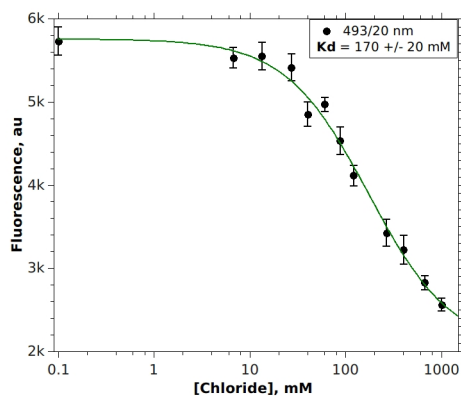


Figure 4.26: Fluorescence intensity of H148G-E²GFP, at increasing chloride concentration, analyzed at emission isosbestic point wavelength (493 nm)

To confirm the high pK value previously obtained from excitation spectra (Section 4.1.5), chloride affinity was measured at various pH values (Figure 4.27)

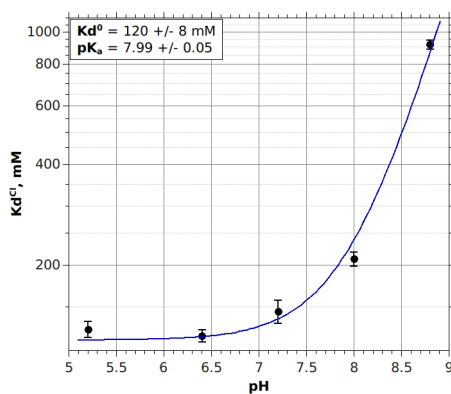


Figure 4.27: H148G-E²GFP chloride dissociation constant (K_d) depends on pH

pH dependence resulted in the high $pK_a = 7.99 \pm 0.05$, outside pH range of interest: in the physiological pH range K_d^{Cl} exhibits a very low pH influence.

Beside its notable high pK_a value, this mutants is not appropriate to measure physiological chloride concentration, being not enough chloride-sensitive for in-cells experiments.

Conclusions From literature review, position 148 plays a key role for reducing GFP dependence on pH. In particular, mutation H148G was reported to increase protein pK_a .

Analyzing pH effect both on fluorescence intensity and on chloride dissociation constant, $pK_a \simeq 7.9$ has been obtained. With this pK_a value, this mutant fluorescence can be considered pH independent (at least in physiological pH range).

Whether mutation H148G has a positive effect on pK_a , it has a negative influence on chloride affinity: at physiological pH this mutant has a $Kd^{Cl} = 160 \pm 10 \text{ mM}$, too high to assure a precise chloride measurement in physiological range.

This GFP-variant is not appropriate to be the next green moiety in ClopHensor, but one characteristic, never observed in all previous mutants, makes it very attractive and interesting: the presence of an isosbestic point in emission, separating two emission peaks influenced by pH in opposite way.

This phenomenon is called *dual emission* and is the key point to bring E²GFP-mutant to a next level.

In detail: Excited state proton transfer

As widely known in literature[50, 51], green fluorescent protein is the only fluorophore which, under excitation with either violet or blue light, gives a fluorescence signal centered at 515 nm.

Its absorption spectrum is bimodal, characterized by two absorption peaks: the main peak around 400 nm (violet) and a smaller one around 475 nm (blue).

The second peak corresponds to the anionic form of the chromophore, present at basic pH values (named “B”), which undergoes normal photophysical excitation-emission cycle.

The major peak corresponds to the neutral chromophore “A” present at acid pH, that would theoretically be expected to emit blue fluorescence (approximately at 450 nm) if excited with violet light.

However, when the neutral chromophore A is excited (becoming A*) the tyrosine residue becomes a strong acid: its proton is transferred (through hydrogen network) to the Glutamic Acid -222 and an anionic-like chromophore is created in an excited state “I*”. This process is named EXCITED STATE PROTON TRANSFER ESPT.

This anionic excited chromophore is responsible for the green emission at 515 nm, just like the normal emission from B*.

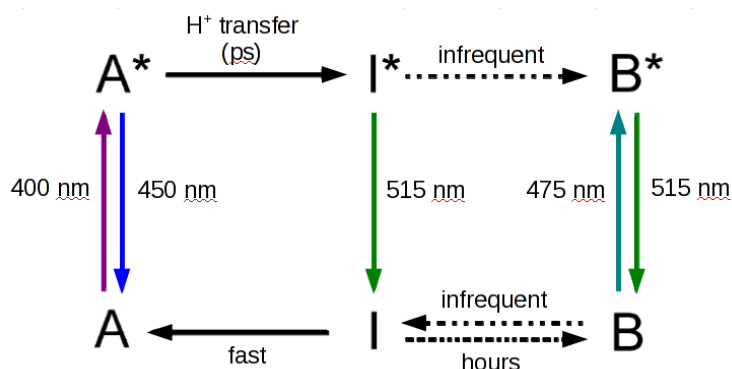


Figure 4.28: Excites State Proton Transfer [50]

Replacing the basic residue 148-Histidine, especially with a nonpolar aminoacid (like Glycine), the normal hydrogen network for proton transfer is altered. The proton acceptor in this case is not more Glutamic Acid -222, but it is this new 148 residue.

If proton transfer is somehow blocked, for example altering the normal hydrogen network, the neutral excited chromophore “A*” can not be converted in the anionic-like excited state “I*”. Direct deexcitation from “A*” to “A” state can then occurs, resulting in a fluorescent blue emission around 450 nm.

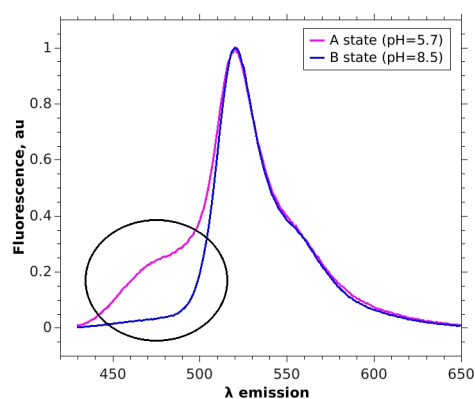


Figure 4.29: Emission spectra showing the different shapes caused by direct deexcitation from “A*” to “A” state (pink spectrum) when compared to a “normal” emission one (blue spectrum).

In conclusion, when position 148 is altered, GFP chromophore shows emission peak at two distinct blue and green wavelengths when excited with violet light.

4.1.6 The mutant: H148G-V224L-E²GFP

The goal of this project is to identify an E²GFP-mutant which keeps the E²GFP ability to measure chloride concentration in cells, but requiring only two excitation wavelengths. The first idea would be to avoid the pH estimation and perform directly the chloride concentration measurement. This task can be achieved engineering a E²GFP-mutant with high pK_a (higher than 8), so that its chloride affinity would be no more pH dependent (at least in the physiological pH range).

With the knowledge gained from all previous GFP-variants analysis, a particular E²GFP-double-mutant was engineered, combining (theoretically) appropriate chloride affinity (from V224L-mutant, section 4.1.1) with an alternative way to measure pH (thanks to the isosbestic point in emission of H148G-mutant, section 4.1.5).

- **V224L**: substitution in position 224 of a VALINE instead of the original LEUCINE creates an extremely chloride sensitive mutant, with a $Kd = 1.2\text{mM}$.⁵
- **H148G**: the presence of nonpolar GLYCINE in position 148, in place of basic HISTIDINE, is responsible for the *dual emission* of this mutant. *Dual emission* can be exploited to measure pH with one excitation line less than in original E²GFP.⁶

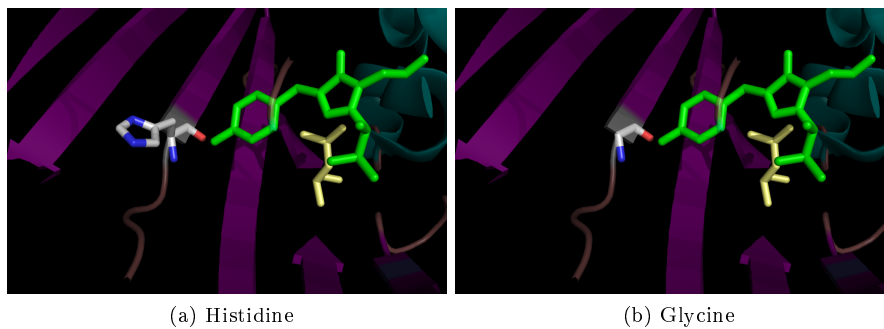


Figure 4.30: E²GFP structure, with highlighted the chromophore (in green), the leucine-224 (in yellow) and the 148-residue (gray for carbon, red for oxygen, blue for nitrogen)

⁵Detailed information on V224L-mutant can be found in section 4.1.1 on page 62

⁶H148G-mutant properties are described in detail in section 4.1.5 on page 86

In-vitro characterization

As already performed for the analysis of all the previous mutants, an in-vitro analysis was carried out to confirm chloride affinity and pH effect on this new mutant. Furthermore, other spectroscopic properties were analyzed for a full characterization.

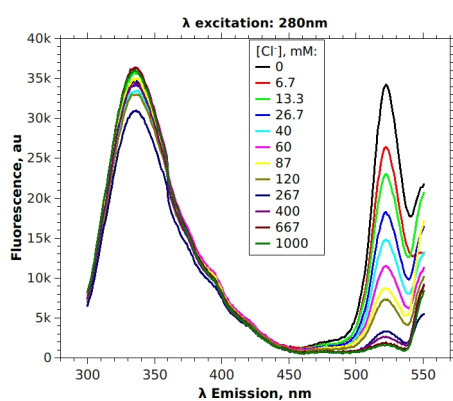
Chloride titration**At physiological pH**

Chloride quenching effect was analyzed acquiring fluorescence spectra at increasing chloride concentration (Figure 4.31).

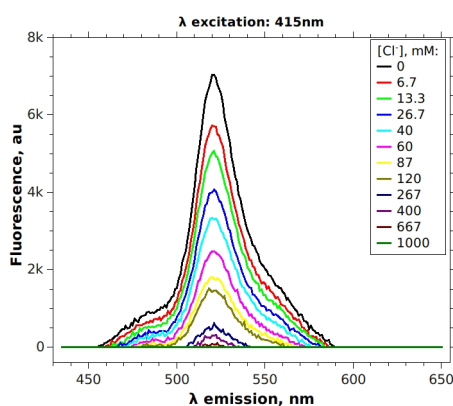
This quenching effect was analyzed in emission spectra upon excitation at 280 nm (Figure 4.31a) and at 415 nm (Figure 4.31b) and in excitation spectra with emission fixed at 515 nm (Figure 4.31c).

For each spectra of Figure 4.31 the spectral region analyzed is:

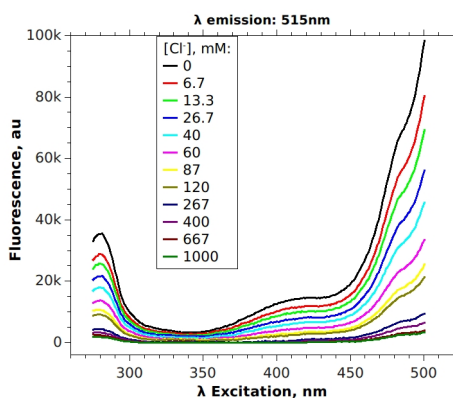
- In spectra 4.31a the area subtended by each curve from 505 nm to 525 nm
- In spectra 4.31b the area between 505 nm and 525 nm, being always an emission graph
- In spectra 4.31c the area subtended from 410 to 420 nm



(a) Emission spectrum for excitation at 280 nm



(b) Emission spectrum for excitation at 415 nm



(c) Excitation spectrum for emission at 515 nm

Figure 4.31: Fluorescence spectra of H148G-V224L-E²GFP at different chloride concentration: from 0mM (the black, highest spectrum) to 1M (the dark green, lower spectrum) at pH=7.2. It is clearly visible the decrease of fluorescence intensity at increasing chloride concentration.

For each spectra of Figure 4.31 the fluorescence intensities have been measured, normalized to their maximum value (corresponding to $[Cl^-] = 0 \text{ mM}$) and then averaged.

Result is shown in Figure 4.32: the resulting chloride dissociation constant is $Kd^{Cl} = 27 \pm 4 \text{ mM}$.

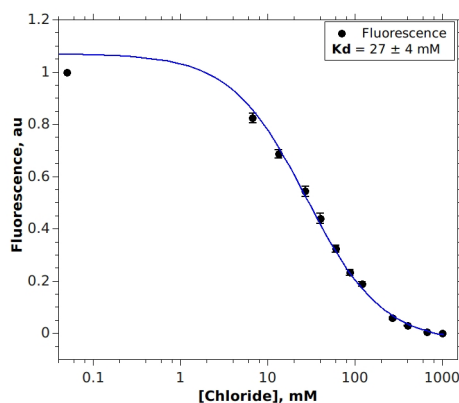


Figure 4.32: H148G-V224L-E²GFP normalized fluorescence intensity at increasing chloride concentration (constant $pH = 7.2$): the halogen quenching effect causes a fluorescence intensity decrease as the chloride concentration increases.

Chloride affinity at different pHs

Performing the same chloride titration previously described, but at different pH values (from 4.7 to 8.2) is possible to characterize Kd dependence on pH .

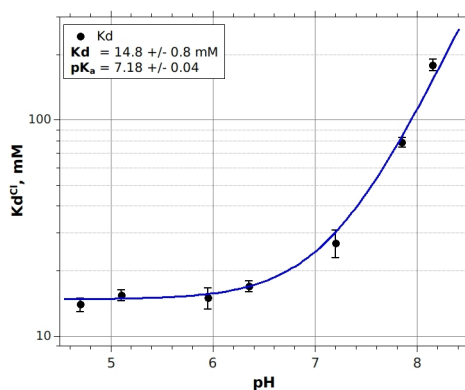


Figure 4.33: H148G-V224L-E²GFP chloride dissociation constant (Kd) depends on pH

As for ClopHensor, also this mutant shows an evident interplay between proton and chloride binding, resulting in a chloride dissociation constant very sensible to pH .

Using equation 3.8 on page 58 it is possible to estimate

- the chloride affinity for the fully protonated protein: $Kd^1 = 14.8 \pm 0.8 \text{ mM}$
- the pH value at which the Kd is double than Kd^1 : $pK_a = 7.18 \pm 0.04$

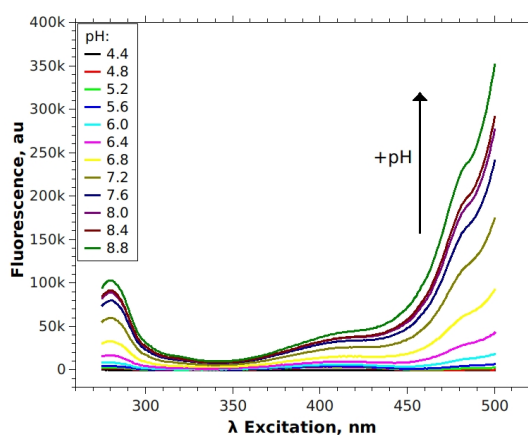
pH titration Fluorescence intensity of H148G-V224L-E²GFP is sensitive to pH . In 4.34a are visible different excitation spectra, for emission fixed at 520 nm, for pH value ranging from 4.4 to 8.8: it is not present any isosbestic point.

The peculiar characteristic of this mutant, which makes this GFP-variant so interesting and promising, is the presence of an isosbestic point in emission spectra, at 498 nm (Figure 4.34b).

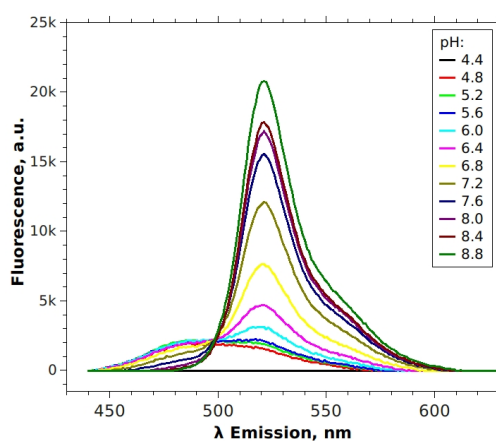
For excitation at 415 nm, in emission spectra are clearly presents two peaks⁷, subjected to pH influence with opposite trends:

- At 520 nm the main emission peak is present, increasing its intensity increasing the pH
- At 480 nm there is a second peak, not present in E²GFP, whose intensity decrease with pH

⁷The explanation of this phenomenon has been reported by McAnaney et al[50], and is detailed discussed in Section 4.1.5 on page 92



(a) Excitation spectra, the isosbestic point is missing



(b) Emission spectra, with an isosbestic point at 495 nm

Figure 4.34: Changes in H148G-V224L-E²GFP fluorescence intensity, for pH value ranging from 4.4 (black line) to 8.8 (green line), for excitation and emission spectra.

In Figure 4.35 the trend of the main emission peak intensity and of the isosbestic band are graphed: the first shows a remarked dependence from pH, while the second is constant, pH independent.

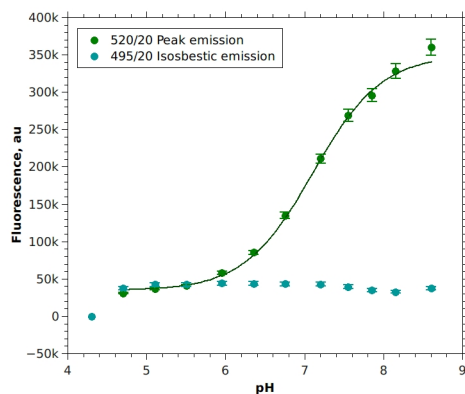


Figure 4.35: Different pH effect on main emission peak (green dots, pH sensitive) and on isosbestic band (cyan dots, pH insensitive) for H148G-V224L-E²GFP

Considering the position (central wavelength and bandwidth) of 520/20 nm for the main emission peak and of 495/20 nm for the isosbestic band, the two signals are perfectly separated and do not interfere one with each other.

Figure 4.36 shows a representation (on the emission graph already reported in Figure 4.34b) of the exact filter bands used to collect emission signal and isosbestic band.

Position of isosbestic emission band is also temperature dependent, so all these analysis were performed at $T = 37^{\circ}\text{C}$ to better reproduce the condition of future applications in live cells.

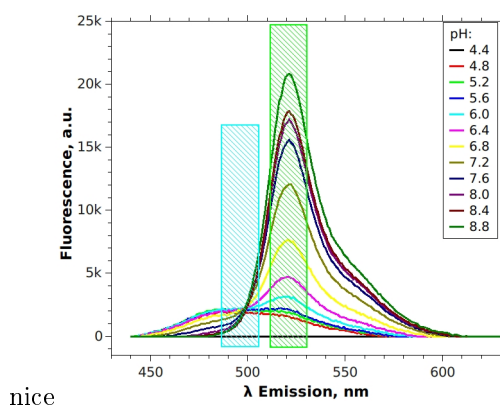


Figure 4.36: Graphics representation of filters used for pH analysis of H148G-V224L-E²GFP, on emission spectra at different pH

Because of different protein expression level from cell to cell, it is necessary to perform a ratio-analysis to avoid different protein concentration bias. Exploiting double emission shown by this mutant, the ratio was performed between the main emission peak signal (chloride and pH sensitive) and the isosbestic band (chloride sensitive, but pH insensitive).

The resulting ratio, at pH values from 4.6 to 8.8, is reported in Figure 4.37 and fitted with Equation 3.10.

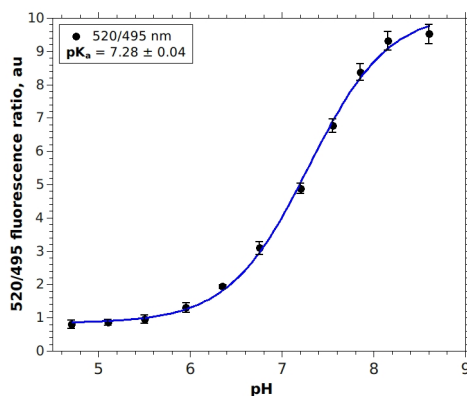


Figure 4.37: Ratio between H148G-V224L-E²GFP main emission peak and isosbestic band is sensible to pHs

The resulting pH dependence is characterized by $pK_a = 7.28 \pm 0.04$, and the two plateau are $A_1 = 10.2 \pm 0.2$ and $A_2 = 0.89 \pm 0.09$.

Some interesting features appears evident:

- with its pK_a falling well-within the physiological pH range, this mutant is appropriate to measure pH values in physiological conditions
- its wide dynamic range, almost 10 folds, assures an accurate pH estimation
- it is protein concentration independent (ratio-analysis)
- most important: this pH estimation requires ONLY ONE EXCITATION WAVELENGTH, and two emission filters

Another important and essential characteristic of this ratio-analysis to estimate pH is that this ratio 520/495 is chloride independent. As shown in Figure 4.38 this ratio remains constant for all the physiological chloride concentration range and for a wide range of pH values. In this way it is possible to estimate pH values without any previous-required knowledge on chloride concentration.

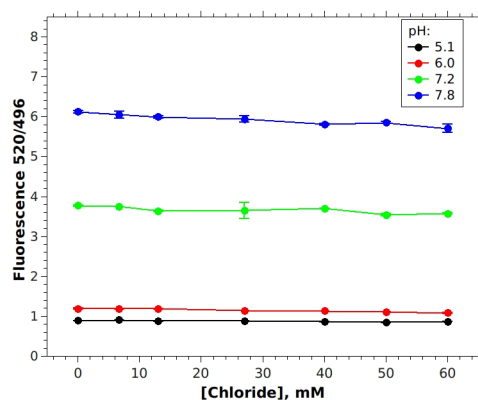


Figure 4.38: *Ratio-pH* 520/495 is independent from chloride concentration in a wide pH range

Chromophore active fraction A certain fraction of recombinant GFP variant may not show any fluorescence because of incomplete conversion of the chromophore. The concentration of GFP with intact chromophore can be determined by exploiting the absorbance characteristics of the base-denatured chromophore. The two typical GFP absorbance peaks in the range 250-520 nm are converted into a single peak at 447 nm when the protein is denaturated in 0,1M NaOH.

Figure 4.39 shows the two absorption spectra necessary for this analysis:

- in black line the spectrum of native-state mutant, with the absorption peak at 278 nm used to determine the protein concentration, and the other two peaks for the neutral and anionic species present in solution.
- in red line the absorption spectrum of the denaturated protein, with an absorption peak at 447 nm.

Knowing the absorption coefficient ϵ at those particular wavelength it is possible to evaluate the total protein concentration (using absorption at 278 nm) and chromophore concentration (with absorption at 447 nm).

From these spectra the intact chromophore fraction for the H148G-V224L-E²GFP results 97%.

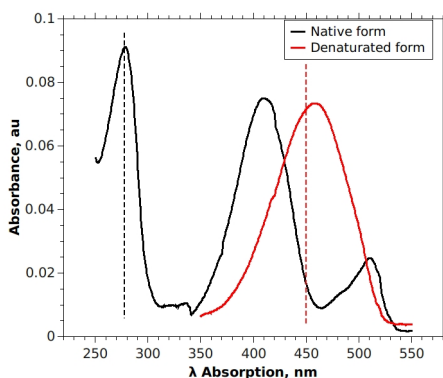


Figure 4.39: Absorbance spectra for native (black line) and base-denatured (red line) H148G-V224L-E²GFP, with highlighted the two wavelength necessary for the analysis

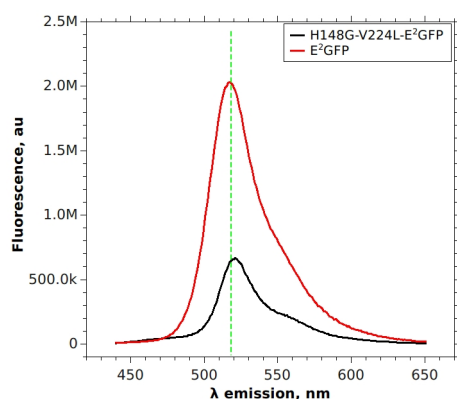
Brightness Brightness is an important spectroscopic characteristic of every fluorophore used for cell imaging.

Measuring absolute brightness is not trivial, so the relative brightness using E²GFP as reference is here reported.

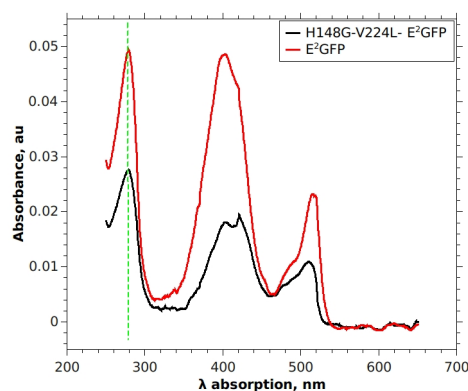
The brightness of the new protein η_{new} , compared to the E²GFP brightness η_{E2} , is computed from the fluorescence intensity F of each protein (at 520 nm) normalized by their respective absorbances A at 280 nm:

$$\frac{\eta_{new}}{\eta_{E2}} = \frac{F_{new} \cdot A_{E2}}{F_{E2} \cdot A_{new}} \quad (4.1)$$

With spectral information represented in Figure 4.40, it is possible to evaluate the H148G-V224L-E²GFP brightness as 60% of E²GFP brightness.



(a) Fluorescence spectra, for excitation at 420 nm



(b) Absorption spectra in UV-Vis range

Figure 4.40: Fluorescence and absorption spectra for E²GFP (red lines) and for H148G-V224L-E²GFP (black lines)

Thermodynamic analysis To discern the entropic and enthalpic contribution in the Gibbs free energy variation associated to chloride binding in H148G-V224L-mutant, a thermodynamic analysis was performed with a Van't Hoff analysis[6, 16].

Van't Hoff equation relates an equilibrium constant, in the present case the chloride dissociation constant K_d , with entropy and enthalpy at a certain temperature.

All measurements were performed at $pH = 5.2$ for two main reasons: (1) at this acid pH the protein is more sensitive to chloride, i.e. all GFPs present in solution are bound to a chloride ion; (2) at acid pH the chloride dissociation constant is less sensitive to occasional pH variations, which can otherwise influence the thermodynamic analysis.

From Van't Hoff linear behavior shown in Figure 4.41 on the facing page

it is possible to evaluate the variations in entropy ΔS ($\frac{cal}{K \cdot mol}$) and enthalpy ΔH ($\frac{Kcal}{mol}$) caused by the chloride insertion in the binding pocket inside the molecule.

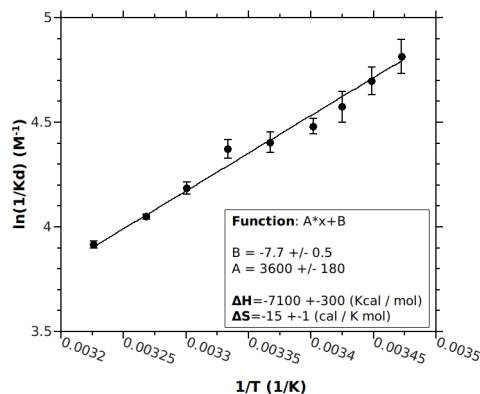


Figure 4.41: H148G-V224L-mutant Van't Hoff isothermal analysis, relating chloride dissociation constant Kd with temperatures T

For $H148G - V224L - E^2GFP$ this analysis estimates a negative variation in entropy and also a negative variation for enthalpy:

$$\begin{aligned}\Delta S &= -15 \pm 1 \frac{cal}{K \cdot mol} \\ \Delta H &= -7100 \pm 300 \frac{Kcal}{mol}\end{aligned}$$

The negative enthalpy variation (a positive slope of data in graph) means this binding reaction is exothermic[31].

Van't Hoff analysis has also been performed on other mutants, in order to reveal if their different chloride affinities were mainly triggered by the entropy or the enthalpy contribution in the Gibbs free energy.

In Figure 4.42 are reported the Van't Hoff analysis for V224L-E²GFP and for E²GFP in comparison with H148G-V224L-E²GFP.

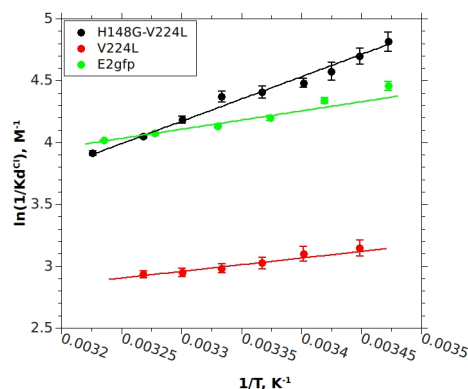


Figure 4.42: Van't Hoff analysis has been performed for E²GFP and for its mutant V224L and V224L-H148G, in order to compare the different entropy and enthalpy contribution to chloride affinity.

Entropy and in enthalpy for different mutants are summarized in table:

Mutant	ΔH ($\frac{Kcal}{mol}$)	ΔS ($\frac{cal}{K \cdot mol}$)
H148G-V224L-E ² GFP	-7100 \pm 300	-15 \pm 1
V224L-E ² GFP	-2100 \pm 700	-1.2 \pm 0.2
E ² GFP	-2900 \pm 200	-1.5 \pm 0.5

The different affinities for chloride cannot be ascribed to just entropy or just enthalpy, but to their overall effect.

In-cell characterization

For in-cell analysis, HEK293 cells have been used, transfected with exogenous DNA plasmid (codifying for *H148G – V224L – E²GFP*) with Effectene (Effectene Transfection Reagent, Qiagen, n°301427).

To calibrate in cells, and avoid the problem of different expression level and concentration variability from cell to cell, the full biosensor has been transfected: this new green moiety linked to red moiety monomeric-DsRed.

To perform a precise calibration, it's necessary to know exactly the chloride concentration and the pH inside cells. This task is achieved by the use of ionophores (see Section 3.1), organic molecules which make the cell wall permeable to ions (in particular chloride) and protons. In this way the environmental conditions inside cells are exactly those of the surrounding buffer, with specific pH and chloride.

pH calibration In in-vitro conditions, to measure pH it is necessary to excite the sample with blue light at 415 nm, and performing the ratio between emission signal detect at 520 nm (green signal) and at 495nm (cyan signal).

For in-cells experiment a custom 415/10 nm filter has been used, and emission were subsequently detected with 520/20 and 495/20 nm filters (respectively green and cyan channel). The red signal, detected with high-pass-620 filter upon 543nm excitation, has also been detected.

In Figure 4.43 it is reported a schematic pH-variation effect (from acid pH to basic pH) on the three different channels:

- green channel intensity (first row) is highly affected by changes in pH value, with an increased emission at basic pH
- cyan channel in the second row is instead unaffected by pH
- also red signal (third row) is constant and pH insensible.

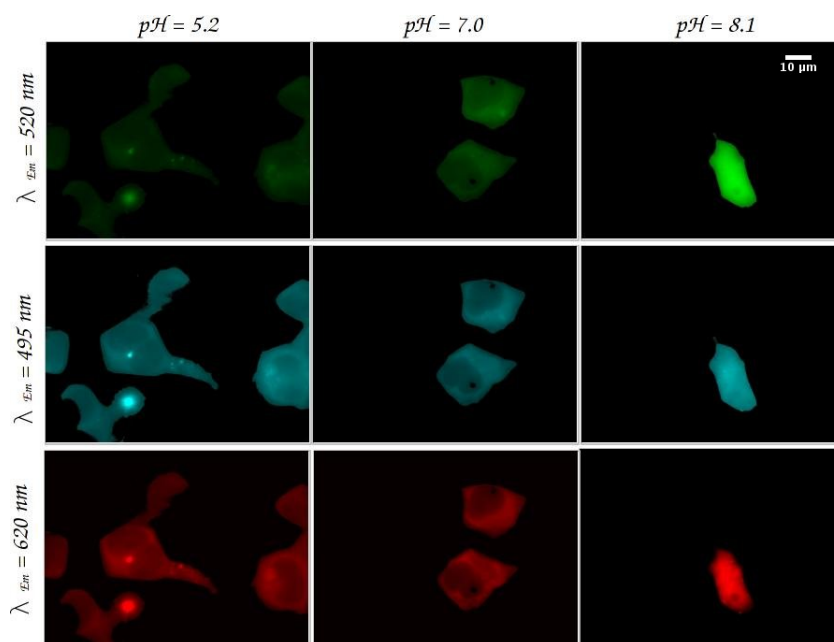


Figure 4.43: pH effect on green, cyan and red channel: green signal intensity is pH sensible, while cyan and red intensity are constant and insensible.

For each pH value, green/cyan ratio has been performed, and result is shown in Figure 4.44 (black dots): as in vitro, this ratio is pH sensitive, with a $pK = 7.42 \pm 0.05$ appropriate to have the best sensibility in the physiological pH range. Moreover this ratio shows a wide dynamic range of about 5 folds, assuring a high pH-detection precision.

To be sure also in cells the emission 495/20 is an isosbestic band, the ratio cyan/red has been performed (DsRed signal is pH independent): in Figure 4.44 this ratio (red dots) is constant, with a slope of $A = (8 \pm 7) \cdot 10^{-3}$ confirming the isosbestic characteristic of this cyan channel.

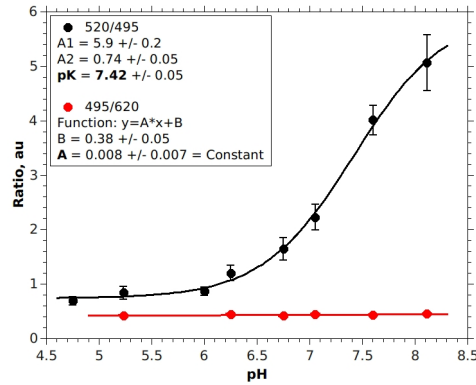
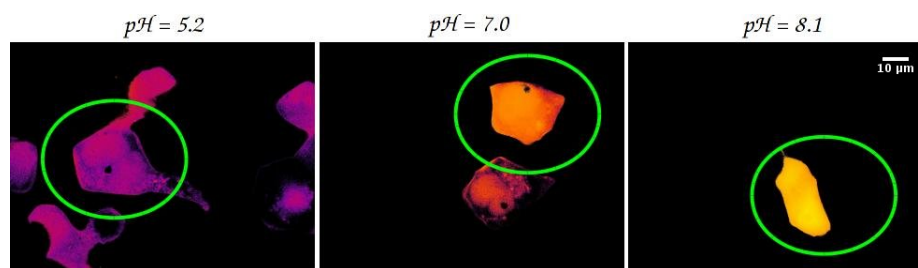


Figure 4.44: Green/cyan *ratio-pH* (black dots) and isosbestic signal cyan/red (red dots) analyzed for different pH values

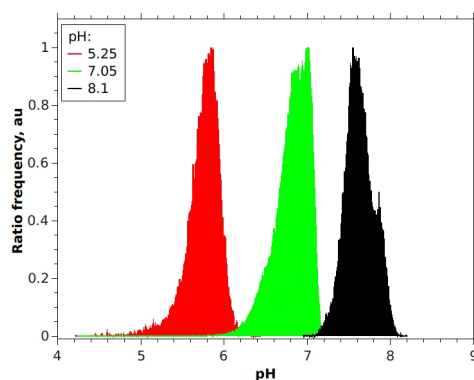
Once performed pH calibration, it is possible to obtain a pH map of cells from pixel-by-pixel ratio between green-channel and cyan-channel images: as example, pH maps of cells clamped with ionophores at three different pH values (and at the same chloride concentration of 0 mM) are shown in Figure 4.45.

Analyzing the pH-ratio intensity distribution for each of these samples, the resulting histograms are well defined and clearly separated for each of these pH conditions (Figure 4.45b).

The whole cell has also a uniform false-color, meaning ionophores act on the cell wall and also on the nuclear wall (Figure 4.45a).



(a) pH maps for cells clamped at different pH values



(b) pH values histogram distribution

Figure 4.45: Examples of pH analysis in cells

pH measurements is independent from in-cell chloride concentration

To perform a correct pH measurements, it is important that this analysis is not affected by other variables, such as chloride concentration. As happens in-vitro (Section 4.1.5 on page 86) also in-cell calibration confirms pH-ratio-analysis to be independent from chloride concentration, for a wide chloride concentration range around physiological pH values (shown in Figure 4.46)

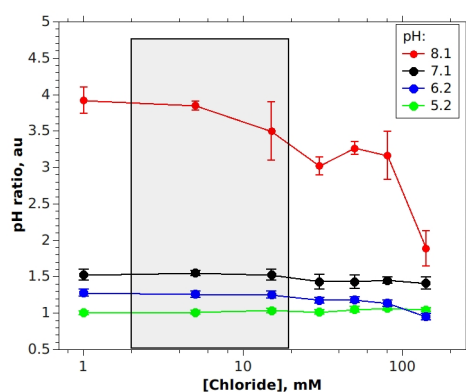


Figure 4.46: *Ratio-pH* analysis is chloride independent (in physiological pH and chloride conditions)

pH measurements is independent from microscope setup

This mutant has an isosbestic point in emission, allowing ratio-imaging with only one excitation wavelength.

Working only on the green moiety, and with only one excitation light, it is possible to change at will:

- Excitation light intensity
- Detector exposure time (which must be however kept equal between green and cyan detection)

In Figure 4.47 the *ratio-pH* is constant and independent from excitation light intensity (from 90% to 50%) and from exposure time (from 6 s to 1 s). This allows the user to be extremely free in setting up the microscope, leaving space to deal with possible sample issues.

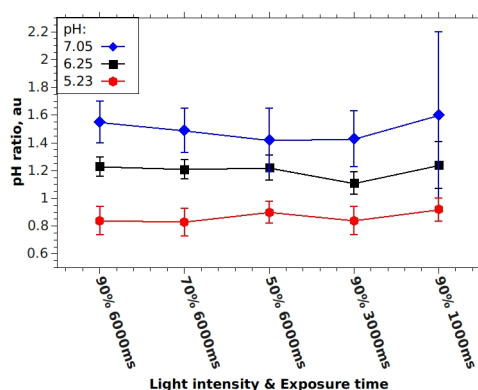


Figure 4.47: pH analysis is independent from microscope setup parameters, such as exposure time and excitation intensity

Background: autofluorescence effect

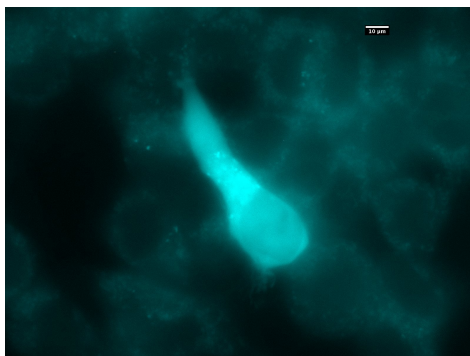
To have isosbestic point in emission, the excitation wavelength must be in very deep violet (415 nm). This is perfect condition for an autofluorescence signal to be generated and detected (autofluorescence has typical emission wavelengths in green range, right where microscope green and cyan filters are).

Autofluorescence is not quenched by chloride and is unaffected by pH variations, so it will represent a bias in all images. Its intensity must be subtracted to obtain a “clean” image.

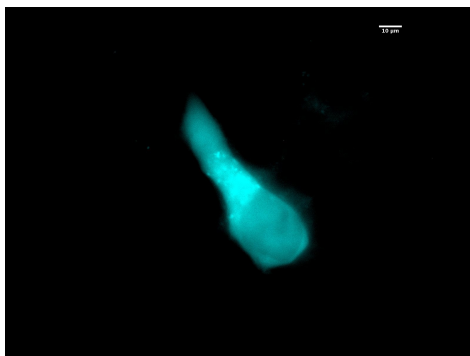
As general assumption, autofluorescence generated in transfected cells (i.e. cells which express the biosensor) has the same intensity as autofluorescence arising from not-transfected ones. In this way it is possible to know this contribution measuring intensity in green and cyan channel in not-transfected cells (cells which don't show any fluorescence signal in red channel⁸).

In Figure 4.48 is reported a typical image as example, acquired in cyan channel, as it appears with autofluorescence contribution (4.48a) and after subtraction to remove this bias signal (4.48b).

⁸Red signal is obtained exciting at 560 nm, faraway from usual autofluorescence excitation.



(a) Original image, with autofluorescence signal



(b) Cleaned image, without autofluorescence signal

Figure 4.48: Example of autofluorescence contribution, in cyan channel

Chloride calibration To measure chloride concentration the chloride sensitive green component alone is not enough.

To perform ratio-analysis and avoid problem of concentration variability from cell to cell it is necessary to measure also the reference signal from DsRed moiety (pH and chloride independent[4]):

Sensitive signal is detected in the cyan channel, with excitation at 415/10 nm and emission at the isobestic point 498/20 nm;

Reference signal is the red channel, characterized by excitation at 543/20 nm and emission with long-pass 620nm filter

In Figure 4.49 it is reported a schematic chloride-variation effect (for chloride concentration $[Cl] = 0 - 15 - 50 mM$) on the three different channels:

- green and cyan channel intensities (first and second row) are highly affected by changes in chloride concentration, with a strong quenching effect on their emission intensities

- red channel in the last row is instead unaffected by increasing chloride concentration.

For each chloride concentration, *ratio-Cl* cyan/red ratio has been performed at several pH values, as visible in Figure 4.50

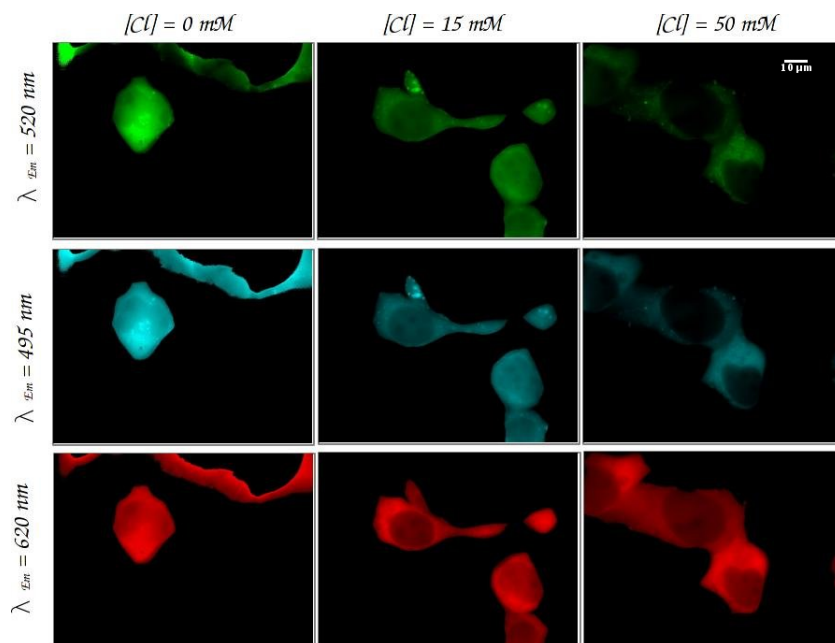


Figure 4.49: Chloride effect on green, cyan and red channel

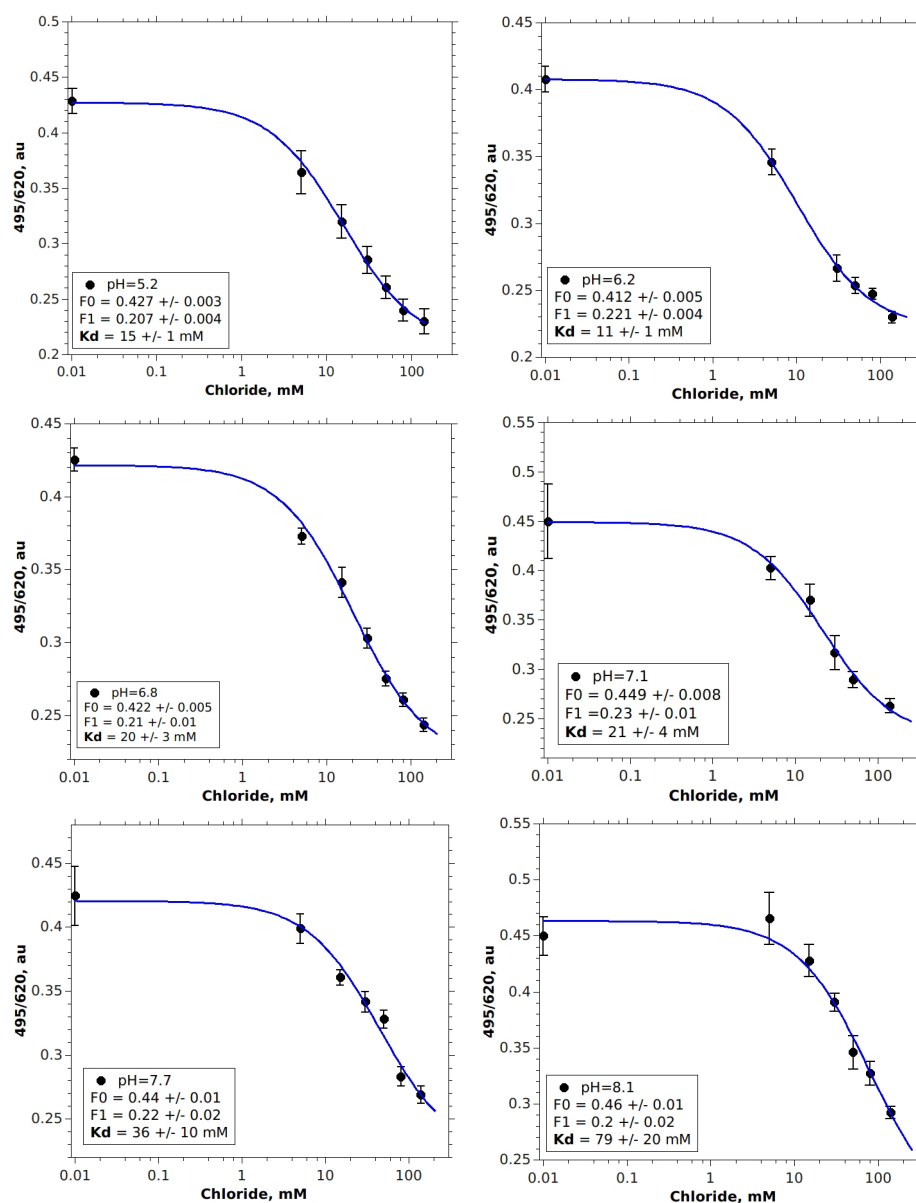


Figure 4.50: Chloride quenching effect on cyan/red *ratio-Cl* at different pH values: for each pH *ratio-Cl* decreases when chloride concentration in solution increases, due to chloride quenching effect. This decrease is affected by pH, chloride dissociation constant K_d is sensible to pH

At each pH, cyan/red ratio is very chloride sensitive, with a decrease more than 50%, even if this chloride affinity is pH sensitive as in-vitro (Figure 4.33 on page 97). At pH higher than ≈ 7.4 the chloride dissociation constant K_d increases significantly, as summarized in Figure 4.51.

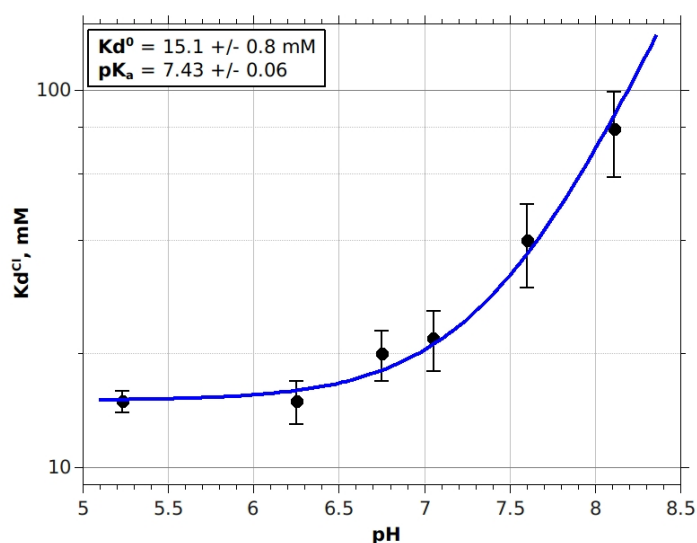
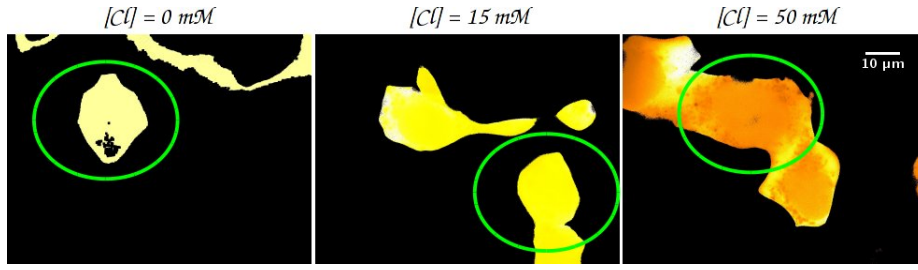


Figure 4.51: Chloride dissociation constant Kd at different pH values: chloride sensibility is affected by proton concentration in solution

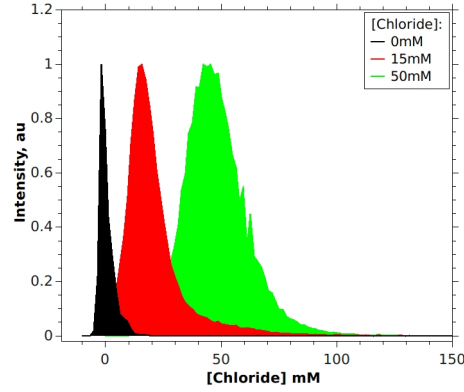
As already obtained in in-vitro analysis (Figure 4.33 on page 97), this mutant H148G-V224L-E²GFP shows a chloride affinity appropriate to measure chloride concentration in physiological conditions ($Kd^{Cl} = 21 \pm 4 \text{ mM}$).

Once performed chloride calibration, it is possible to obtain a chloride concentration map of cells from the pixel-by-pixel ratio-image between cyan-channel and red-channel images: as example, maps of cells clamped with ionophores at three different chloride concentrations (at the same pH = 7.2) are shown in Figure 4.52a.

Analyzing the [Cl]-ratio intensity distribution for each of these samples, clear and well defined chloride-distribution histograms are obtained for each different conditions (Figure 4.52b).



(a) [Cl] maps for cells clamped at different chloride concentration



(b) [Cl] values histogram distribution

Figure 4.52: Example of chloride analysis in cells

Measuring $[\text{Cl}^-]$ from ratio value R^{Cl}

To convert the ratio value R obtained after ratio-analysis of cyan and red image, after having the calibration values Kd^1 and pK_a , Equation 4.2 is used[4]:

$$[\text{Cl}^-] = \frac{(R_{(pH)}^0 - R)}{R - R_{(pH)}^{\text{inf}}} \cdot \left(Kd^1 \cdot \frac{1 + 10^{(pK_a - pH)}}{10^{(pK_a - pH)}} \right) \quad (4.2)$$

where R^0 and R^{inf} are the ratio-value extrapolated at zero and at infinite chloride concentration, respectively.

Their theoretical pH dependence is not present for cyan/red ratio-analysis because fluorescence coming from both these channel is pH independent. It is confirmed by analysis reported in Figure 4.53:

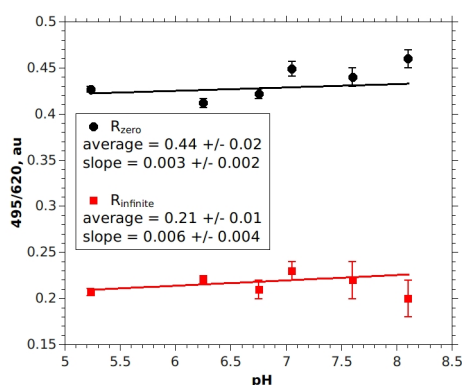


Figure 4.53: R^0 and R^{inf} are pH independent

Both R^0 and R^{inf} are constant with pH (their slope is comparable to zero). Their values to be used in Formula 4.2 are $R^0 = 0.44$ and $R^{\text{inf}} = 0.21$

Conclusions

Several E^2GFP mutants were screened, and two mutants were found to be of particular interest:

V224L-mutant is extremely sensitive to chloride concentration, presenting an incredible low chloride dissociation constant

H148G-mutant presents a *dual emission* characteristic, which can be exploited to measure pH with one excitation line less than in original E^2GFP

With a double site-specific mutagenesis, the best characteristics of these two single mutations has been gathered in one GFP-mutant. The result is $H148G - V224L - E^2GFP$, the most promising candidate to be the future green moiety in ClopHensor next-generation.

Major properties:

- with a chloride affinity $Kd^{Cl} = 21 \text{ mM}$ (at $pH = 7.2$) it is well suited to measure chloride concentration in intracellular environment
- it is also able to measure physiological in-cells pH with high precision, thanks to its $pK_a = 7.4$ and wide dynamic range (5-folds)
- thanks to its emission isosbestic point, pH measurement can be performed using only one excitation wavelength (instead of two with E^2GFP in ClopHensor).

It shows also other interesting spectroscopic features:

- pH measurements is independent from chloride concentration
- pH ratio analysis is independent from microscope setup, such as detector exposure time, excitation light intensity and excitation light stability
- thanks to ratio-imaging techniques, pH and chloride assessments are protein concentration independent
- its chromophore shows an high active fraction, up to 97% of proteins have a correctly folding chromophore

4.1.7 Mutant H148D-V224L-E²GFP

With the promising H148G-V224L-E²GFP as template, a new double site-specific mutant has been engineered to drastically alter aminoacid-148 characteristics.

- **V224L**: to increase chloride affinity ($Kd = 1.2\text{ mM}$)⁹
- **H148D**: the basic aminoacid HISTIDINE¹⁰ has been removed from position 148 and ASPARTIC ACID¹¹ has taken its place. A positive electrical charged residue was substituted with a negative charged one, significantly changing electrostatic conditions around the chromophore.

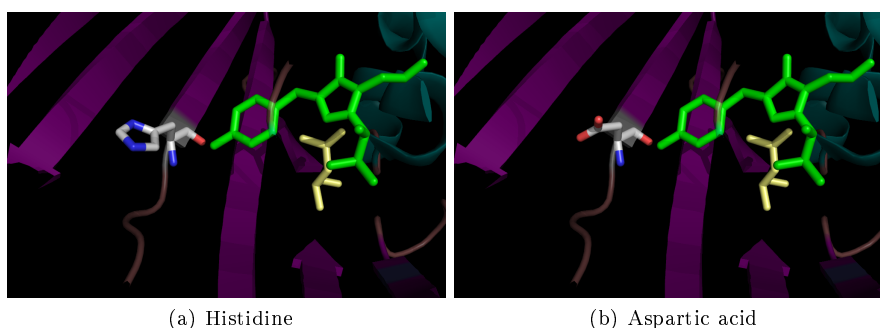


Figure 4.54: E²GFP structure, with highlighted the chromophore (in green), the leucine-224 (in yellow) and the 148-residue (gray for carbon, red for oxygen, blue for nitrogen)

In-vitro characterization

Chloride and pH titration At physiological pH, this mutant showed a low chloride affinity, as reported in Figure 4.55: $Kd = 230 \pm 50\text{ mM}$.

⁹Detailed information on V224L-mutant can be found in section 4.1.1 on page 62

¹⁰highly polar aminoacid, due to its imidazole functional group with its aromatic ring.

¹¹together with Glutamic acid, is classified as an acidic aminoacid (with a intrinsic pK of 3.9)

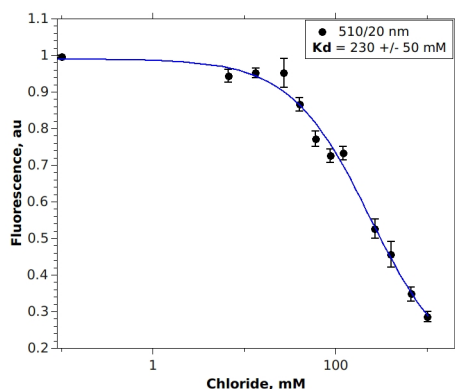


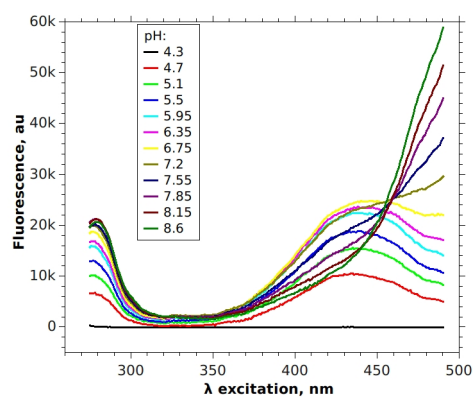
Figure 4.55: H148D-V224L-E²GFP fluorescence emission intensity (at 510/20 nm) at $pH = 7.2$ at increased chloride concentration up to 1M

Changing electrostatic environment around the chromophore reduced the chloride binding affinity. This can be explained by a long-distance electrostatic repulsion between negative-charged chloride ion and negative-charged new aminoacid in position 148.

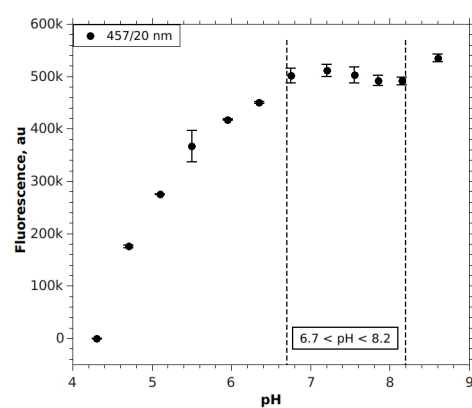
Moreover, new negative 148-residue plays an important role in defining the excitation isosbestic point.

Excitation spectra, acquired at different pH, are reported in Figure 4.56a: isosbestic point is present at 457 nm only in the pH range from 6.7 to 8.2. This result is better visible in Figure 4.56b, where the fluorescence intensity of the isosbestic band (457/20 nm) is reported.

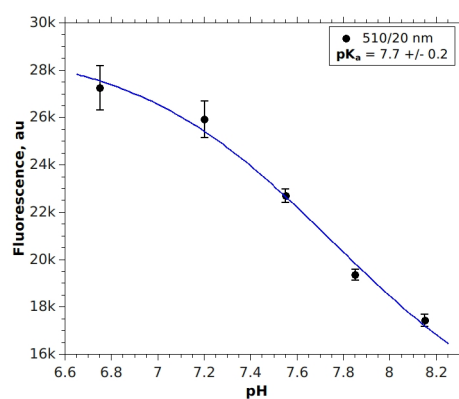
In the isosbestic-point-present pH range, the emission fluorescence intensity is influenced by pH with a $pK_a = 7.7 \pm 0.1$ (Figure 4.56c).



(a) Excitation spectra of H148D-V224L-E²GFP (for emission at 510 nm) acquired in different pH conditions, from $pH = 4.7$ (red spectrum) to 8.6 (dark green spectrum)



(b) Isosbestic band intensity (457/20 nm) from excitation spectra of Figure 4.56a: isosbestic feature is present only in a very limited pH range



(c) Intensity variation of the main emission peak (510 nm) due to pH effect, analyzed only in the pH region where isosbestic excitation point is present

Figure 4.56: pH effect on H148D-V224L-E²GFP fluorescence spectra shapes and intensities

Conclusions Mutation H148D significantly alters electrostatic environment around the chromophore, affecting both chloride and proton affinity.

Chloride affinity is lower than in E²GFP, with a K_d increased by more than one order of magnitude, probably explained by electrostatic repulsion with the negative-charged chloride ion. This GFP variant is not enough sensitive for an accurate chloride concentration measurements in physiological concentration range.

Mutation H148D has a strong effect on proton affinity, increasing pK of almost one point if compared to E²GFP, but it also affects in a critical way the presence of the isosbestic point in excitation, only present in a limited pH range.

4.1.8 Site-specific mutants results

Spectroscopic characteristics for E²GFP-mutants obtained by site-specific mutagenesis are here summarized.

- Kd^1 is the chloride dissociation constant for the fully-protonated protein form, i.e. measured at acid pH¹².
- pK_a is the specific pH value at which the chloride dissociation constant becomes double than Kd^1 .
- The *Isosbestic point* graph schematically shows the excitation spectra¹³ changes due to pH influence (at two extreme conditions: acid pH in black line, basic pH in red line)

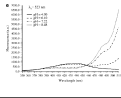
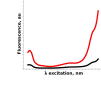
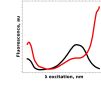
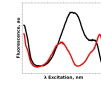
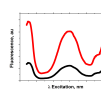
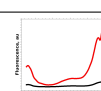
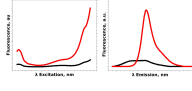
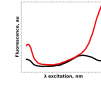
Mutation(s)	pK_a	Kd^1 (mM)	Isosbestic point
<i>E²GFP</i> [9]	7.1 ± 0.2	11.7 ± 0.8	
<i>V224L</i>	6.6 ± 0.1	1.2 ± 0.2	
<i>V224Q</i>	8.7 ± 0.1	1600 ± 30	
<i>V224N</i>	6.1 ± 0.2	13 ± 0.5	
<i>L42H-V224L</i>	6.9 ± 0.1	3.1 ± 0.3	
<i>H148G</i>	8 ± 0.05	120 ± 8	
<i>H148G-V224L</i>	7.2 ± 0.04	14.8 ± 0.8	
<i>H148D-V224L</i>	7.7 ± 0.2	$230 \pm 50^*$	

Table 4.1: Recap of site-specific E²GFP main spectroscopic characteristics.

¹²Chloride affinity for H148D-V224L-mutant was measured at physiological pH.

¹³For H148G-V224L-mutant are also reported the emission spectra.

4.2 Mutants from Random Mutagenesis

All mutants described so far have been obtained by site-specific mutagenesis.

Parallel to this strategy, E²GFP were also mutated in random position, where original aminoacid were substituted with random new ones.

With this procedure is very common to obtain mutant which are not fluorescent, because the mutation may alter the folding properties of the GFP, may alter its second and third structure, or prevent correct chromophore formation.

Even among correctly folded and fluorescent mutants, lots of them will not show any chloride affinity (halogen binding is not a common GFP property).

Random mutagenesis efforts are still in progress, but so far a couple of interesting mutants have already arisen.

4.2.1 P192A-E²GFP

This mutants presents in position -192 the non-polar aminoacid ALANINE in substitution of the non-polar PROLINE. Position -192 is not located near the chromophore as happened with all previous mutants. Mutation on this position doesn't a direct effect on binding characteristics, but in some way it affects the chromophore fluorescence features, as now described.

Chloride affinity and pH effect

Alanine in position -192 significantly increases chloride affinity. This mutant displayed the lowest $Kd_{pH=5.2}^{Cl} = 0.81 \pm 0.06 \text{ mM}$ ever met in our experiments.

However, this mutant resulted highly dependent on pH, with $pK_a = 6.33 \pm 0.05$.

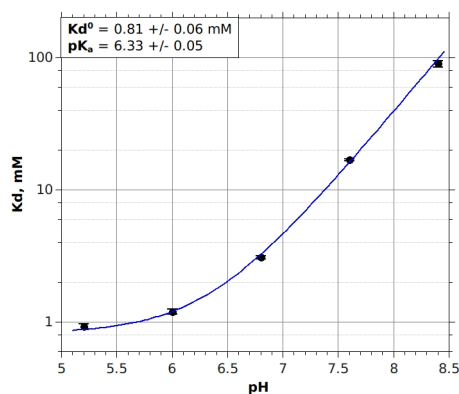


Figure 4.57: P192A-E²GFP chloride affinity is strongly influenced by pH already at acid pH conditions, as reported from the very low pK_a

In the physiological pH range this mutant is more sensitive to chloride than E²GFP, with an estimated K_d of 7 mM at $pH = 7.2$.

4.2.2 K101E-E²GFP

In this mutant there's a significant change in electrical charge of position -101: the basic aminoacid LYSINE (positive charged) has been replaced with the GLUTAMIC ACID (negative charged).

Chloride affinity and pH effect

GLUTAMIC ACID in position -101 creates a mutant with chloride affinity and proton sensitivity very similar to E²GFP ($K_d^1 = 13 \pm 2$ mM and $pK_a = 7.4 \pm 0.1$).

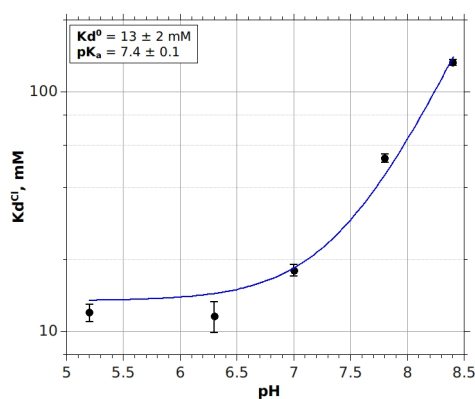


Figure 4.58: K101E-E²GFP chloride dissociation constant at different pH values. Chloride affinity and pH influence are very similar to those of template E²GFP

Mutation K101E plays a role in defining spectroscopic fluorescence features of this GFP variants, slightly increasing chloride dissociation constant and decreasing pH effects, even if there's not a significant improvement from E²GFP characteristics.

4.2.3 S202N-E²GFP

ASPARAGINE is the polar aminoacid which substitute SERINE (still polar aminoacid) in position 202 in this E²GFP mutant.

Even if there isn't a change in electrostatic characteristics, ASPARAGINE influences protein's spectroscopic characteristics.

Chloride affinity and pH effect

Spectroscopic features of S202N-mutant are very similar to those of its template, E²GFP.

Its chloride affinity for the fully-protonated form is $Kd_1^{Cl} = 16 \pm 1 \text{ mM}$, while at physiological $pH = 7.2$ it is estimated to be $\sim 25 \text{ mM}$ (Figure 4.59). With such a chloride sensitivity this mutant is perfectly able to measure physiological chloride concentration in cells.

S202N-E²GFP also preserves the important isosbestic point in excitation as it was in the template E²GFP (Figure 4.60a).

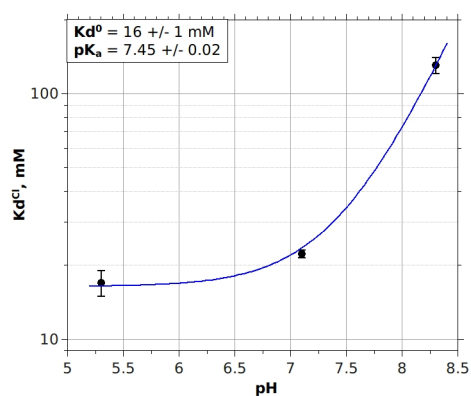
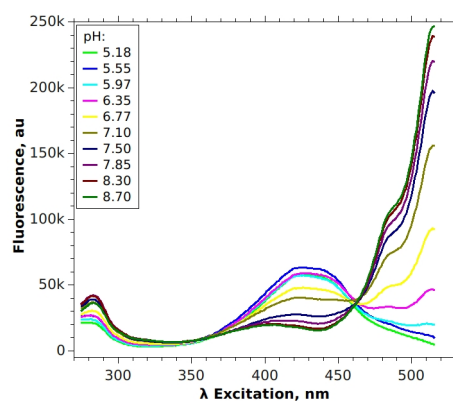
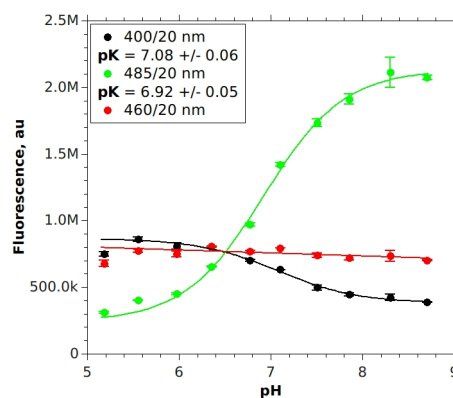


Figure 4.59: S202N-E²GFP chloride dissociation constant (Kd^1), and its pH sensibility (pK_a) are very similar to those of its template E²GFP



(a) pH effect on fluorescence spectra. This mutant presents an isobestic point in excitation, necessary for a correct and independent pH and chloride measurements



(b) Fluorescence intensities, at 430 nm from Figure 4.60a normalized, are influenced by pHs

Figure 4.60: S202N-E²GFP pH effect on fluorescence spectra

With these very interesting and promising spectroscopic characteristics about chloride affinity and pH dependence, mutant S202N-E²GFP has been selected as template for forthcoming experiments of random mutagenesis.

4.3 In-cell applications

H148G-V224L-E²GFP has shown its ability to in-vitro and in-cell measure pH and chloride concentration. It exhibits pH and chloride sensitivities similar to original ClopHensor's, but this combined estimation of pH and chloride can be performed with only two excitation wavelengths (instead of three as ClopHensor).

With these advantageous features, new *H148G-V224L-E²GFP+DsRed biosensor* were further tested in biological applications.

Different experiments were performed, as expression in eukaryotic cells after transfection or direct uploading in cells of the in-vitro purified version.

4.3.1 Uptake in cells of already-purified biosensor

Design of new carriers for drug delivery is one of the main subject of nanomedical research. Efficient substance loading, ability to delivery to the targeted cells, high cost-effectiveness and biocompatibility are just some of the prerequisites an efficient carrier should have.

Inorganic nanoparticles are very promising about these criteria. In particular, porous calcium carbonate in form of polycrystalline vaterite spheres.

Only recently these particles have been successfully sized-down to submicrometer size, achieving monodispersed size distribution around 400 nm[58]. This dimensions allows vaterite spheres the access inside cells and tissue structure, increasing this system's potential for future drug delivery applications.

It has been known that these vaterite sphere are biocompatible and naturally uptaken by cells[58], but the specific entry pathway is still unclear. The possibility to simultaneous measure pH and chloride concentration during vaterite sphere uptake would be very useful in better understanding cells' behavior in the presence of these polymeric nanoparticles.

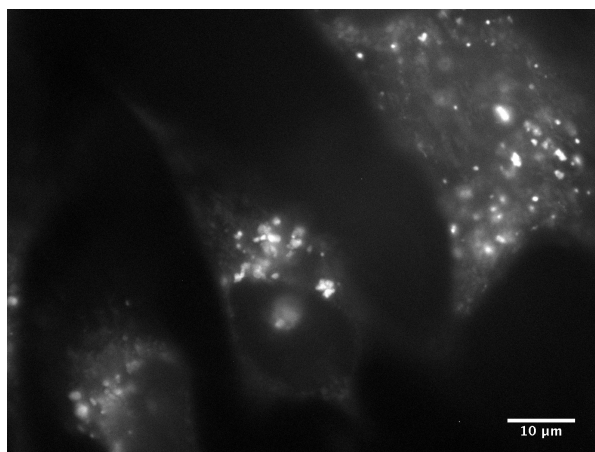
As proof-of-concept, preliminary experiments have been performed loading¹⁴ vaterite particles with purified H148G-V224L-E²GFP.

Biosensor was previously expressed in competent bacteria and then purified by liquid chromatography, alike for in-vitro characterization experiments. Once loaded, vaterite spheres are diluted in cells growing medium and added to cells for incubation (variable time from 2 to 46 hours). Before image acquisition, cells have been washed several times with fresh medium, to remove free carriers not yet uptaken.

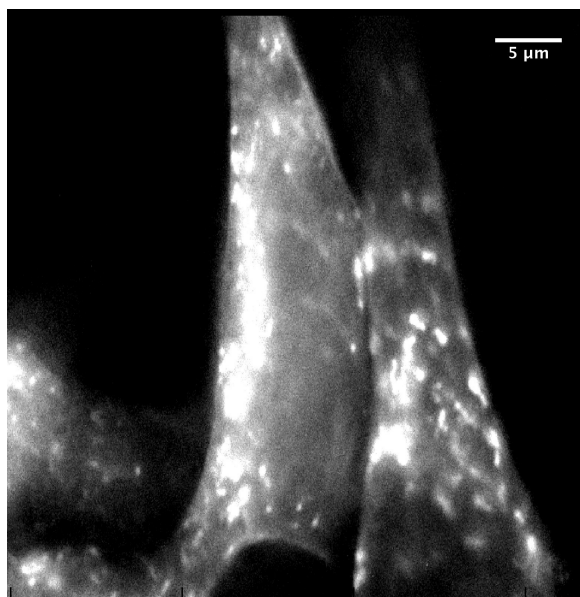
Inside HEK293 cells are clearly visible bright fluorescent dots (Figure 4.61).

¹⁴Standard protocol have been followed[58]

These bright dots are present only when cells are incubated with vaterite particles previously loaded of GFP-based biosensor. Background obtained from images of cells incubated with free biosensor in the growing medium (i.e. biosensor not loaded in vaterite spheres) was subtracted before image analysis.



(a) Bright dots inside HEK293 cells are vaterite nanospheres (or their aggregates), loaded with H148G-V224L-mutant, up-taken inside cells.



(b) Vaterite nanospheres with their fluorescent payload inside HEK293 cells.

Figure 4.61: Vaterite nanosphere loaded with H148G-V224L-E²GFP uptaken in HEK293 cells

Fluorescent dots sizes were about 500nm in diameter, compatible with sin-

gle vaterite spheres dimensions as measured independently by dynamic light scattering.

Vaterite spheres have the tendency to cluster in large aggregates (micrometer sized) when present at high concentration. Some of these micrometer-sized bright dots are visible in Figure 4.61. Vaterite particles preparation protocol is still under optimization, in order to decrease the percentage of nanoparticle clusters without over-reducing the single particles uptaken in cells.

As already reported for vaterite spheres filled with Rhodamine-6G and TRITC-dextran[58], also GFP-based biosensor can be efficiently loaded in vaterite nanoparticles. To load fluorescent dyes inside nanospheres, a preparation of vaterite containers is diluted in phosphate buffer ($pH = 7.2$) with 0.2 mg/ml of H148G-V224L-E²GFP for 1h. The nanospheres are then washed by centrifugation for at least 4 times, each time replacing the supernatant with fresh buffer.

The loading efficiency is defined as the amount of payload (in this case fluorescent dyes, but in future a specific drug) loaded per milligram of vaterite nanospheres. Vaterite nanospheres loading efficiency for H148G-V224L-E²GFP has been estimated subtracting the concentration of GFP-mutant in the supernatant (after first centrifugation washing) from the GFP-mutant concentration of the initial immersion solution.

Optimization of GFP-mutant loading process is still in progress, but preliminary measurements has revealed an efficiency of $\sim 0.2\% w/w$ ($20\ \mu\text{g}$ of GFP-mutant each 10 mg of vaterite particles), of the same order of those obtained with TRITC-dextran[58].

These experiments had shown the feasibility of this approach. H148G-V224L-E²GFP previously purified could be successfully loaded into vaterite nanoparticles, preserving its fluorescent property during cells uptakes.

This approach allows experiments for direct pH and chloride concentration assessment during nanospheres internalization, to better understand and characterize vaterite nanoparticles endocytotic pathways.

4.3.2 Intracellular functional characterization [53]

Chinese hamster ovary (CHO) cells are a cell line derived from the ovary of the Chinese hamster. This cell line is often used in biological and medical research because of their rapid growth and high protein production.

H148G-V224L-E²GFP+DsRed biosensor was transiently expressed in CHO-K1 cell line.

The first analysis was directed to determine its intracellular distribution in this cell line: observations confirms that H148G-V224L-ClopHensor variant exhibits a cytoplasmatic distribution (Figure 4.62) as already experienced during trasfection in HEK293 cells (Section 4.1.6).

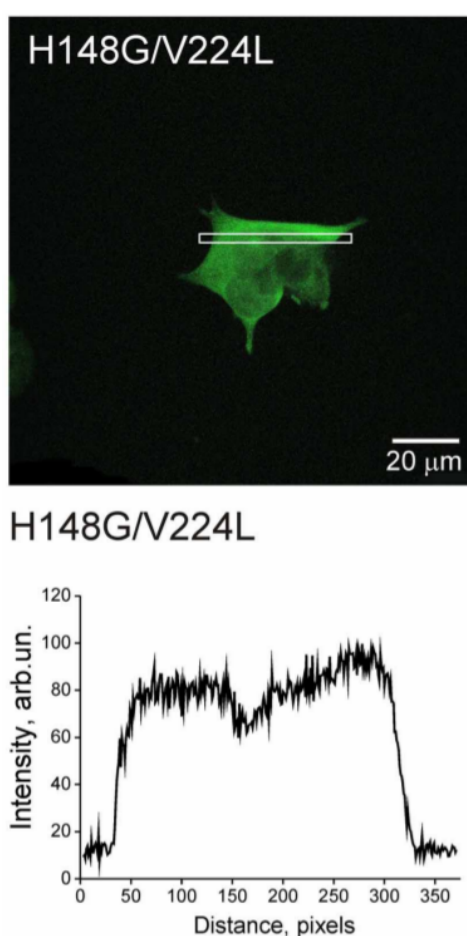


Figure 4.62: Expression of H148G-V224L-E²GFP+DsRed biosensor in CHO-K1 cell: (*above*) confocal image of CHO cell expressing genetically encoded H148G-V224L-ClopHensor variant; (*bottom*) illustrative profile of signal intensity distribution within the corresponding selcted area. Note the fluorescence distribution pattern being predominantly cytoplasmatic.[53]

After intracellular calibration, this new biosensor was exploited to simultaneously record changes in chloride concentration and pH during activation of Chloride-selective GlyR (glycine-receptors) channels.

The glycine receptor, or GlyR, is the specific cell receptor for the aminoacid neurotransmitter glycine, and it is one of the most widely distributed inhibitory receptors in the central nervous system. GlyR is an ionotropic receptor, a transmembrane protein which allows ions to pass through the cell membrane in response to the binding of a chemical messenger (such as a neurotransmitter, like glycine). GlyR produces its effects through chloride current.

H148G-V224L-E²GFP+DsRed biosensor was co-expressed with GlyR in CHO cells.

By dispensing glycine at 200 μ M locally, chloride-selective glycine receptor channels open, causing a variation in in-cell chloride concentration. *H148G-V224L-E²GFP+DsRed biosensor* was perfectly able to resolve this channel activation response: in Figure 4.63 is visible the recorded pH and chloride concentration variation (top trace and bottom trace, respectively) with well evident the spikes caused by glycine adding.

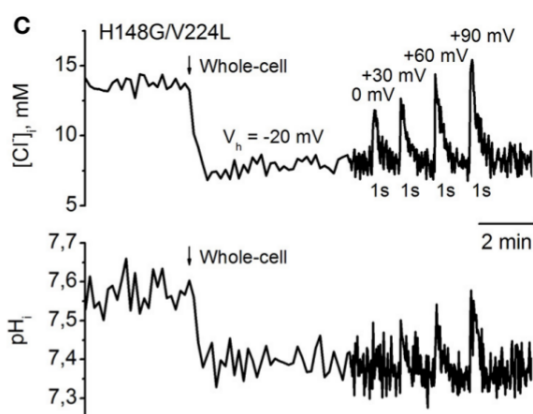


Figure 4.63: Monitoring of transients in chloride concentration and pH in response to GlyR activation, using H148G-V224L-ClopHensor variant. Changes in $[Cl^-]$ (above) and in pH (bottom) show an evident chloride concentration change during glycine treatment, associated with a pH fluctuation.[53]

These observations of the GlyR channels activation effects on chloride concentration (and pH fluctuations) confirm that *H148G-V224L-E²GFP+DsRed* is a suitable tool for stable, long-lasting and non-invasive monitoring of $[Cl^-]$ and pH , also in CHO cell line[53].

4.3.3 pH and chloride distribution in neuron-like cells

Hydrogen (H^+) and chloride ions (Cl^-) are fundamental in a wide range of nervous system processes, and often they are co-regulated.

Regulation of intracellular chloride is becoming widely recognized as an important neuronal process, and alterations in its homeostasis implies severe nervous system disorders.

Tools to accurately (and independently) measure pH and chloride concentration are important to understand the role these ions play in physiological and pathological neuronal network states.

ClopHensor has already demonstrated its ability to simultaneously and independently perform pH and $[Cl^-]$ measurements in different cell lines.

ClopHensor-variant composed of H148G-V224L-E²GFP as sensitive moiety and monomeric-DsRed as reference moiety has been here exploited.

In Section 4.1.6 on page 94 this new ClopHensor-variant has shown its ability measuring pH and chloride concentration in HEK293 cells. Now it has been expressed in neuron-like cells, NSC-34 differentiated (as explained on page 56), considered a standard template for nervous system cells.

New ClopHensor-variant plasmid has been transfected in NSC-34 cells as proof-of-concept that this E²GFP-mutant can be successfully expressed in neuron-like cells, significantly different than HEK293 cells previously exploited.

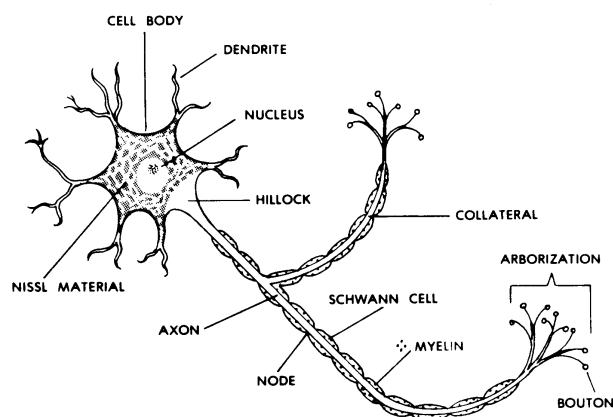


Figure 4.64: Schematic representation of a typical neuron cell

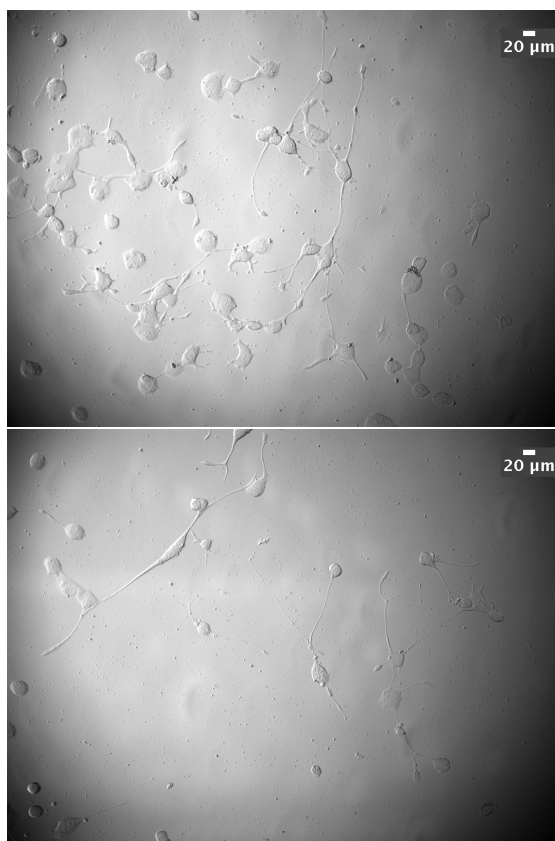


Figure 4.65: Transmission-light images of NSC-34 neuron-like cells

The thin and long projections from the cell body (named *Soma*) are the so-called *Processes*, responsible for the neuronal signal transmission from cell to cell in the brain.

To test the transfection feasibility in this delicate neuron-like cell line, *H148G-V224L-E²GFP+DsRed* biosensor was at first expressed in NSC-34 before differentiation, while they are still in the quiescent form, not yet neuron-like.

Resulting fluorescence, after standard 48-hours expression, was very intense, comparable with what previously observed in HEK293 cells. In Figure 4.66 is reported as example a typical “red” image in not-differentiated NSC-34.

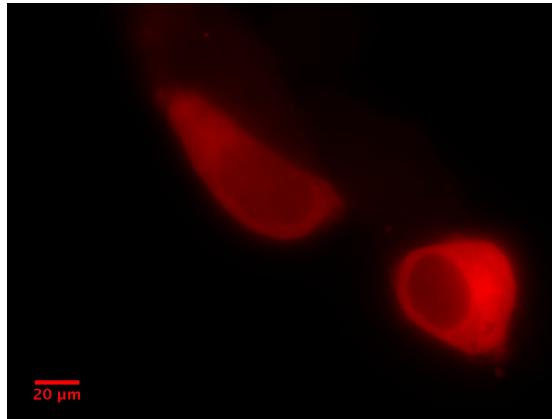


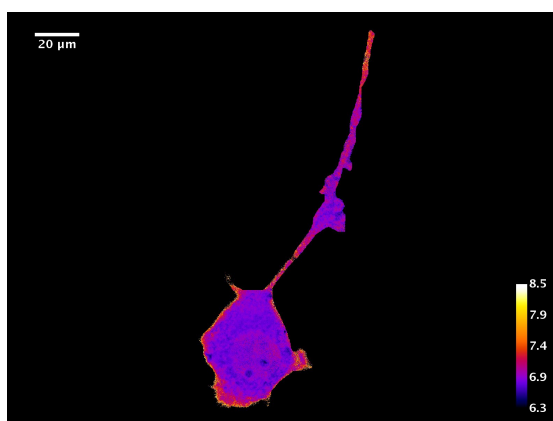
Figure 4.66: DsRed fluorescent signal from not-differentiated NSC-34 cells. In not-differentiated cells the new biosensor is very nicely expressed.

H148G-V224L-E²GFP+DsRed biosensor was then transfected in differentiated NSC-34 cells, after a 7-day differentiation (typical transmission light images are reported in Figure 4.65) and incubated for 48h before image acquisition.

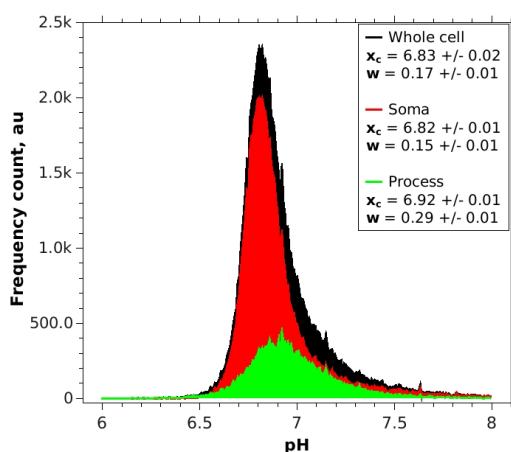
Following pH-ratio analysis protocol (as described on page 56) the pH resulted to be $pH_{soma} = 6.85 \pm 0.1$ in soma and similar $pH_{process} = 6.9 \pm 0.2$ in processes (Figure 4.67a).

These results are in perfect agreement with $pH \simeq 7$ reported in literature for neurons [72, 78].

These pH values were estimated fitting pH distribution with a Gaussian statistic: the pH value is the peak of the distribution (Xc), while the Gaussian variance (w) indicates the spread of pH values around the main peak.



(a) pH map of a differentiated NSC-34 cell (neuron-like cell): the soma and the process show a similar pH, around 6.9, in agreement with literature.



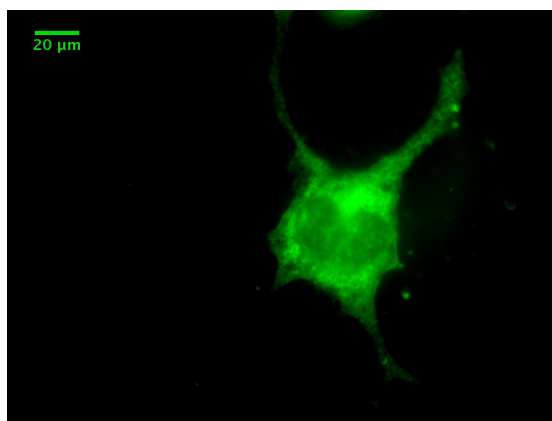
(b) Pixel-value distribution of pH in the map of Figure 4.67a. pH distribution results centered around $pH \simeq 6.9$ with a variance of 0.2

Figure 4.67: pH map inside an NSC-34 neuron-like cell

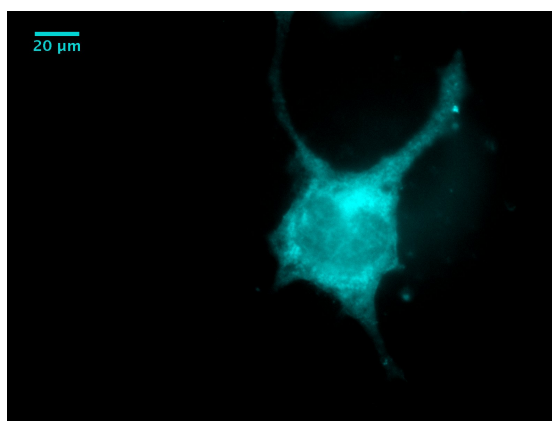
H148G-V224L-E²GFP+DsRed biosensor is then confirmed to be a sensitive and reliable probes for pH measurements in neuronal cells.

Unfortunately, using our standard procedure, fluorescence intensity of the red protein resulted substantially lower than in HEK293 cells. As a consequence, we were unable to compute reliable chloride maps in this case. In fact the red signal is used in the denominator of our (image) ratio, where a weak signal determines high uncertainty in the computed ratio.

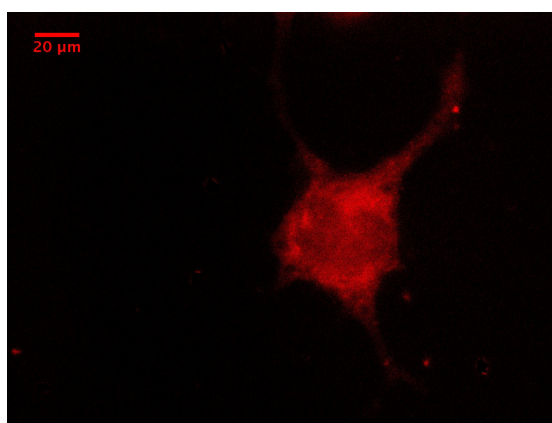
In Figure 4.68 it is possible to note the intense fluorescent signal arising from green and cyan channel (images *a* and *b*), while the red channel (image *c*) has a very low intensity.



(a) $Exc = 415/10\text{ nm}$, $Em = 520/20\text{ nm}$ (pH and chloride sensitive)



(b) $Exc = 415/10\text{ nm}$, $Em = 498/20\text{ nm}$ (Isosbestic emission, pH insensitive)



(c) $Exc = 543/20\text{ nm}$, $Em > 620\text{ nm}$ (Red reference signal)

Figure 4.68: New ClopHensor-variant (H148G-V224L-E²GFP+DsRed) expressed in neuron-like NSC-34 differentiated cells. Red signal is far less intense than what expected

To quantify these differences, it has been analyzed the ratio between the red fluorescent intensity inside cells and the background intensity (Figure 4.69). To avoid the influence of different expression level from cell to cell, a statistical analysis has been performed on several cells ($n > 20$). Experimentally the red background intensity has always had a similar intensity for all the images.

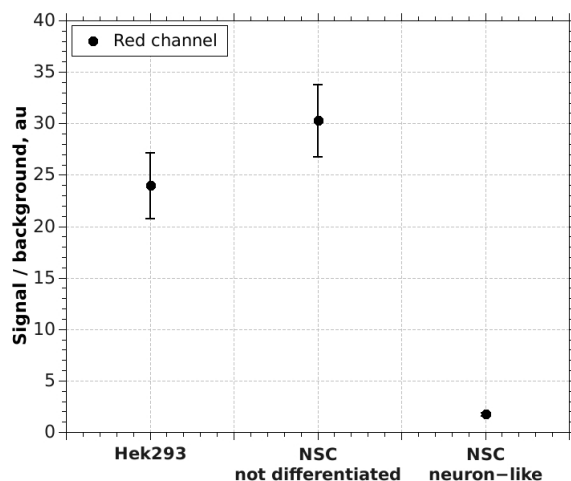


Figure 4.69: The ratio between red fluorescent intensity and background clearly show the extremely low red intensity when new ClopHensor-variant is expressed in neuron-like cells

As shown in Figure 4.69, signal over background ratio is significantly higher in HEK293 and not-differentiated NSC-34 cells than in neuron-like NSC-34, reflecting what by-eye observed.

Why the red fluorescent protein exhibited an anomalous turnover in differentiated NSC-34 cells remains an open question. Nevertheless, the new *H148G-V224L-E²GFP+DsRed biosensor* has clearly shown its ability to measure pH in *soma* and in *processes* of neuron-like cells.

These encouraging results let us be very confident on the future possibility to obtain also reliable chloride concentration estimation in neuronal cells.

Chapter 5

Conclusions

In this thesis a new genetically encoded pH-chloride indicator is presented.

This biosensor consists of two fluorescent protein linked by a short aminoacid linker, DsRed and a H148G-V224L-E²GFP. This construct is very similar to ClopHensor: it is composed of the same reference moiety (DsRed) and a double-mutated E²GFP as sensitive moiety.

As ClopHensor, it is not based on FRET between the two molecules, but on the ratiometric analysis of fluorescence emission intensities under different combination of excitation-emission wavelengths.

This new ClopHensor-variant exhibits chloride affinity and proton affinity very similar to *ClopHensor*.

With a chloride affinity $Kd^{Cl} = 21 \text{ mM}$ (at $pH = 7.2$) it is appropriate to measure chloride concentration in intracellular environment (in the order of some millimolar). It is also able to measure pH, in the physiological pH range, with high precision, thanks to its $pK_a = 7.4$ and its wide dynamic range. Its pK_a is just slightly higher than E²GFP, diminishing but not abolishing the pH dependence of the chloride affinity. Thus an independent pH measurement is still required for a precise chloride concentration estimation.

H148G-V224L-E²GFP+DsRed biosensor is characterized by an isosbestic point in emission, not in excitation as *ClopHensor*. In this way the pH measurements can be performed using only one excitation wavelength (instead of two with ClopHensor). The pH-ratio is now obtained analyzing *H148G-V224L-E²GFP* emission intensities at two different specific spectral bands, 520/20 and 495/20 nm.

This is a significant improvement: with only two excitation wavelengths for pH and chloride analysis, *H148G-V224L-E²GFP+DsRed biosensor* requires a

microscope setup less expensive, easier in alignment, optimization and maintenance. Moreover, ratio-imaging techniques for pH measurements is independent from excitation intensity, excitation light stability and detector exposure time. pH estimation is also independent from chloride concentration, allowing a reliable pH measurements regardless chloride concentration.

Previously-purified *H148G-V224L-E²GFP* was successfully loaded into vaterite nanoparticles, biocompatible artificial polymeric nanospheres whose endocytosis scheme is still unclear. *H148G-V224L-E²GFP* fluorescent properties are preserved during loading process and particles uptake inside cells.

These experiments showed the feasibility of this approach for direct ratio-imaging analysis during nanospheres internalization, to better understand and characterize these vaterite nanoparticles during their endocytotic pathways.

Genetically-encoded feature of this new ClopHensor-variant allows its direct expression in cells.

H148G-V224L-E²GFP+DsRed biosensor plasmid was transfected in differentiated NSC-34 cells, neuron-like cells considered a standard model for nervous system cells. Preliminary results revealed that this new ClopHensor-variant can be expressed in neuron-like cells, so that ratio-imaging analysis can be performed also in these particular cell lines. Further analysis and optimization are still in progress, but these results let us be very confident in future applications in brain neurons, for pH and chloride studies in physiological and pathological conditions.

H148G-V224L-E²GFP+DsRed biosensor was also transiently expressed in CHO-K1 cells [53]. These observations confirmed its cytoplasmatic distribution and its appropriate chloride affinity for intracellular $[Cl^-]$ measurements. This new biosensor, co-expressed with GlyR in CHO cells, was also able to resolve $[Cl^-]$ variations associated to GlyR channel activation.

Genetically encoded fluorescent probes have recently become the main tools for imaging studies of ions and proteins in live cells. Their continuous development and improvement, together with the progress in optical imaging techniques, has opened new avenues for noninvasive monitoring of ions flux in several cell lines and within specific cell compartments, in physiological and pathological conditions.

H148G-V224L-E²GFP+DsRed biosensor joins a pool of ratiometric genetically-encoded fluorescent biosensors widely exploited for their in-cell chloride sensitivity. *Clomeleon*, *SuperClomeleon*, *Cl-sensor*, *ClopHensor* and *ClopHensorN* are the top exponent of this chloride-sensitive pool.

Clomeleon, *SuperClomeleon* and *Cl-sensor* are FRET-based biosensors whose

chloride readouts is intrinsically pH dependence. An independent pH estimation is then necessary, but these biosensors are unable to self-measure pH. The used of a second external pH-sensitive probes is then necessary.

ClopHensor is perfectly able to measure pH and chloride concentration, but this double estimation requires the use of three excitation light. As consequence, it requires an expensive microscope setup, with non-trivial alignment and maintenance, most of all in the view of two-photon-excitation applications.

ClopHensorN, the most recent Clophensor-variant for chloride measurements in neurons, has an improved red reference moiety, but it shares the same green sensitive moiety (E²GFP) with *ClopHensor*. It still requires three excitation wavelengths for its ratio-imaging application.

H148G-V224L-E²GFP+DsRed biosensor has the same pH and chloride sensitivity as *ClopHensor*, but its spectroscopic characteristics make it able to efficiently measure both these parameters with only two excitation light lines.

Acknowledgments

Caro avventuriero ed esploratore scientifico, sei ora giunto alla conclusione del mio “diario” di questa spedizione scientifica alla ricerca della GFP perfetta. Mi hai seguito evitando pericoli nascosti ed insidiosi ostacoli, fino alla scoperta del mutante definitivo. Devi però sapere che questo lavoro, che porta ufficialmente solo il mio nome, è stato in realtà frutto di un lavoro di gruppo più grande di quanto immagini. Non avrei mai concluso questo viaggio senza l’aiuto (scientifico e non) di alcune persone, e questa tesi non sarebbe mai stata scritta senza il loro supporto.

A queste persone va tutta la mia gratitudine ed i miei ringraziamenti!

Grazie al mio supervisor DANIELE, per avermi accolto nel suo gruppo, per avermi guidato nel mondo dei biosensori di cloro, tra spettroscopia e microscopia, per i suggerimenti e le discussioni (e le frequenti incomprensioni) e per il grande supporto nella correzione finale della tesi.

Grazie anche ai miei genitori, per aver sempre creduto in me, per il loro costante sostegno e per essere sempre stati sicuri che sarei riuscito ad arrivare fino alla fine dell’impresa.

Nel mio percorso di dottorato ho avuto la fortuna di incontrare grandi persone, oltre che ottimi colleghi ed impareggiabili compagni di viaggio.

Certamente un grazie a LAVINIA: hai avuto il difficile compito di insegnare le basi di biologia ad un fisico, tralasciando le parti teoriche e catapultandomi direttamente nella pratica di laboratorio; grazie per tutto l’aiuto, scientifico e non solo, per il costante sostegno e supporto nei numerosi momenti difficili, per la pazienza e per l’allegria ogni giorno, per avermi guidato ogni giorno nel mondo del laboratorio!

Grazie a VALERIA: il passaggio dai banchi ottici di microscopia alle culture cellulare poteva rivelarsi difficile, invece grazie ai tuoi insegnamenti e alla tua pazienza non solo non ho mai combinato disastri con cellule e batteri, ma mi sono divertito ed ho conosciuto un mondo totalmente nuovo!

Non devo assolutamente dimenticare i miei colleghi JOSÈ, AURORA, SONJA e LIAISAN: oltre ad avermi aiutato ed assistito con le parti di biologia pura, mutazione e clonaggi vari, siete sempre stati un punto di riferimenti per risolvere dubbi ed incertezze scientifiche, sempre pronti a discutere per trovare una soluzione, e sempre presenti anche quando si trattava di ridere e divertirsi! Grazie per le lezioni di spagnolo (ora posso ordinare una cervesa come un vero spagnolo) e per i passi di danza (non dimenticherò mai il tuo danzare nei corridoi ed il tuo perenne sorriso).

Anche se non direttamente parte del mio gruppo, ci sono alcune colleghe senza le quali non sarei mai arrivato alla fine di questa tesi e di questo dottorato, alle quali va tutta la mia riconoscenza per l'impegno, la pazienza ed il tempo che hanno investito su di me in questi anni. MANUELA è senza dubbio una delle prima che devo ringraziare: mentre ti destreggiavi tra mille progetti, scadenze ed esperimenti, hai sempre trovato il tempo per aiutarmi e consigliarmi, spaziando dalle attività sperimentali di laboratorio (sai tutto di tutto, devo ancora trovare un problema in grado di metterti in difficoltà) alla stesura della tesi, senza dimenticare aperitivi e spritz!

Lo stesso discorso vale per LAURA T: grazie per tutti i consigli ed i suggerimenti, per le sempre utili discussioni su ogni argomento, dalla biologia alla microscopia, grazie per la pazienza nel leggere la mia tesi e per l'aiuto nella preparazione di Lisbona (e per essere stata la nostra guida turistica!) ed infine grazie anche per avermi fatto scoprire un po' della tua Cambridge!

Anche se è l'ultima arrivata in lab, un grande grazie va a VALENTINA: appena arrivata ti sei subito mostrata presente quando ne avevo bisogno, mi hai dato tantissimi suggerimenti, soprattutto per quanto riguarda la stesura della tesi (e l'odiata tabella riassuntiva!) ed importantissimo grazie per avermi guidato ogni mattina verso il caffè al bar! Grazie per l'allegria e per le risate in ufficio, mi sono sempre divertito!

Non posso certo tralasciare GAIA, compagna di scrivania e "custode" delle mie biro-penne-matite-scotch-etc, e LORENZA, fisico infiltrato nel mondo della biologia!

La tesi che state leggendo non sarebbe mai arrivata ad una versione definitiva senza il prezioso contributo del COCOSTE, il comitato per il controllo della scrittura della tesi. Un gruppo di futuri premi Nobel sparsi per il mondo che ha avuto il difficile compito di spronare il dottorando a scrivere la tesi, a fare ancora quell'ultimo esperimento, quell'ultimo grafico, a migliorare l'inglese (ricordandomi che di Shakespeare ce n'era solo uno) e a leggere articoli per avere una solida base di partenza. E per aver festeggiato con me, con un adeguato numero di spritz, ogni piccolo traguardo raggiunto verso la conclusione di questo

lavoro! Quando fonderò il laboratorio FBB (Fondazione Bora Bora) siete il gruppo che vorrei con me!

Un grazie anche al Tecnico MATTEO (sto ancora aspettando il giro di birre al bingo!), a GABRIELLA, MAURO, CARLO, CRISTINA, LAURA P, CECILIA e tutti i colleghi che ho avuto il piacere di incontrare in questi anni passati in laboratorio, grazie!

MARTA, non ti preoccupare, non mi sono dimenticato di te, e se ti ho lasciata per ultima è perchè ti meriti un posto particolare nei miei ringraziamenti: tu sei stata la vera presenza fissa in questi anni di dottorato, l'unica che ho visto dal primo giorno, in cui spaesato ed emozionato sono entrato in ufficio, e che vedrò fino all'ultimo giorno, quando felice e triste me ne andrò. Hai sopportato giorno dopo giorno le mie lamentele, i miei problemi, le mie giornate negative, i miei esperimenti falliti e le mie idee spesso assurde, ma sei stata anche pronta a festeggiare i successi, a ridere e scherzare, consigliarmi ed aiutarmi nel risolvere problemi e trovare soluzioni a tutto. E grazie anche per tutto l'aiuto al di fuori delle pareti del laboratorio, mi sei stata accanto anche da lontano, nei mesi in cui non ero in laboratorio tu sei sempre stata presente e mi hai sempre tenuto compagnia, sempre sicura che tutto sarebbe finito per il meglio! Grazie per essere sempre riuscita a farmi sorridere, ogni giorno!

Non hanno idea di cosa sia una proteina e non hanno mai visto una cellula, ma questi anni passati a Trento non sarebbe stati così felici e allegri senza i miei coinquilini Pedrodattili! Innanzitutto il capostipite, il grande Zio BERNA, il migliore compagno di stanza che si possa avere e fedele compagno nella lotta al disordine casalingo (Zandronen e Rolls, ne sapete qualcosa?), grazie per le sveglie mattutine a suon di Fugazzi, per aver affrontato con me la bertuccia e per le dritte per le varie applications; grazie anche a ROLLS, l'ultimo baluardo dei Pedrodattili originali, per la compagnia e l'allegria che ha sempre portato in casa, per le ottime cene e aver introdotto il rito del tisanone serale; un grazie anche a ZANDRONEN, che prima di esportare il pedrodattilismo nella terra dei crauti è stato il nostro barman, falegname, tuttofare in casa, portando sempre risate ed allegria, e affrontando in scontri epici il temibile Piergio (un'antica incisione ritrovata su una mensola lo testimonia). Ricordate: insalatona per tutti!

Anche se non ufficialmente coinquilini, voglio ringraziare anche LINDA, per aver portato colore e sempre più allegria in casa, ed il CIOPPE, che ogni sera entrava digitalmente in casa, coinquilina virtuale.

Anche se lontani da Trento ed estranei al mondo scientifico, un grande grazie va ai miei storici amici LAURA G, MARCO e NICOLAS, nella mia vita

praticamente da sempre, ed anche in questi anni sempre pronti a sostenermi, ad aiutarmi e a distrarmi, a farmi ridere ed a congratularsi e festeggiare con me ogni risultato raggiunto!

Un ringraziamento particolare va a STE: mi sei sempre rimasta accanto nonostante la distanza, sei sempre stata presente, soprattutto nei momenti difficili! Grazie per i consigli, le idee, le telefonate a mezzogiorno, i suggerimenti e la pazienza di ascoltarmi sempre! Anche a te andrà tutto bene!

LAURA A, da che parte posso iniziare per ringraziarti di tutto? Forse un'equazione potrà parlarti al posto mio meglio di mille parole: $(\delta + m) \psi = 0$. Questa è l'equazione di Dirac, la più bella equazione conosciuta della fisica. Grazie a questa si descrive il fenomeno dell'entanglement quantistico, che in pratica afferma che: "Se due sistemi interagiscono tra loro per un certo periodo di tempo e poi vengono separati, non possiamo più descriverli come due sistemi distinti, ma in qualche modo sottile diventano un unico sistema. Quello che accade a uno di loro continua ad influenzare l'altro, anche se distanti chilometri o anni luce".

Per concludere, grazie a te, avventuriero ed esploratore scientifico, per essere giunto alla conclusione di questo "diario" di viaggio. Spero tu possa esserti divertito, e magari un giorno ti ritroverai anche tu a chiederti: "E se provassimo questa mutazione...?".

Bibliography

- [1] *Strep -tagged Protein Purification Handbook, 04/2007.*
- [2] C. C. Aickin and A. F. Brading. Measurement of intracellular chloride in guinea-pig vas deferens by ion analysis, 36Cl^- efflux and micro-electrodes. *J Physiol*, 326:139–154, May 1982.
- [3] Daniele Arosio, Gianpiero Garau, Fernanda Ricci, Laura Marchetti, Ranieri Bizzarri, Riccardo Nifosi, and Fabio Beltram. Spectroscopic and structural study of proton and halide ion cooperative binding to gfp. *Biophys J*, 93(1):232–244, Jul 2007.
- [4] Daniele Arosio, Fernanda Ricci, Laura Marchetti, Roberta Gualdani, Lorenzo Albertazzi, and Fabio Beltram. Simultaneous intracellular chloride and ph measurements using a gfp-based sensor. *Nat Methods*, 7(7):516–518, Jul 2010.
- [5] Francis M. Ashcroft. *Ion channels and diseases*. San Diego Academi Press, 2000.
- [6] P.W. Atkins. *Physical Chemistry*. OXFORD UNIVERSITY PRESS, 1978.
- [7] T. Awaji, A. Hirasawa, H. Shirakawa, G. Tsujimoto, and S. Miyazaki. Novel green fluorescent protein-based ratiometric indicators for monitoring ph in defined intracellular microdomains. *Biochem Biophys Res Commun*, 289(2):457–462, Nov 2001.
- [8] Ken Berglund, Wolfram Schleich, Hong Wang, Guoping Feng, William C. Hall, Thomas Kuner, and George J. Augustine. Imaging synaptic inhibition throughout the brain via genetically targeted clomeleon. *Brain Cell Biol*, 36(1-4):101–118, Aug 2008.
- [9] Ranieri Bizzarri, Caterina Arcangeli, Daniele Arosio, Fernanda Ricci, Paolo Faraci, Francesco Cardarelli, and Fabio Beltram. Development of a

- novel gfp-based ratiometric excitation and emission ph indicator for intracellular studies. *Biophys J*, 90(9):3300–3314, May 2006.
- [10] Ranieri Bizzarri, Riccardo Nifosi, Stefania Abbruzzetti, Walter Rocchia, Sara Guidi, Daniele Arosio, Gianpiero Garau, Barbara Campanini, Elena Grandi, Fernanda Ricci, Cristiano Viappiani, and Fabio Beltram. Green fluorescent protein ground states: the influence of a second protonation site near the chromophore. *Biochemistry*, 46(18):5494–5504, May 2007.
- [11] Ranieri Bizzarri, Michela Serresi, Stefano Luin, and Fabio Beltram. Green fluorescent protein based ph indicators for in vivo use: a review. *Anal Bioanal Chem*, 393(4):1107–1122, Feb 2009.
- [12] Walter Boron and Emile Boulpaep. *Medical physiology: a cellular and molecular approach*. 2004.
- [13] Chiara Bosisio, Valentina Quercioli, Giuseppe Chirico, Laura D’Alfonso, Stefano Bettati, Samanta Raboni, Barbara Campanini, and Maddalena Collini. Effect of the point mutation h148g on gfpmut2 unfolding kinetics by fluorescence spectroscopy. *Biophys Chem*, 157(1-3):24–32, Aug 2011.
- [14] Piotr Bregestovski, Tatyana Waseem, and Marat Mukhtarov. Genetically encoded optical sensors for monitoring of intracellular chloride and chloride-selective channel activity. *Front Mol Neurosci*, 2:15, 2009.
- [15] Tsung-Yu Chen and Tzyh-Chang Hwang. Clc-0 and cftr: chloride channels evolved from transporters. *Physiol Rev*, 88(2):351–387, Apr 2008.
- [16] Normann Craig. Entropy diagrams. *J. Chem. Educ.*, 73:710, 1996.
- [17] E. DiCera. *Thermodynamic theory of site specific binding process in biological macromolecules*. Cambridge Univeristy press, 2005.
- [18] Colette T. Dooley, Timothy M. Dore, George T. Hanson, W Coyt Jackson, S James Remington, and Roger Y. Tsien. Imaging dynamic redox changes in mammalian cells with green fluorescent protein indicators. *J Biol Chem*, 279(21):22284–22293, May 2004.
- [19] J. Eisinger and J. Flores. Front-face fluorometry of liquid samples. *Anal Biochem*, 94(1):15–21, Apr 1979.
- [20] M. A. Elsliger, R. M. Wachter, G. T. Hanson, K. Kallio, and S. J. Remington. Structural and spectral response of green fluorescent protein variants to changes in ph. *Biochemistry*, 38(17):5296–5301, Apr 1999.

- [21] Alessandro Esposito, Matthias Gralle, Maria Angela C. Dani, Dirk Lange, and Fred S. Wouters. phlameleons: a family of fret-based protein sensors for quantitative ph imaging. *Biochemistry*, 47(49):13115–13126, Dec 2008.
- [22] Marta Fernandez-Suarez and Alice Y. Ting. Fluorescent probes for super-resolution imaging in living cells. *Nature Reviews*, 9:929–943, 2008.
- [23] J. Flach, M. Bossie, J. Vogel, A. Corbett, T. Jinks, D. A. Willins, and P. A. Silver. A yeast rna-binding protein shuttles between the nucleus and the cytoplasm. *Mol Cell Biol*, 14(12):8399–8407, Dec 1994.
- [24] L. J. Galletta, P. M. Haggie, and A. S. Verkman. Green fluorescent protein-based halide indicators with improved chloride and iodide affinities. *FEBS Lett*, 499(3):220–224, Jun 2001.
- [25] C. D. Geddes, K. Apperson, J. Karolin, and D. J. Birch. Chloride-sensitive fluorescent indicators. *Anal Biochem*, 293(1):60–66, Jun 2001.
- [26] Joshua S. Grimley, Li Li, Weina Wang, Lei Wen, Lorena S. Beese, Homme W. Hellinga, and George J. Augustine. Visualization of synaptic inhibition with an optogenetic sensor developed by cell-free protein engineering automation. *J Neurosci*, 33(41):16297–16309, Oct 2013.
- [27] G. Grynkiewicz, M. Poenie, and R. Y. Tsien. A new generation of ca^{2+} indicators with greatly improved fluorescence properties. *J Biol Chem*, 260(6):3440–3450, Mar 1985.
- [28] O. P. Hamill, J. Bormann, and B. Sakmann. Activation of multiple-conductance state chloride channels in spinal neurones by glycine and gaba. *Nature*, 305(5937):805–808, 1983.
- [29] George T. Hanson, Tim B. McAnaney, Eun Sun Park, Marla E P. Rendell, Daniel K. Yarbrough, Shaoyou Chu, Lixuan Xi, Steven G. Boxer, Marshall H. Montrose, and S James Remington. Green fluorescent protein variants as ratiometric dual emission ph sensors. 1. structural characterization and preliminary application. *Biochemistry*, 41(52):15477–15488, Dec 2002.
- [30] Stefan W. Hell. Far-field optical nanoscopy. *Science*, 316(5828):1153–1158, May 2007.
- [31] Takayuki Ichikawa. Thermodynamic properties of metal amides determined by ammonia pressure-composition isotherms. *J. Chem. Thermodynamics*, 42:140, 2010.

- [32] N. P. Illsley and A. S. Verkman. Membrane chloride transport measured using a chloride-sensitive fluorescent probe. *Biochemistry*, 26(5):1215–1219, Mar 1987.
- [33] S. Jayaraman, J. Biwersi, and A. S. Verkman. Synthesis and characterization of dual-wavelength cl-sensitive fluorescent indicators for ratio imaging. *Am J Physiol*, 276(3 Pt 1):C747–C757, Mar 1999.
- [34] S. Jayaraman, P. Haggie, R. M. Wachter, S. J. Remington, and A. S. Verkman. Mechanism and cellular applications of a green fluorescent protein-based halide sensor. *J Biol Chem*, 275(9):6047–6050, Mar 2000.
- [35] J. Kere, H. Lohi, and P. Hägglund. Genetic disorders of membrane transport iii. congenital chloride diarrhea. *Am J Physiol*, 276(1 Pt 1):G7–G13, Jan 1999.
- [36] B. Kerem, J. M. Rommens, J. A. Buchanan, D. Markiewicz, T. K. Cox, A. Chakravarti, M. Buchwald, and L. C. Tsui. Identification of the cystic fibrosis gene: genetic analysis. *Science*, 245(4922):1073–1080, Sep 1989.
- [37] R. D. KEYNES. Chloride in the squid giant axon. *J Physiol*, 169:690–705, Dec 1963.
- [38] Kazuya Kikuchi. Design, synthesis, and biological application of fluorescent sensor molecules for cellular imaging. *Adv Biochem Eng Biotechnol*, 119:63–78, 2010.
- [39] M. Kneen, J. Farinas, Y. Li, and A. S. Verkman. Green fluorescent protein as a noninvasive intracellular ph indicator. *Biophys J*, 74(3):1591–1599, Mar 1998.
- [40] M. C. Koch, K. Steinmeyer, C. Lorenz, K. Ricker, F. Wolf, M. Otto, B. Zoll, F. Lehmann-Horn, K. H. Grzeschik, and T. J. Jentsch. The skeletal muscle chloride channel in dominant and recessive human myotonia. *Science*, 257(5071):797–800, Aug 1992.
- [41] T. Kuner and G. J. Augustine. A genetically encoded ratiometric indicator for chloride: capturing chloride transients in cultured hippocampal neurons. *Neuron*, 27(3):447–459, Sep 2000.
- [42] Holger Lerche, Yvonne G. Weber, Karin Jurkat-Rott, and Frank Lehmann-Horn. Ion channel defects in idiopathic epilepsies. *Curr Pharm Des*, 11(21):2737–2752, 2005.

- [43] J. Llopis, J. M. McCaffery, A. Miyawaki, M. G. Farquhar, and R. Y. Tsien. Measurement of cytosolic, mitochondrial, and golgi pH in single living cells with green fluorescent proteins. *Proc Natl Acad Sci U S A*, 95(12):6803–6808, Jun 1998.
- [44] S. E. Lloyd, S. H. Pearce, S. E. Fisher, K. Steinmeyer, B. Schwappach, S. J. Scheinman, B. Harding, A. Bolino, M. Devoto, P. Goodyer, S. P. Rigden, O. Wrong, T. J. Jentsch, I. W. Craig, and R. V. Thakker. A common molecular basis for three inherited kidney stone diseases. *Nature*, 379(6564):445–449, Feb 1996.
- [45] Oliver Maier, Julia BÄ¶hm, Michael Dahm, Stefan BrÄ¶eck, Cordian Beyer, and Sonja Johann. Differentiated nsc-34 motoneuron-like cells as experimental model for cholinergic neurodegeneration. *Neurochem Int*, 62(8):1029–1038, Jun 2013.
- [46] James J. Mancuso, Jinsook Kim, Soojung Lee, Sachiko Tsuda, Nicholas B H. Chow, and George J. Augustine. Optogenetic probing of functional brain circuitry. *Exp Physiol*, 96(1):26–33, Jan 2011.
- [47] M. K. Mansoura, J. Biwersi, M. A. Ashlock, and A. S. Verkman. Fluorescent chloride indicators to assess the efficacy of cftr cDNA delivery. *Hum Gene Ther*, 10(6):861–875, Apr 1999.
- [48] Nima Marandi, Arthur Konnerth, and Olga Garaschuk. Two-photon chloride imaging in neurons of brain slices. *Pflugers Arch*, 445(3):357–365, Dec 2002.
- [49] Olga Markova, Marat Mukhtarov, Eleonore Real, Yves Jacob, and Piotr Bregestovski. Genetically encoded chloride indicator with improved sensitivity. *J Neurosci Methods*, 170(1):67–76, May 2008.
- [50] Tim B. McAnaney, Eun Sun Park, George T. Hanson, S James Remington, and Steven G. Boxer. Green fluorescent protein variants as ratiometric dual emission pH sensors. 2. excited-state dynamics. *Biochemistry*, 41(52):15489–15494, Dec 2002.
- [51] Tim B. McAnaney, Xinghua Shi, Paul Abbyad, Henry Jung, S James Remington, and Steven G. Boxer. Green fluorescent protein variants as ratiometric dual emission pH sensors. 3. temperature dependence of proton transfer. *Biochemistry*, 44(24):8701–8711, Jun 2005.
- [52] A. Miyawaki, O. Griesbeck, R. Heim, and R. Y. Tsien. Dynamic and quantitative Ca^{2+} measurements using improved cameleons. *Proc Natl Acad Sci U S A*, 96(5):2135–2140, Mar 1999.

- [53] M. Mukhtarov, L. Liguori, T. Waseem, F. Rocca, S. Buldakova, D. Arosio, and P. Bregestovski. Calibration and functional analysis of three genetically encoded cl(-)/ph sensors. *Front Mol Neurosci*, 6:9, 2013.
- [54] Marat Mukhtarov, Olga Markova, Eleonore Real, Yves Jacob, Svetlana Buldakova, and Piotr Bregestovski. Monitoring of chloride and activity of glycine receptor channels using genetically encoded fluorescent sensors. *Philos Trans A Math Phys Eng Sci*, 366(1880):3445–3462, Oct 2008.
- [55] T. Nakamura, H. Kaneko, and N. Nishida. Direct measurement of the chloride concentration in newt olfactory receptors with the fluorescent probe. *Neurosci Lett*, 237(1):5–8, Nov 1997.
- [56] T. O. Neild and R. C. Thomas. Intracellular chloride activity and the effects of acetylcholine in snail neurones. *J Physiol*, 242(2):453–470, Oct 1974.
- [57] M. OrmÅ¶, A. B. Cubitt, K. Kallio, L. A. Gross, R. Y. Tsien, and S. J. Remington. Crystal structure of the aequorea victoria green fluorescent protein. *Science*, 273(5280):1392–1395, Sep 1996.
- [58] B. V. Parakhonskiy, Cristina Foss, Eleonora Carletti, Mariangela Fedel, albrecht Haase, Antonella Motta, Claudio Migliaresi, and Renzo Antolini. Tailored intracellular delivery via a crystal pahase transition in 400 nm walerite particles. *Biomaterials Science*, 1:1273–1281, 2013.
- [59] G. J. Phillips. Green fluorescent protein—a bright idea for the study of bacterial protein localization. *FEMS Microbiol Lett*, 204(1):9–18, Oct 2001.
- [60] Brooks B. Pond, Ken Berglund, Thomas Kuner, Guoping Feng, George J. Augustine, and Rochelle D. Schwartz-Bloom. The chloride transporter na(+)-k(+)-cl- cotransporter isoform-1 contributes to intracellular chloride increases after in vitro ischemia. *J Neurosci*, 26(5):1396–1406, Feb 2006.
- [61] Lauren J. Pouwels, Liping Zhang, Nam H. Chan, Pieter C. Dorrestein, and Rebekka M. Wachter. Kinetic isotope effect studies on the de novo rate of chromophore formation in fast- and slow-maturing gfp variants. *Biochemistry*, 47(38):10111–10122, Sep 2008.
- [62] Joseph V. Raimondo, Bradley Joyce, Louise Kay, Theresa Schlagheck, Sarah E. Newey, Shankar Srinivas, and Colin J. Akerman. A genetically-encoded chloride and ph sensor for dissociating ion dynamics in the nervous system. *Front Cell Neurosci*, 7:202, 2013.

- [63] B. G. Reid and G. C. Flynn. Chromophore formation in green fluorescent protein. *Biochemistry*, 36(22):6786–6791, Jun 1997.
- [64] D Rendell. *Fluorescence and Phosphorescence (Analytical Chemistry by Open Learning)*. July 1987.
- [65] J.M. Russel. Sodium-potassium-chloride cotransport. *Physiol. Rev.*, 80:211–276, 2000.
- [66] J. M. Russell and W. F. Boron. Role of chloride transport in regulation of intracellular ph. *Nature*, 264(5581):73–74, Nov 1976.
- [67] Z. Servetnyk and G. M. Roomans. Chloride transport in ncl-sg3 sweat gland cells: channels involved. *Exp Mol Pathol*, 83(1):47–53, Aug 2007.
- [68] Nathan C. Shaner, George H. Patterson, and Michael W. Davidson. Advances in fluorescent protein technology. *J Cell Sci*, 120(Pt 24):4247–4260, Dec 2007.
- [69] R. Shiang, S. G. Ryan, Y. Z. Zhu, A. F. Hahn, P. O’Connell, and J. J. Wasmuth. Mutations in the alpha 1 subunit of the inhibitory glycine receptor cause the dominant neurologic disorder, hyperekplexia. *Nat Genet*, 5(4):351–358, Dec 1993.
- [70] D. B. Simon and R. P. Lifton. The molecular basis of inherited hypokalemic alkalosis: Bartter’s and gitelman’s syndromes. *Am J Physiol*, 271(5 Pt 2):F961–F966, Nov 1996.
- [71] M. Suzuki, T. Morita, and T. Iwamoto. Diversity of cl(-) channels. *Cell Mol Life Sci*, 63(1):12–24, Jan 2006.
- [72] Nataliya Svichar, Susana Esquenazi, Huei-Ying Chen, and Mitchell Chesler. Preemptive regulation of intracellular ph in hippocampal neurons by a dual mechanism of depolarization-induced alkalization. *J Neurosci*, 31(19):6997–7004, May 2011.
- [73] Karel Svoboda and Ryohei Yasuda. Principles of two-photon excitation microscopy and its applications to neuroscience. *Neuron*, 50(6):823–839, Jun 2006.
- [74] R. C. Thomas. The role of bicarbonate, chloride and sodium ions in the regulation of intracellular ph in snail neurones. *J Physiol*, 273(1):317–338, Dec 1977.

- [75] A. Y. Ting, K. H. Kain, R. L. Klemke, and R. Y. Tsien. Genetically encoded fluorescent reporters of protein tyrosine kinase activities in living cells. *Proc Natl Acad Sci U S A*, 98(26):15003–15008, Dec 2001.
- [76] R. Y. Tsien. The green fluorescent protein. *Annu Rev Biochem*, 67:509–544, 1998.
- [77] A. S. Verkman, M. C. Sellers, A. C. Chao, T. Leung, and R. Ketcham. Synthesis and characterization of improved chloride-sensitive fluorescent indicators for biological applications. *Anal Biochem*, 178(2):355–361, May 1989.
- [78] S. Vorstrup, K. E. Jensen, C. Thomsen, O. Henriksen, N. A. Lassen, and O. B. Paulson. Neuronal pH regulation: constant normal intracellular pH is maintained in brain during low extracellular pH induced by acetazolamide—³¹p nmr study. *J Cereb Blood Flow Metab*, 9(3):417–421, Jun 1989.
- [79] R. M. Wachter, M. A. Elsliger, K. Kallio, G. T. Hanson, and S. J. Remington. Structural basis of spectral shifts in the yellow-emission variants of green fluorescent protein. *Structure*, 6(10):1267–1277, Oct 1998.
- [80] R. M. Wachter and S. J. Remington. Sensitivity of the yellow variant of green fluorescent protein to halides and nitrate. *Curr Biol*, 9(17):R628–R629, Sep 1999.
- [81] R. M. Wachter, D. Yarbrough, K. Kallio, and S. J. Remington. Crystallographic and energetic analysis of binding of selected anions to the yellow variants of green fluorescent protein. *J Mol Biol*, 301(1):157–171, Aug 2000.
- [82] J.L. Walker. Ion-specific liquid ion exchanger micro-electrodes. *Analyt. Chem.*, 43:89–93, 1971.
- [83] Tatyana Waseem, Marat Mukhtarov, Svetlana Buldakova, Igor Medina, and Piotr Bregestovski. Genetically encoded cl-sensor as a tool for monitoring of cl-dependent processes in small neuronal compartments. *J Neurosci Methods*, 193(1):14–23, Oct 2010.
- [84] Roberto Weigert, Monika Sramkova, Laura Parente, Panomwat Amornphimoltham, and Andrius Masedunskas. Intravital microscopy: a novel tool to study cell biology in living animals. *Histochem Cell Biol*, 133(5):481–491, May 2010.

- [85] Z. Xia, Q. Zhou, J. Lin, and Y. Liu. Stable snare complex prior to evoked synaptic vesicle fusion revealed by fluorescence resonance energy transfer. *J Biol Chem*, 276(3):1766–1771, Jan 2001.